

Investigations on histamine and neuropeptide Y receptors by label-free and label-dependent methods

Dissertation

zur Erlangung des Doktorgrades der Naturwissenschaften
(Dr. rer. nat.)
an der Fakultät für Chemie und Pharmazie der Universität Regensburg



vorgelegt von
Sebastian Lieb
aus München

2016

Die vorliegende Arbeit entstand in der Zeit von September 2012 bis August 2016 unter der Leitung von Herrn Prof. Dr. Armin Buschauer und Herrn Prof. Dr. Joachim Wegener am Institut für Pharmazie der Fakultät für Chemie und Pharmazie der Universität Regensburg.

Das Promotionsgesuch wurde eingereicht im August 2016.

Tag der mündlichen Prüfung: 14. Oktober 2016

Prüfungsausschuss:

Prof. Dr. J. Heilmann	(Vorsitzender)
Prof. Dr. A. Buschauer	(Erstgutachter)
Prof. Dr. J. Wegener	(Zweitgutachter)
Prof. Dr. S. Elz	(Drittprüfer)

für meine Mutter

Contents

Contents.....	I
Publications and posters	V
Acknowledgements and declaration of collaborations.....	VII
Abbreviations.....	IX
1 General introduction.....	1
1.1 G-protein coupled receptors	1
1.2 G-protein mediated GPCR signaling	1
1.3 G-protein independent GPCR signaling.....	3
1.4 Traditional GPCR assays	3
1.5 Label-free assay platforms	6
1.5.1 Dynamic mass redistribution (DMR)	9
1.5.2 Surface plasmon resonance (SPR)	9
1.5.3 Electric cell-substrate impedance sensing (ECIS)	10
1.5.4 ECIS-SPR assay combination.....	11
1.5.5 Information on G-protein coupling gained from DMR and ECIS.....	11
1.6 References	13
2 Scope and objectives.....	21
3 The critical impact of cell adhesion in optical and impedance-based label-free assays	23
3.1 Introduction.....	24
3.2 Materials and methods	28
3.2.1 Cells and culture conditions	28
3.2.2 Transfections	28
3.2.3 Chemicals and test compounds.....	29
3.2.4 Impedimetric assay.....	30
3.2.5 RWG-based cell assays (EnSpire	32
3.2.6 Experimental setup for ECIS-SPR assays.....	32
3.2.7 Fura-2 calcium assay.....	34
3.2.8 Data analysis.....	34
3.3 Results and discussion	35
3.3.1 Impedance and DMR response of U-373 MG cells upon hH ₁ R stimulation.....	35
3.3.2 Impedance and DMR response of BAECs upon β_2 -adrenergic receptor stimulation ..	37
3.3.3 Comparing U-373 MG (H ₁ R) and BAE cells (β_2 -AR) stimulation by ECIS-SPR analysis..	40
3.3.4 Comparison of HEK293T-CRE-Luc-hH ₁ R with and without hMSR1 co-transfection	42
3.4 Conclusion	46
3.5 Appendix.....	47

3.5.1	Detection of hMSR1 expression in HEK293T-CRE-Luc-hH ₁ R-hMSR1 cells by immunoblotting.....	47
3.5.2	SDS-PAGE and western blot	48
3.6	References	49
4	Label-free versus conventional cellular assays: Functional investigations on the human histamine H₁ receptor	51
4.1	Introduction.....	52
4.2	Materials and methods	54
4.2.1	Histamine receptor ligands	54
4.2.2	Genetically engineered cells and culture conditions	55
4.2.2.1	HEK293T-CRE-Luc-hH ₁ R and HEK293T-CRE-Luc-hH ₁ R-hMSR1 cells.....	55
4.2.2.2	HEK293T-CRE-Luc-hH ₁ R-mtAEQ cells	55
4.2.2.3	HEK293T-ARRB1-H ₁ R and HEK293T-ARRB2-H ₁ R cells for the hH ₁ R- β -arrestin luciferase fragment complementation assay.....	55
4.2.3	Radioligand competition binding assay.....	56
4.2.4	Aequorin calcium assay	57
4.2.5	Fura-2 calcium assay.....	57
4.2.6	Luciferase gene reporter assay	58
4.2.7	β -Arrestin recruitment assay.....	59
4.2.8	Impedimetric assay.....	59
4.2.9	Dynamic mass redistribution assay	60
4.2.10	Data analysis.....	61
4.3	Results and discussion	61
4.3.1	Functional characterization of H ₁ receptor agonists	61
4.3.2	Cellular response to H ₁ R agonists in various assays.....	65
4.3.3	Investigation of G protein coupling.....	67
4.3.4	Functional characterization of H ₁ receptor antagonists.....	72
4.4	Conclusion	75
4.5	Appendix.....	76
4.5.1	H ₁ R-ELucC/ELucN-ARRB expression in HEK293T cells.....	76
4.5.2	Radioligand saturation binding on HEK293T cells, expressing the H ₁ R-ELucC and ELucN-ARRB constructs.....	78
4.5.3	Cytotoxicity of selected H ₁ R agonists in the crystal violet chemosensitivity assay.....	79
4.5.4	H ₁ R agonism of histaprodifen-derived hH ₁ R ligands in the β -arrestin recruitment assay	82
4.6	References	82
5	Functional investigations of human NPY Y₂ and Y₄ receptors: Comparison of label-free and calcium-based methods.....	87
5.1	Introduction.....	87
5.2	Materials and Methods	88
5.2.1	Human neuropeptide Y ₂ and Y ₄ receptor ligands.....	88
5.2.2	Cell culture.....	89

5.2.3	Aequorin calcium assay	89
5.2.4	Fura-2 calcium assay.....	90
5.2.5	Impedimetric assay.....	90
5.2.6	Dynamic mass redistribution assay	90
5.3	Results and discussion	91
5.3.1	Determination of the optimal cell density for CHO-hY ₂ -G _{q15} -mtAEQ cells in label-free assays	91
5.3.2	Effective range of measurement depending on the frequency of the alternating current (AC).....	92
5.3.3	Functional characterization of hY ₂ receptor ligands	93
5.3.4	Investigation of G-protein coupling of the human NPY Y ₂ receptor	96
5.3.5	Functional characterization of hY ₄ receptor ligands in the DMR and aequorin calcium assay	99
5.4	Conclusion	101
5.5	References	102
6	Summary.....	105

Publications and posters

Research articles (published results prior to the submission of this thesis):

Lieb, S., Michaelis S., Plank, N., Bernhardt G., Buschauer, A., Wegener J.

Label-free analysis of GPCR-stimulation: The critical impact of cell adhesion
Pharmacol. Res. **2016**, Apr 28; 108:65-74

Lieb, S., Littmann, T., Plank, N., Felixberger, J., Tanaka, M., Krief, S., Elz, S., Bernhardt G., Wegener J., Ozawa, T., Buschauer, A.

Label-free versus conventional cellular assays: Functional investigations on the human histamine H₁ receptor, submitted

Poster presentations:

Lieb, S., Plank, N., Bernhardt, G., Wegener, J., Buschauer, A.

Impedance-based label-free versus conventional methods for the determination of functional data on GPCRs: The human histamine H₁ receptor as an example. *Frontiers in Medicinal Chemistry* **2014**, Tübingen, Germany

Lieb, S., Plank, N., Bernhardt, G., Wegener, J., Buschauer, A.

Comparison of label-free methods with classical assays for the functional characterization of the human histamine H₁ receptor *7th Summer School Medicinal Chemistry* **2014**, Regensburg, Germany and *Annual meeting of the German Pharmaceutical Society* **2014**, Frankfurt a.M., Germany

Lieb, S., Kuhn, K., Bernhardt, G., Buschauer, A.

Dynamic mass redistribution: a label-free method for investigations on human NPY Y₂ and Y₄ receptors *11th NPY-PYY-PP Meeting* **2015**, Leipzig, Germany

Lieb, S., Michaelis S., Plank, N., Bernhardt G., Buschauer, A., Wegener J.

Label-free analysis of GPCR-stimulation: The critical impact of cell adhesion *3rd Conference on Impedance-Based Cellular Assays* **2016**, Regensburg, Germany

Acknowledgements and declaration of collaborations

First, I am especially grateful to my supervisor Prof. Dr. Armin Buschauer who gave me the possibility to work on my scientific project in his research group and want to thank him for his guidance and support on this thesis.

I wish to thank my second supervisor Prof. Dr. Joachim Wegener (Institute of Analytical Chemistry, Bioanalysis and Biosensors, University of Regensburg) for scientific advice and valuable discussions on this thesis. Furthermore, I want to thank his group for collaboration concerning electric cell-substrate impedance sensing (ECIS). Special thanks are addressed to his coworkers Dr. Judith Stolwijk, Kathrin Hajek, Christina Hupf, Sonja Lukic, Zlatko Paric and Barbara Goricnik for personal support. Investigations on and comparison with different label-free methods (Chapter 3) were carried out together with Dr. Stefanie Michaelis. The contribution of Dr. Nicole Plank to this chapter is gratefully acknowledged. I wish to express my warmest thanks for this successful collaboration.

I owe sincere gratitude to Prof. Dr. Sigurd Elz for giving me the possibility to work in his research group and for his participation in the examination committee.

I wish to express my gratitude to Prof. Dr. Jörg Heilmann for participation in the evaluation committee.

I want to thank Prof. Dr. Günther Bernhardt for giving me hints to improve the style of this thesis and for his scientific advice.

Comparison of label-free methods with conventional assays (Chapter 4) was concerted work (with equal contributions) with Dr. Nicole Plank and Timo Littmann. The contribution of Dr. Johannes Felixberger and Dr. Stéphane Krief (Bioproject Biotech, Saint-Grégoire, France), Prof. Dr. Takeaki Ozawa and Dr. Miho Tanaka (Both Department of Chemistry, School of Science, The University of Tokyo, Japan) as well as Prof. Dr. Sigurd Elz to this chapter is gratefully acknowledged. I wish to express my warmest thanks for this successful collaboration.

Elvira Schreiber from our group is gratefully acknowledged for outstanding technical assistance with regard to performing fura-2 calcium assays (Chapter 4+5).

I want to thank all technicians for the fruitful collaboration. Special thanks are addressed to Lydia Schneider and Peter Richthammer for their humor and encouraging words.

I want to thank all former and present colleagues for providing a very enjoyable atmosphere and constructive mutual assistance. I am especially grateful to Kilian Kuhn, José-Esteban Obrequé-Balboa and Matthias Scholler for the support and highly philosophical discussions.

For technical assistance I also wish to thank my student apprentices Christiane Luther, Angelina Welsch, Christina Seisenberger, Christoph Müller and Markus Busch.

Many thanks are due to the Hanns-Seidel-Stiftung for a PhD fellowship.

Finally, I thank my wife Verena Lieb and my family for their support and for believing in me.

Abbreviations

°C	degrees Celsius
μ	10 ⁻⁶
λ	lambda, wavelength (nm)
Δ	delta, difference
AC	alternating current
BAEC	bovine aortic endothelial cells
BSA	bovine serum albumin
cAMP	cyclic 3'-5'-adenosine monophosphate
cf.	(Lat.: <i>conferre</i>) compare
C	capacitance
C _m	specific membrane capacitance (ECIS model)
CHO	Chinese hamster ovary (cells)
DAG	diacylglycerol
DMEM	Dulbecco's modified eagle medium
DMR	dynamic mass redistribution
DMSO	dimethyl sulfoxide
ECIS	electric cell-substrate impedance sensing
EMEM	Eagle's minimal essential medium
FCS	fetal calf serum
Fig.	figure
g	gram
G418	geneticin
GDP	guanosine-5'-diphosphate
GTP	guanosine-5'-triphosphate
GPCR	G protein-coupled receptor
G protein	guanine nucleotide-binding protein
H	human
HEK	human embryonic kidney (cells)
IP ₃	inositol-1,3,4-triphosphate

I	current
L	liter
m	meter
m	milli
min	minutes
M	molar (mol/l)
N	number of experiments
n	nano (10^{-9})
nd	not determined
p	pico (10^{-12})
pEC ₅₀	negative logarithm (base 10) of half maximal effect concentration (EC ₅₀)
PBS	phosphate buffered saline
PKA	protein kinase A
pH	negative logarithm (base 10) of the molar concentration of dissolved hydronium ions (H ₃ O ⁺)
PKC	protein kinase C
PLC	phospholipase C
PTX	pertussis toxin
R	resistance
R _b	specific barrier resistance /ECIS model)
RWG	resonant waveguide grating
SEM	standard error of the mean
SPR	surface plasmon resonance
t	time
Tab.	Table
U	Voltage
Z	impedance
Z	impedance magnitude
8W10E	eight wells, ten electrodes
96W1E+	96 wells, one electrode

2 Scope and objectives

Conventional methods for the functional characterization of GPCR ligands in cellular assays monitor individual signaling pathways such as alterations in calcium-, cAMP or IP₃ levels. By contrast, although being less specific, label-free assays are integrative approaches, harbouring the potential to detect complex signaling networks as the sum of intracellular processes upon GPCR activation.

The aim of this doctoral thesis was to optimize and to explore the potential of two label-free methods, namely DMR and ECIS, to functionally characterize ligands of prototypical aminergic and peptidergic G-protein coupled receptors. For this purpose, histamine H₁ and neuropeptide Y (NPY) Y₂ and Y₄ receptors were selected as examples, as appropriate pairs of selective agonists and antagonist as well as corresponding data from various label-dependent assays have been available.

With regard to optimization, various cell types expressing the human H₁ receptor (H₁R), comprising constitutively H₁R expressing tumor cells as well as different genetically engineered HEK293T cells co-expressing the H₁R and the firefly luciferase, were chosen. Moreover, to study the effect of adhesion in the label-free assays, the co-expression of human macrophage scavenger receptor 1 (hMSR1) was aimed at. As a model system for peptidergic GPCR, CHO-G_{q15}-mtAEQ cells co-expressing the human NPY Y₂ (Y₂R) or Y₄ receptor (Y₄R), the chimeric G α protein G_{q15} and mitochondrially tagged aequorin were selected.

To study the contribution of individual signaling pathways to the holistic readouts, the selective G-protein inhibitors FR900359 (also known as UBO-QIC) and pertussis toxin (PTX) were considered appropriate tools.

1 General introduction

1.1 G-protein coupled receptors

G-protein coupled receptors (GPCR) represent the largest and most versatile group of membrane receptors [1-3]. More than 800 GPCRs are encoded in the human genome [4]. The GPCRs are grouped in five major phylogenetic classes [5]. The largest branch with about 700 members comprises the rhodopsin-like receptors [5]. The other groups are the adhesion, secretin, glutamate and frizzled/taste receptors [5]. Furthermore, there are more than 100 (orphan) GPCRs with no identified endogenous ligand or function [6-8]. The G-protein coupled receptors are sharing structural similarities comprising an N-terminal extracellular domain, seven transmembrane domains, connected by three extracellular and three intracellular loops, and a C-terminal intracellular domain [9]. A broad range of chemical and physical stimuli, for example neurotransmitters, ions or light, can activate specific GPCRs, which subsequently transduce the signal into cellular responses [10]. Consequently, GPCRs are involved in many physiological functions and in a plethora of diseases [11,12]. The majority of GPCRs are signaling via heterotrimeric guanosin-5'-triphosphate binding proteins (G-proteins) [3], whereas other signaling mechanisms are G-protein independent, involving β -arrestins or GPCR heteromerization [13,14]. Therefore, GPCRs are more precisely referred to as seven transmembrane receptors (7TMRs) [15]. More than 30 % of all approved drugs are addressing GPCRs [2,10,16], although only about 30 GPCRs are currently targeted [17]. Therefore, there is still a large number of GPCRs to be validated for drug discovery.

1.2 G-protein mediated GPCR signaling

The heterotrimeric G-proteins were discovered more than 40 years ago [18]. The GPCR mediated signal transduction is triggered by agonist binding which induces conformational changes of the receptor resulting in the activation of heterotrimeric G-proteins [19]. The G-proteins consist of three polypeptides, the 39-52 kDa GDP/GTP-binding $G\alpha$ subunit and the $G\beta\gamma$ dimer [20]. Before activation, the $G\beta\gamma$ is non-covalently bound to the $G\alpha$ subunit. G-protein activation is resulting in the exchange of guanidine diphosphate (inactive G-protein) for guanidine triphosphate (active G-protein) in the $G\alpha$ subunit. After GDP-GTP-exchange, the G-protein dissociates from the receptor and falls apart into the α - and the $\beta\gamma$ -subunit. Both subunits are then free to stimulate distinct pathways [21]. The duration of signaling depends on the rate of the intrinsic GTP hydrolysis by the $G\alpha$ -subunit and the following re-association

of $G\alpha$ -GDP with $G\beta\gamma$ [22-24]. Up to now, 16 mammalian $G\alpha$ subunits are described and based on sequence of the α -subunit and their functional properties, G-proteins are classically divided into four classes: $G\alpha_{i/o}$, $G\alpha_s$, $G\alpha_{q/11}$ and $G\alpha_{12/13}$ [22,25,26]. Moreover, 5 $G\beta$ - and 12 $G\gamma$ subunits are known [25]. When coupled to $G\alpha_s$ or $G\alpha_{i/o}$ proteins, GPCRs either activate or inhibit adenylyl cyclase (AC) activity, followed by an increase or decrease in intracellular cyclic AMP (cAMP) levels [27-30]. The second messenger cAMP can, for example, activate cAMP-dependent protein kinase A (PKA), the Rap guanine exchange factor Epac (exchange protein activated by cAMP) or the transcription factor CREB (cAMP response element binding protein) [26,31-33]. $G\alpha_{i/o}$ proteins are also involved in AC-independent responses, e. g. the blockade of calcium channels, in the stimulation of G-protein inwardly rectifying potassium channels (GIRK) and in the stimulation of phosphodiesterases [3,31]. Furthermore, not only $G\alpha_{i/o}$ - and $G\alpha_s$ -proteins can influence ACs, but also $G\beta\gamma$ subunits via calcium-calmodulin [25]. Interaction with $G\alpha_{q/11}$ triggers the stimulation of phospholipase C (PLC) which results in the formation of inositol trisphosphate (IP_3) and diacylglycerol (DAG). For the α_1 -adrenergic receptors coupling to both the $G\alpha_q$ and the $G\alpha_{11}$ subunit was described [34,35]. The stimulation of IP_3 -sensitive receptors, located in the membrane of the endoplasmatic reticulum, results in a release of calcium ions into the cytosol. Diacylglycerol can activate the protein kinase C (PKC) [26,31,36]. G12 was the last identified $G\alpha$ protein subfamily and consists of two members, $G\alpha_{12}$ and the $G\alpha_{13}$ protein [37]. About 25 different GPCRs have been associated to the activation of the G12 subfamily [38]. GPCRs coupling to $G\alpha_{12/13}$ are activating small GTPases like RhoA [21]. Moreover, $G\alpha_{12/13}$ have received attention in the context of cell proliferation and morphological changes [39]. The $G\beta\gamma$ subunits interact with effectors like mitogen-activated protein kinases (MAPKs), phosphatidylinositol-3-kinase (PI3K) and small GTP-binding proteins [40]. Dissociated $G\beta\gamma$ subunits are also involved in GPCR desensitization and downregulation [41]. Receptor desensitization after agonist activation terminates the signaling process and constitutes a significant step in the regulation of GPCR mediated effects [42]. Traditionally, GPCRs are characterized by their preferential coupling to distinct G-proteins. However, an increasing number of GPCRs has been identified as promiscuous receptors capable of coupling to various G-proteins [43,44]. It is worth to mention, that the signaling depends on the cellular background [45,46].

1.3 G-protein independent GPCR signaling

G-protein coupled receptors do not only use canonical (G-protein mediated) but also non-canonical (G-protein independent) signaling pathways, for example via β -arrestins [47-50], to transduce ligand binding into a cellular response. Historically, arrestins were discovered because of their ability to terminate G-protein mediated signaling by interacting with phosphorylated ligand-activated GPCRs [51] and subsequent receptor internalization [52,53]. This process involves G-protein coupled receptor kinases (GRKs). After internalization, the GPCRs are either degraded or recycled by re-integration into the membrane [54]. Arrestins are able to regulate the signaling of the vast majority of GPCRs [55]. In addition to their role in receptor desensitization and trafficking these proteins are capable to trigger various signaling pathways [56], which are different from classical G-protein mediated effectuation [51]. The arrestin family consists of four isoforms (arrestin 1-4) sharing a high sequence homology. Arrestin 1 and arrestin 4 are exclusively expressed in the visual system, whereas arrestin 2 (β -arrestin 1) and arrestin 3 (β -arrestin 2) are expressed ubiquitously [57]. Depending on their affinity to β -arrestin 1 or 2, the receptors are divided into Class A or Class B receptors. Class A receptors bind with a higher affinity to β -arrestin 2 [54]. Among the most intensively investigated signaling molecules involved in β -arrestin pathways are mitogen active protein kinase (MAPK) and the Src-family tyrosine kinases [56,58-60].

1.4 Traditional GPCR assays

A variety of detection techniques have been established to investigate GPCR-ligand interactions, receptor activation and receptor triggered signaling pathways. Traditional GPCR assays can be grouped into two categories, namely in ligand-binding assays and functional assays. Since the early 1970s, GPCR research advanced with the development of radioligand-binding techniques [61,62]. Basically, three kinds of ligand-binding experiments can be carried out [63]. There are kinetic experiments, where the association (k_{on}) and dissociation (k_{off}) constants of a compound of interest are determined. Saturation experiments are used, to determine the dissociation-constant (K_d) of the radioligand and the quantity of specific binding sites for the compound. Finally, competition experiments are used to determine the binding constants (K_i) of non-labeled ligands by displacement of a radioligand. Radioligand-binding assays do not provide information on the quality of action, i. e., whether the compound is an agonist, inverse agonist or an antagonist [4].

Functional assays using laboratory animals and preparations of isolated were already performed in the nineteenth century, and played a central role in drug research prior to the development of reductionistic cellular and molecular approaches. Nowadays GPCR ligands are usually studied on the human receptor of interest expressed in various host cells containing the required signaling machinery, enabling the detection and quantification of a distinct readout to characterize agonists, antagonists or inverse agonists.

Classical functional assays for GPCRs are measuring $G\alpha_s$ or $q/11$ or i/o subtype dependent changes of intracellular concentrations of second messengers (e.g. Ca^{2+} , cAMP, IP_3) or alterations in the expression of reporter genes (**Fig. 1.1**). These assays are often performed as endpoint assays requiring cell lysis. Furthermore, GPCR activation resulting in G-protein-independent signaling can be determined by measuring the arrestin recruitment, e. g. by luciferase complementation assays.

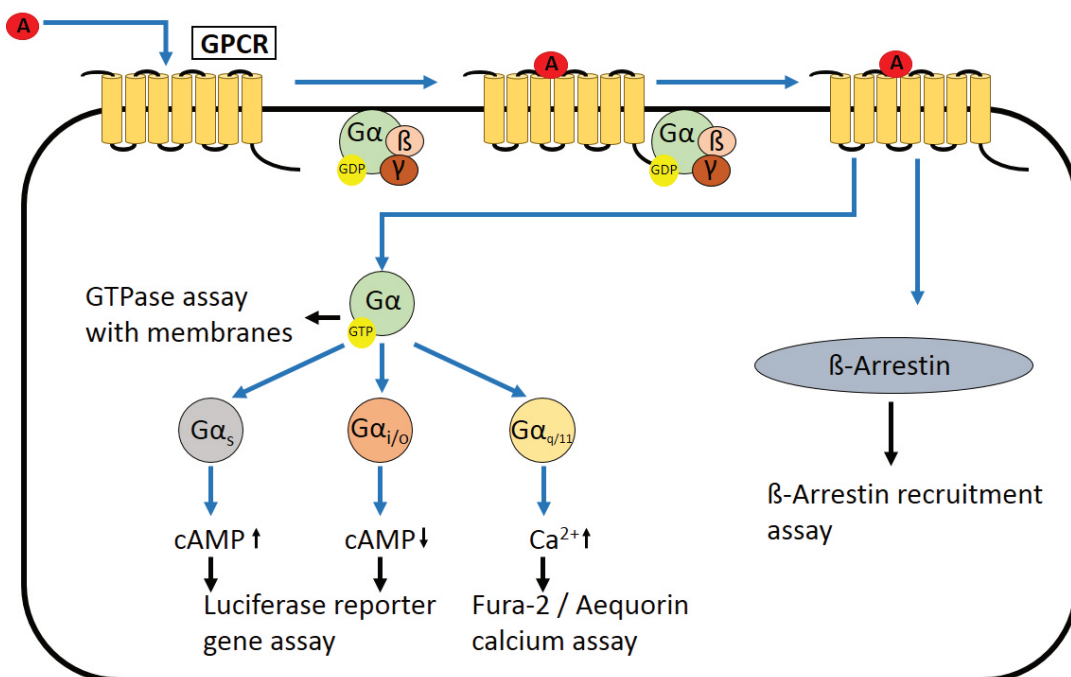


Fig. 1.1: Examples of cellular signaling pathways activated by GPCRs and exploited for quantification in traditional functional assays.

Examples of proximal assays measuring GPCR activation are the $[^{35}S]GTP\gamma S$ binding and the steady-state $[^{32}P]GTPase$ assay, which are performed with membrane preparations of cells, for example Sf9 insect cells, expressing the receptor of interest [64,65].

Methods for the determination of transient changes in the cytosolic calcium concentration ($[Ca^{2+}]_i$), e. g. due to calcium release from intracellular stores such as the endoplasmatic

reticulum (ER), are popular because of the availability of calcium-sensitive fluorescent dyes [66,67]. Calcium sensitive fluorescent dyes, such as Fura-2, Fluo-3 or Fluo-4, can be used to monitor intracellular Ca^{2+} in real time to obtain data from agonist, antagonist and allosteric modulators, but not inverse agonists [66,68]. Instead of fluorescent calcium indicators the calcium-dependent luminescence emitted by the recombinantly expressed jellyfish photoprotein aequorin can be exploited to measure changes in intracellular Ca^{2+} concentrations [69,70]. This method requires genetical engineering of the cells and incubation with a luciferin substrate [66,71]. The GPCR-mediated calcium signal is predominantly depending on $\text{G}\alpha_{q/11}$ coupling [72]. However, calcium assays can also be performed in case that the cells expressing the receptor of interest are either equipped with promiscuous G proteins ($\text{G}\alpha_{15}$ or $\text{G}\alpha_{16}$) or genetically modified to re-direct $\text{G}\alpha_s$ and $\text{G}\alpha_i$ signaling to calcium release using chimeric G-proteins [43,73-75]. The latter has been achieved by replacing the last five to nine C-terminal amino acids of $\text{G}\alpha_s$ or $\text{G}\alpha_i$ with those of $\text{G}\alpha_{q/11}$ [76-79].

To quantify GPCR activity in a reporter gene assay the GPCR dependent gene expression results in the biosynthesis of a conveniently detectable protein or enzymatic activity of the latter (e. g. luciferase) [66,80]. Luciferases can be grouped according to source, cofactor dependence, brightness, emission wavelength, etc. [81]. The most frequently used luciferase is the firefly luciferase, which was isolated from *Photinus pyralis* [82]. The enzyme uses d-luciferin as a substrate, which is adenosylated, oxydized and, upon AMP release, converted to a dioxetanone, falls apart into CO_2 and oxyluciferin under emission of light at a maximum wavelength of about 560 nm [82,83]. In principle, gene reporter assays are broadly applicable to GPCRs and allow the detection of weak agonists (due to signal amplification) and allosteric modulators [4,80].

In addition, G-protein dependent effects the quantification of β -arrestin recruitment is required to identify functionally selective GPCR ligands. Misawa *et al.* [84] developed a split click beetle luciferase complementation assay which is ideal for this purpose. Two inactive fragments of luciferase are attached to the receptor and arrestin, respectively. Upon GPCR activation and arrestin recruitment, the fragments come into close proximity and reconstitute enzymatically active luciferase [85,86], which provides a robust signals at a low background.

The current knowledge of GPCR pharmacology has been essentially gained from results obtained from conventional second messenger based functional assays, making these

technologies indispensable. However, neither method is universal and ideal. Only in rare cases, such assays can be performed with native cells reflecting the physiological situation. Assay-specific manipulation range from the addition of indicators to complex genetic alterations of the cells regarding expression of receptors, effector proteins and gene reporters [4]. Moreover, such reductionist approaches, focusing on specific signaling pathways, are inappropriate to uncover complex signaling networks which contribute to an overall physiological cellular response [8], and attempts to identify orphan receptors or their ligands will most probably fail. Label-free assay technologies could overcome some of these problems by detecting holistic cellular responses. The most commonly used label-free assays rely on impedance-based or optical readouts [87-91]. Label-free assays have been successfully applied to characterize not only GPCRs but also various other biological targets such as kinases, ion channels and immunoreceptors [92-98].

1.5 Label-free assay platforms

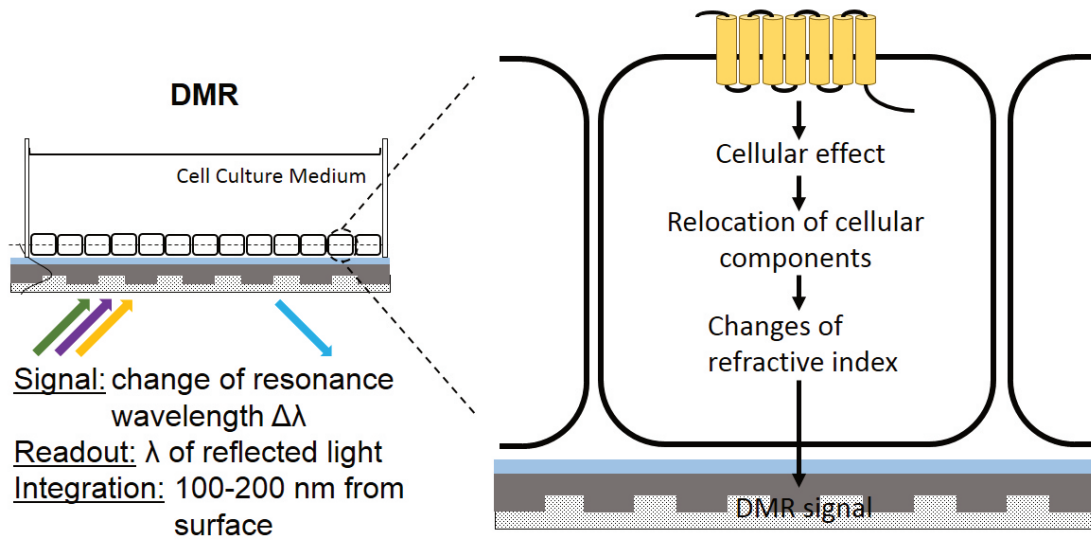
Label-free assays usually employ a biosensor to record ligand-induced cellular effects in a non-invasive manner [99,100]. Living cells, expressing the GPCR of interest are allowed to attach to the surface of an appropriate support (e. g. electrode or optical waveguide). A confluent cell monolayer is ideal to obtain a stable baseline and to improve the reproducibility of the readout [101]. Upon addition of a GPCR ligand, on, minute changes in cellular morphology are detected by the sensor [102]. In principle, such a sensor converts a plethora of cellular effects (e. g., minor alterations in cell shape, cell adhesion, cell proliferation, cell migration, cell death) into a quantifiable signal [102-111]. Up to now, the processes reflected in the signal are not fully understood, although. It is assumed that minor cytoskeletal re-arrangements or alterations of cell-cell interactions play a major role [90]. Therefore, the signal from a label-free assay is commonly referred to as a “black box” readout [90], and it remains challenging to deconvolute the response and to trace the complex signal back to the contributing pathways.

It is characteristic of label-free technologies that, in contrast to traditional assays, knowledge of the involved signaling pathways is unnecessary, real time measurements are performed without addition of molecular probes and genetic modifications to enable a distinct readout [91]. Label-free techniques are in principle applicable to any GPCR including orphans, provided that the receptor is expressed in an appropriate cell type [112]. As label-free assays are

quantifying effects rather than resolving individual pathways contributing to an overall response, these approach increase the chance to identify biologically active compounds which would escape traditional label-dependent assays [54].

Biosensors can be grouped into distinct groups, according to the method of signal transduction. Among others, calorimetric, acoustic or magnetic biosensors are described in literature [100,113]. Optical biosensors, detecting and quantifying the index of refraction in the cell in close proximity to the optical sensor [114,115], and impedance-based biosensors [91,116], using electrodes as support for the cells, were employed in this doctoral project and are, therefore, explained in more detail in the following and illustrated in Chapter 3, **Fig. 3.1**. A schematic representation of the used label-free methods is shown below (**Fig. 1.2**).

A



B

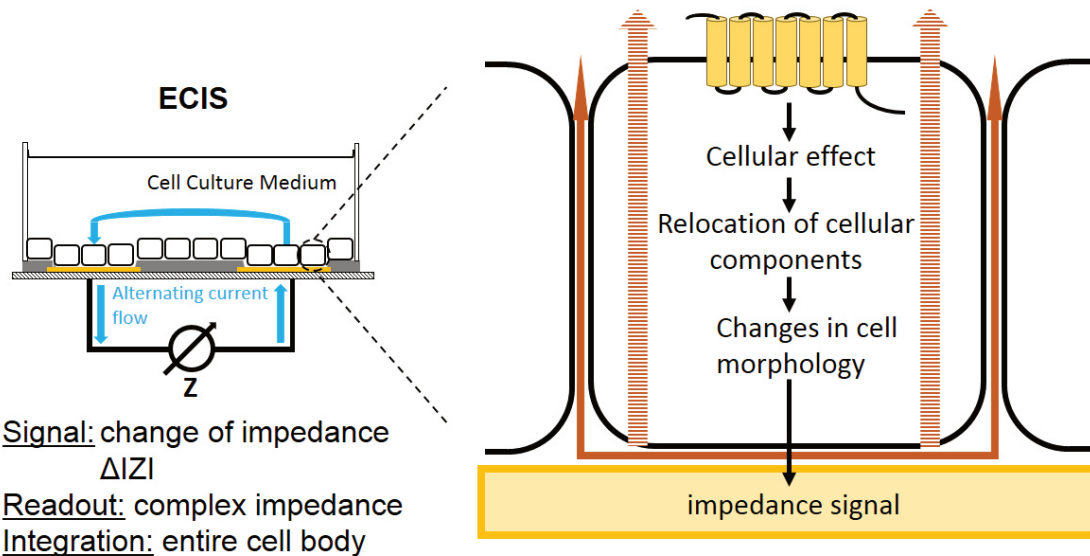


Fig. 1.2: Schematic representation of the label-free techniques DMR and ECIS. (A) Surfaces on the bottom of well, containing resonant waveguide grating (RWG), reflecting monochromatic light of a specific wavelength λ when illuminated with polychromatic light. Mass redistribution within 200 nm from the surface is recorded. (B) Electric cell-substrate impedance sensing (ECIS) records the electrical impedance of a confluent cell-layer. The impedance signal depends on the shape of the cells on the electrode.

1.5.1 Dynamic mass redistribution (DMR)

Ligand-triggered cellular dynamic mass redistribution (DMR) can be recorded by an optical sensor such as a resonant waveguide grating (RWG). RWG came up in the 1990s and was originally used to investigate binding of compounds to immobilized receptors [117]. Explained in a simplified form, the biosensor consists of a substrate layer, a waveguide film wherein an optical grating structure is embedded, a medium and a cell layer [87]. When illuminated from the microplate bottom side with broadband light centred at 830 nm in a specific angle, the light is moving in parallel through the bottom of each well of the microtiter plate [118]. Resulting from the interaction of light with the grating, an evanescent electromagnetic field is generated, which decays exponentially from the sensor surface [102]. The electromagnetic field interacts with cells in the sensor vicinity and depending on the local refractive index, changes of the reflected wavelength can be measured. The readout is recorded as the shift in resonant wavelength in picometer (pm) as a function of time [103]. The GPCR-induced cellular response leads to alterations in the refractive index close to the sensor surface [87,99]. Mass redistributions perpendicular to the sensor are detectable: the signal increases, when mass movement is directed to the surface of the sensor, whereas mass movement in the opposite direction decrease the signal; mass redistribution parallel to the sensor are not detectable [102]. The limiting factor of the DMR method is the penetration depth of the evanescent field, which lies between 150 – 200 nm. Just DMR events within this penetration depth can be recorded. It is worth to mention that the used long-wavelength light is strong enough to illuminate the biosensor but not the cell. Thus, the optical RWG method can be considered as a non-invasive analysing technique [8,89,91,99,103,119].

1.5.2 Surface plasmon resonance (SPR)

Another optical biosensor, transducing ligand-triggered DMR into a quantifiable signal is the surface plasmon resonance (SPR) technology. SPR was first described by Otto in the late 1960s and was made commercially available for biomolecular investigations in 1990 [120,121]. Like RWG, SPR has proven to be applicable for versatile investigations like receptor-drug, enzyme-substrate or lipid membrane-protein interactions, among others [122-124]. In general, SPR spectroscopy can be applied for monitoring changes of the refractive index of cells, cultivated on a metal (usually gold) sensor [125]. Surface plasmon resonance takes place, when a monochromatic parallel-polarized (p-polarized) light beam hits the layer of gold under

conditions of total internal reflection [126]. P-polarized light is defined as light with an electric field direction parallel to the plane of incidence on the metal layer. It is worth to mention, that s-polarized light (perpendicular to the surface) does not cause plasmon resonance and increases just the background intensity of reflected light [127]. Several instrumental configurations exist which are used to excite surface plasmons. These configurations are using prisms, gratings or optical waveguides [127]. At a specific angle of incidence, electrons of the gold surface are excited to move parallel to the surface (plasmons). The plasmons generate an electric field which decays exponentially on both sides of the gold film [128]. DMR within a distance of about 300 nm from the sensor surface can be recorded [126]. The interaction of incident light with electrons of the golden surface layer is resulting in a dip of the recorded intensity level of the reflected light. The angle at which the maximal reduction of the reflected light intensity occurs is named resonance angle. The resonance angle depends on optical characteristics of the system, like the refractive indices of the media at both sides of the gold layer. Because the refractive index at the side of the prism is not changing, the refractive index in the direct vicinity of the gold surface alters, if dynamic mass redistribution is directed to the sensor [127].

1.5.3 Electric cell-substrate impedance sensing (ECIS)

The applicability of electric biosensors to detect morphological changes in live cells upon biological, chemical or physical stimuli was first described in the early 1980s [104]. ECIS exploits confluent monolayers of cells on gold electrodes [106], for example, embedded in wells of microtiter plates, to quantify alterations in the impedance. The cell-covered electrodes and reference electrodes are electrically connected by cell culture medium on top of the cell layer. Subsequently, small sinusoidal alternating current (AC) voltages at varying frequencies are applied to these electrodes and impedance alterations are measured [129]. The cells behave as insulators because of the capacitive, non-conducting properties of the cell membrane [129]. Due to this characteristic, the current is forced to flow around the cellular bodies along narrow gaps under and between adjacent cells at lower frequencies (< 10 kHz). At higher frequencies (> 30 kHz), the current can couple capacitively through the cell membrane [129]. The technique is quantifying changes in complex impedance (Z) as readout, calculated by the ratio of the voltage (is measured by ECIS) to current (is applied by ECIS), as defined by Ohm's law ($Z = U(t)/I(t)$) [130]. In turn, the complex impedance can be dissected into three parameters R_b , α and C_m [131,132]. In the ECIS model, cells are represented as disk

shaped objects with insulating membranes, filled with conducting electrolyte solution, which are levitating above the electrodes. R_b quantifies the impedance contribution generated by adjacent cells. The parameter α describes the impedance due to the restricted current flow between cells and electrode. The radius of the cells and the cell-electrode distance are the main factors contributing to α . Lastly, C_m describes the average capacitance of the cell plasma membrane. It is worth to mention, that it is not possible to distinguish between the apical and basal membrane [131,132].

ECIS is a versatile technique to investigate the cell in a frequency-dependent manner, reflecting minute morphological changes, and to distinguish between impedance contributions from cell-electrode contact, cell-cell contact and membrane properties. It was demonstrated ECIS can be applied to various biological targets including, e.g., GPCRs, tyrosine kinase and nuclear receptors [130].

1.5.4 ECIS-SPR assay combination

In the last years several approaches were performed, to combine SPR with other analytical methods to increase the information depth [133-135]. The combination of the two most widespread label-free techniques is therefore a logical step to record cellular response from one and the same cell population [133]. Both techniques are based on different physical principles (as shown before) generating complementary readout. Whereas the impedimetric assay is providing data integrated over the whole cell body, the optical measurement technique detects alterations up to 300 nm perpendicular to the sensor surface. The combination of the impedimetric and optic label-free techniques may increase the information obtained from the same cell population [133].

1.5.5 Information on G-protein coupling gained from DMR and ECIS

Although being considered holistic approaches, the shape of the DMR and ECIS traces can be roughly associated with ligand-GPCR interactions resulting in distinct G-protein subtype activation [136-138]. Typical signatures of $G\alpha_{q/11}$, $G\alpha_s$ and $G\alpha_{i/o}$ mediated cellular responses monitored by DMR and ECIS are shown in **Fig. 1.3**

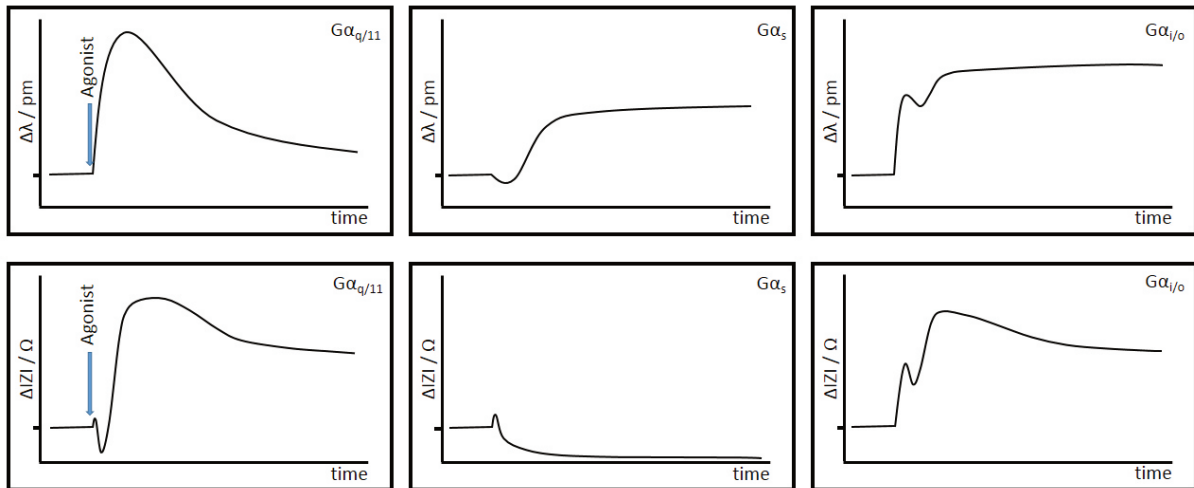


Fig. 1.3: Characteristic DMR (first row) and ECIS (second row) traces as signatures of $G\alpha_{q/11}$, $G\alpha_s$ and $G\alpha_{i/o}$ coupling of GPCRs.

Nevertheless, it should be emphasized that the overall response monitored by label-free methods can depend on the cell-type, the GPCR, specific or promiscuous G-protein coupling, the pharmacological properties of the ligand, the extent of activation/inhibition of different pathways including G-protein independent signaling, and possibly many other factors. Therefore, these aspects have to be considered when investigating a particular GPCR in a specific cellular background by label-free techniques. By analogy with classical experimental pharmacology, e. g. on isolated organs, detailed investigations with molecular tools such as pathway inhibitors and selective ligands (agonists, antagonists) are mandatory to identify the contributing signaling mechanisms in holistic label-free cellular assays.

1.6 References

- 1 Bockaert J, Pin JP. Molecular tinkering of G protein-coupled receptors: an evolutionary success. *EMBO J* 1999;18:1723-1729.
- 2 Overington JP, Al-Lazikani B, Hopkins AL. How many drug targets are there? *Nat Rev Drug Discov* 2006;5:993-996.
- 3 Pierce KL, Premont RT, Lefkowitz RJ. Seven-transmembrane receptors. *Nat Rev Mol Cell Biol* 2002;3:639-650.
- 4 Lundstrom K. Present and future approaches to screening of G-protein-coupled receptors. *Future Med Chem* 2013;5:523-538.
- 5 Fredriksson R, Schiöth HB. The repertoire of G-Protein-coupled receptors in fully sequenced genomes. *Mol Pharmacol* 2005;67:1414-1425.
- 6 Lagerstrom MC, Schiöth HB. Structural diversity of G protein-coupled receptors and significance for drug discovery. *Nat Rev Drug Discov* 2008;7:339-357.
- 7 Schlyer S, Horuk R. I want a new drug: G-protein-coupled receptors in drug development. *Drug Discovery Today* 2006;11:481-493.
- 8 Zhang R, Xie X. Tools for GPCR drug discovery. *Acta Pharmacol Sin* 2012;33:372-384.
- 9 Oldham WM, Hamm HE. Heterotrimeric G-protein activation by G-protein coupled receptors. *Nat Rev Mol Cell Biol* 2008;9:60-71.
- 10 Hill SJ. G-protein-coupled receptors: past, present and future. *Br J Pharmacol* 2006;147:S27-S37.
- 11 Heng BC, Aubel D, Fussenegger M. An overview of the diverse roles of G-protein coupled receptors (GPCRs) in the pathophysiology of various human diseases. *Biotechnol Adv* 2013;31:1676-1694.
- 12 Thompson MD, Burnham WM, Cole DEC. The G protein-coupled receptors: Pharmacogenetics and Disease. *Crit Rev Clin Lab Sci* 2005;42:311-389.
- 13 Luttrell LM, Lefkowitz RJ. The role of β -arrestins in the termination and transduction of G-protein-coupled receptor signals. *J Cell Sci* 2002;115:455-465.
- 14 Rozenfeld R, Devi LA. Exploring a role for heteromerization in GPCR signaling specificity. *Biochem J* 2010;433:11-18.
- 15 Fredriksson R, Lagerström MC, Lundin L-G, Schiöth HB. The G-protein-coupled receptors in the human genome form five main families. Phylogenetic analysis, paralogon groups, and fingerprints. *Mol Pharmacol* 2003;63:1256-1272.
- 16 Lappano R, Maggiolini M. G-protein coupled receptors: Novel targets for drug discovery in cancer. *Nat Rev Drug Discov* 2011;10:47-60.
- 17 Alan Wise, Steven C. Jupe, Rees S. The identification of ligands at orphan G-Protein coupled receptors. *Annu Rev Pharmacol Toxicol* 2004;44:43-66.
- 18 Sprang SR. Activation of G proteins by GTP and the mechanism of $G\alpha$ -catalyzed GTP hydrolysis. *Biopolymers* 2016;105:14.
- 19 Gilchrist A. A perspective on more effective GPCR-targeted drug discovery efforts. *Expert Opin Drug Discovery* 2008;3:375-389.
- 20 Gilman AG. G-Proteins: Transducers of receptor-generated signals. *Annu Rev Biochem* 1987;56:615-649.
- 21 Cabrera-Vera TM, Vanhauwe J, Thomas TO, Medkova M, Preininger A, Mazzoni MR, Hamm HE. Insights into G Protein Structure, Function, and Regulation. *Endocr Rev* 2003;24:765-781.
- 22 Hamm HE. The many faces of G-Protein signaling. *J Biol Chem* 1998;273:669-672.

- 23 Hendriks-Balk MC, Peters SLM, Michel MC, Alewijse AE. Regulation of G protein-coupled receptor signalling: Focus on the cardiovascular system and regulator of G protein signalling proteins. *Eur J Pharmacol* 2008;585:278-291.
- 24 Sprang SR. G-Protein mechanisms: Insights from structural analysis. *Annu Rev Biochem* 1997;66:639-678.
- 25 Luttrell LM. Reviews in molecular biology and biotechnology: Transmembrane signaling by G Protein-coupled receptors. *Mol Biotechnol* 2008;39:239-264.
- 26 Milligan G, Kostenis E. Heterotrimeric G-proteins: a short history. *Br J Pharmacol* 2006;147:S46-S55.
- 27 Bokoch GM, Katada T, Northup JK, Ui M, Gilman AG. Purification and properties of the inhibitory guanine nucleotide-binding regulatory component of adenylate cyclase. *J Biol Chem* 1984;259:3560-3567.
- 28 E M Ross a, Gilman AG. Biochemical properties of hormone-sensitive adenylate cyclase. *Annu Rev Biochem* 1980;49:533-564.
- 29 Northup JK, Sternweis PC, Smigel MD, Schleifer LS, Ross EM, Gilman AG. Purification of the regulatory component of adenylate cyclase. *Proc Natl Acad Sci U S A* 1980;77:6516-6520.
- 30 Sternweis PC, Northup JK, Smigel MD, Gilman AG. The regulatory component of adenylate cyclase. Purification and properties. *J Biol Chem* 1981;256:11517-11526.
- 31 Andrew W, Evgeni GP. G Protein - Mediated signaling: Same receptor, multiple effectors. *Curr Mol Pharmacol* 2009;2:237-248.
- 32 Gloerich M, Bos JL. Epac: Defining a new mechanism for cAMP action. *Annu Rev Pharmacol Toxicol* 2010;50:355-375.
- 33 Schmidt M, Sand C, Jakobs KH, Michel MC, Weernink PAO. Epac and the cardiovascular system. *Curr Opin Pharmacol* 2007;7:193-200.
- 34 Wu D, Katz A, Lee CH, Simon MI. Activation of phospholipase C by alpha 1-adrenergic receptors is mediated by the alpha subunits of Gq family. *J Biol Chem* 1992;267:25798-25802.
- 35 Macrez-Leprêtre N, Kalkbrenner F, Schultz G, Mironneau J. Distinct functions of Gq and G11 proteins in coupling α 1-adrenoreceptors to Ca²⁺ release and Ca²⁺ entry in rat portal vein myocytes. *J Biol Chem* 1997;272:5261-5268.
- 36 Kamato D, Thach L, Bernard R, Chan V, Zheng W, Kaur H, Brimble M, Osman N, Little PJ. Structure, function, pharmacology, and therapeutic potential of the G-Protein, G α (q/11). *Front Cardiovasc Med* 2015;2:14.
- 37 Kelly P, Casey PJ, Meigs TE. Biologic functions of the G12 subfamily of heterotrimeric G-Proteins: Growth, migration, and metastasis. *Biochemistry* 2007;46:6677-6687.
- 38 Riobo NA, Manning DR. Receptors coupled to heterotrimeric G proteins of the G12 family. *Trends Pharmacol Sci* 2005;26:146-154.
- 39 Radhika V., Dhanasekaran N. Transforming G proteins. *Oncogene* 2001;20:1607-1614.
- 40 Schwindinger WF, Robishaw JD. Heterotrimeric G-protein betagamma-dimers in growth and differentiation. *Oncogene* 2001;20:1653-1660.
- 41 Desai AN, Salim S, Standifer KM, Eikenburg DC. Involvement of G Protein-coupled receptor kinase (GRK) 3 and GRK2 in down-regulation of the α 2B-adrenoceptor. *J Pharmacol Exp Ther* 2006;317:1027-1035.
- 42 Drake MT, Shenoy SK, Lefkowitz RJ. Trafficking of G-Protein coupled receptors. *Circ Res* 2006;99:570-582.
- 43 Kostenis E, Waelbroeck M, Milligan G. Techniques: Promiscuous Galpha; proteins in basic research and drug discovery. *Trends Pharmacol Sci*;26:595-602.

- 44 Hermans E. Biochemical and pharmacological control of the multiplicity of coupling at G-protein-coupled receptors. *Pharmacol Ther* 2003;99:25-44.
- 45 Schmidt CJ, Thomas TC, Levine MA, Neer EJ. Specificity of G protein beta and gamma subunit interactions. *J Biol Chem* 1992;267:13807-13810.
- 46 Grundmann M, Kostenis E. Label-Free Biosensor Assays in GPCR Screening. In: Prazeres FDM, Martins MSA, eds. *G Protein-Coupled Receptor Screening Assays: Methods and Protocols*. New York, NY: Springer New York, 2015: pp 199-213.
- 47 Abbas A, Roth BL. Arresting serotonin. *Proc Natl Acad Sci U S A* 2008;105:831-832.
- 48 Dorn GW. GRK mythology: G-protein receptor kinases in cardiovascular disease. *J Mol Med* 2009;87:455-463.
- 49 Lefkowitz RJ. Seven transmembrane receptors: something old, something new. *Acta Physiol* 2007;190:9-19.
- 50 Lefkowitz RJ, Shenoy SK. Transduction of receptor signals by β -arrestins. *Science* 2005;308:512-517.
- 51 Park JY, Lee SY, Kim HR, Seo M-D, Chung KY. Structural mechanism of GPCR-arrestin interaction: recent breakthroughs. *Arch Pharm Res* 2016;39:293-301.
- 52 Ferguson SSG, Downey WE, Colapietro A-M, Barak LS, Ménard L, Caron MG. Role of β -Arrestin in Mediating Agonist-Promoted G Protein-Coupled Receptor Internalization. *Science* 1996;271:363-366.
- 53 Goodman OB, Krupnick JG, Santini F, Gurevich VV, Penn RB, Gagnon AW, Keen JH, Benovic JL. β -Arrestin acts as a clathrin adaptor in endocytosis of the β 2-adrenergic receptor. *Nature* 1996;383:447-450.
- 54 Prazeres DMF, Martins SAM. G protein-Coupled Receptors: An Overview of Signaling Mechanisms and Screening Assays. In: Prazeres FDM, Martins MSA, eds. *G Protein-Coupled Receptor Screening Assays: Methods and Protocols*. New York, NY: Springer New York, 2015: pp 3-19.
- 55 Lefkowitz RJ, Whalen EJ. β -arrestins: traffic cops of cell signaling. *Curr Opin Cell Biol* 2004;16:162-168.
- 56 Luttrell LM, Ferguson SSG, Daaka Y, Miller WE, Maudsley S, Della Rocca GJ, Lin F-T, Kawakatsu H, Owada K, Luttrell DK, Caron MG, Lefkowitz RJ. β -Arrestin-Dependent Formation of β 2 Adrenergic Receptor-Src Protein Kinase Complexes. *Science* 1999;283:655-661.
- 57 Lohse MJ, Hoffmann C. Arrestin interactions with G protein-coupled receptors. *Handb Exp Pharmacol* 2014;219:15-56.
- 58 DeFea KA. Beta-arrestins as regulators of signal termination and transduction: How do they determine what to scaffold? *Cell Signal* 2011;23:621-629.
- 59 Luttrell LM. Chapter Eighteen - Arrestin Pathways as Drug Targets. In: Louis ML, ed. *Progress in Molecular Biology and Translational Science: Academic Press*, 2013: pp 469-497.
- 60 Shenoy SK, Lefkowitz RJ. β -arrestin-mediated receptor trafficking and signal transduction. *Trends Pharmacol Sci* 2011;32:521-533.
- 61 Lefkowitz RJ, Roth J, Pastan I. Radioreceptor assay of adrenocorticotrophic hormone: New approach to assay of polypeptide hormones in plasma. *Science* 1970;170:633-635.
- 62 Bylund DB, Toews ML. Radioligand binding methods: practical guide and tips. *Am J Physiol* 1993;265:L421-429.
- 63 Hulme EC, Trevethick MA. Ligand binding assays at equilibrium: validation and interpretation. *Br J Pharmacol* 2010;161:1219-1237.

- 64 Clark MJ, Traynor JR. Assays for G-Protein coupled receptor signaling using RGS-insensitive G α subunits. *Methods Enzymol*: Academic Press, 2004: pp 155-169.
- 65 Schneider EH, Seifert R. Sf9 cells: A versatile model system to investigate the pharmacological properties of G protein-coupled receptors. *Pharmacol Ther* 2010;128:387-418.
- 66 Thomsen W, Frazer J, Unett D. Functional assays for screening GPCR targets. *Curr Opin Biotechnol* 2005;16:655-665.
- 67 Bootman MD, Rietdorf K, Collins T, Walker S, Sanderson M. Ca²⁺-sensitive fluorescent dyes and intracellular Ca²⁺ imaging. *Cold Spring Harbor Protocols* 2013;2013:pdb.top066050.
- 68 Takahashi A, Camacho P, Lechleiter JD, Herman B. Measurement of Intracellular Calcium. *Physiol Rev* 1999;79:1089-1125.
- 69 Paredes RM, Etzler JC, Watts LT, Lechleiter JD. Chemical calcium indicators. *Methods* 2008;46:143-151.
- 70 Eglén RM, Reisine T. Photoproteins: Important new tools in drug discovery. *Assay Drug Dev Technol* 2008;6:659-672.
- 71 Chen L, Jin L, Zhou N. An update of novel screening methods for GPCR in drug discovery. *Expert Opin Drug Discovery* 2012;7:791-806.
- 72 Emkey R, Rankl NB. Screening G Protein-coupled receptors: Measurement of intracellular calcium using the fluorometric imaging plate reader. In: Janzen PW, Bernasconi P, eds. *High Throughput Screening: Methods and Protocols*, Second Edition. Totowa, NJ: Humana Press, 2009: pp 145-158.
- 73 Liu AMF, Ho MKC, Wong CSS, Chan JHP, Pau AHM, Wong YH. G α 16/z chimeras efficiently link a wide range of G-Protein coupled receptors to calcium mobilization. *J Biomol Screening* 2003;8:39-49.
- 74 New DC, Wong YH. Characterization of CHO cells stably expressing a G α 16/z chimera for high throughput screening of GPCRs. *Assay Drug Dev Technol* 2004;2:269-280.
- 75 Zhu T, Fang L-y, Xie X. Development of a universal high-throughput calcium assay for G-protein-coupled receptors with promiscuous G-protein G α 15/16. *Acta Pharmacol Sin* 2008;29:507-516.
- 76 Conklin BR, Farfel Z, Lustig KD, Julius D, Bourne HR. Substitution of three amino acids switches receptor specificity of G α_q to that of G α_i . *Nature* 1993;363:274-276.
- 77 Coward P, Chan SDH, Wada HG, Humphries GM, Conklin BR. Chimeric G-Proteins allow a high-throughput signaling assay of Gi-coupled receptors. *Anal Biochem* 1999;270:242-248.
- 78 Kostenis E. Potentiation of GPCR-signaling via membrane targeting of G protein α subunits. *J Recept Signal Transduct Res* 2002;22:267-281.
- 79 Milligan G, Rees S. Chimeric G alpha proteins: their potential use in drug discovery. *Trends Pharmacol Sci* 1999;20:7.
- 80 Cheng Z, Garvin D, Paguio A, Stecha P, Wood K, Fan F. Luciferase reporter assay system for deciphering GPCR pathways. *Curr Chem Genomics* 2010;4:84-91.
- 81 Wilson T, Hastings JW. Bioluminescence. 1998: 197-230.
- 82 Loren JM, Frederick JK, Robert D. Seeing the light: Luminescent reporter gene assays. *Comb Chem High Throughput Screening* 2011;14:648-657.
- 83 Zomer G. Chapter 2 The Nature of Chemiluminescent Reactions. *Chemiluminescence and Bioluminescence: Past, Present and Future: The Royal Society of Chemistry*, 2011: pp 51-90.

- 84 Misawa N, Kafi AK, Hattori M, Miura K, Masuda K, Ozawa T. Rapid and high-sensitivity cell-based assays of protein-protein interactions using split click beetle luciferase complementation: an approach to the study of G-protein-coupled receptors. *Anal Chem* 2010;82:2552-2560.
- 85 Azad T, Tashakor A, Hosseinkhani S. Split-luciferase complementary assay: applications, recent developments, and future perspectives. *Anal Bioanal Chem* 2014;406:5541-5560.
- 86 Vidi P-A, Ejendal KFK, Przybyla JA, Watts VJ. Fluorescent protein complementation assays: new tools to study G protein-coupled receptor oligomerization and GPCR-mediated signaling. *Mol Cell Endocrinol* 2011;331:185-193.
- 87 Fang Y, Ferrie AM, Fontaine NH, Mauro J, Balakrishnan J. Resonant waveguide grating biosensor for living cell sensing. *Biophys J* 2006;91:1925-1940.
- 88 Kenakin T. A holistic view of GPCR signaling. *Nat Biotechnol* 2010;28:928-929.
- 89 Kenakin TP. Cellular assays as portals to seven-transmembrane receptor-based drug discovery. *Nat Rev Drug Discov* 2009;8:617-626.
- 90 Rocheville M, Jerman JC. 7TM pharmacology measured by label-free: a holistic approach to cell signalling. *Curr Opin Pharmacol* 2009;9:643-649.
- 91 Scott CW, Peters MF. Label-free whole-cell assays: expanding the scope of GPCR screening. *Drug Discovery Today* 2010;15:704-716.
- 92 Abassi YA, Jackson JA, Zhu J, Oconnell J, Wang X, Xu X. Label-free, real-time monitoring of IgE-mediated mast cell activation on microelectronic cell sensor arrays. *J Immunol Methods* 2004;292:195-205.
- 93 Atienza JM, Yu N, Wang X, Xu X, Abassi Y. Label-free and real-time cell-based kinase assay for screening selective and potent receptor tyrosine kinase inhibitors using microelectronic sensor array. *J Biomol Screening* 2006;11:634-643.
- 94 Du Y, Li Z, Li L, Chen Z, Sun S-Y, Chen P, Shin DM, Khuri FR, Fu H. Distinct growth factor-induced dynamic mass redistribution (DMR) profiles for monitoring oncogenic signaling pathways in various cancer cells. *J Recept Signal Transduct Res* 2009;29:182-194.
- 95 Fang Y, Ferrie AM, Fontaine NH, Yuen PK. Characteristics of dynamic mass redistribution of epidermal growth factor receptor signaling in living cells measured with label-free optical biosensors. *Anal Chem* 2005;77:5720-5725.
- 96 Fleming MR, Kaczmarek LK. The use of optical biosensors to detect modulation of Slack potassium channels by G-protein coupled receptors. *J Recept Signal Transduct Res* 2009;29:173-181.
- 97 Pänke O, Weigel W, Schmidt S, Steude A, Robitzki AA. A cell-based impedance assay for monitoring transient receptor potential (TRP) ion channel activity. *Biosens Bioelectron* 2011;26:2376-2382.
- 98 Yanase Y, Hiragun T, Ishii K, Kawaguchi T, Yanase T, Kawai M, Sakamoto K, Hide M. Surface plasmon resonance for cell-based clinical diagnosis. *Sensors* 2014;14:4948-4959.
- 99 Fang Y. Label-Free Receptor Assays. *Drug discovery today Technologies* 2011;7:e5-e11.
- 100 Fang Y, Frutos AG, Verklereen R. Label-free cell-based assays for GPCR screening. *Comb Chem High Throughput Screen* 2008;11:357-369.
- 101 Ferrie AM, Wu Q, Fang Y. Resonant waveguide grating imager for live cell sensing. *Appl Phys Lett* 2010;97:223704.
- 102 Fang Y. Label-free cell-based assays with optical biosensors in drug discovery. *Assay Drug Dev Technol* 2006;4:583-595.
- 103 Fang Y. The development of label-free cellular assays for drug discovery. *Expert Opin Drug Discovery* 2011;6:1285-1298.

- 104 Giaever I, Keese CR. Monitoring fibroblast behavior in tissue culture with an applied electric field. *Proc Natl Acad Sci U S A* 1984;81:3761-3764.
- 105 Giaever I, Keese CR. A morphological biosensor for mammalian cells. *Nature* 1993;366:591-592.
- 106 Opp D, Wafula B, Lim J, Huang E, Lo J-C, Lo C-M. Use of electric cell-substrate impedance sensing to assess in vitro cytotoxicity. *Biosens Bioelectron* 2009;24:2625-2629.
- 107 Ramsden JJ, Horvath R. Optical biosensors for cell adhesion. *J Recept Signal Transduct Res* 2009;29:211-223.
- 108 Spiering D, Schmolke M, Ohnesorge N, Schmidt M, Goebeler M, Wegener J, Wixler V, Ludwig S. MEK5/ERK5 signaling modulates endothelial cell migration and focal contact turnover. *J Biol Chem* 2009;284:24972-24980.
- 109 Wang L, Zhu J, Deng C, Xing W-I, Cheng J. An automatic and quantitative on-chip cell migration assay using self-assembled monolayers combined with real-time cellular impedance sensing. *Lab on a Chip* 2008;8:872-878.
- 110 Wegener J, Keese CR, Giaever I. Electric cell-substrate impedance sensing (ECIS) as a noninvasive means to monitor the kinetics of cell spreading to artificial surfaces. *Exp Cell Res* 2000;259:158-166.
- 111 Xing JZ, Zhu L, Jackson JA, Gabos S, Sun X-J, Wang X-b, Xu X. Dynamic monitoring of cytotoxicity on microelectronic sensors. *Chem Res Toxicol* 2005;18:154-161.
- 112 Peters MF, Vaillancourt F, Heroux M, Valiquette M, Scott CW. Comparing label-free biosensors for pharmacological screening with cell-based functional assays. *Assay Drug Dev Technol* 2010;8:219-227.
- 113 Nirschl M, Reuter F. Review of transducer principles for label-free biomolecular interaction analysis. *Biosensors* 2011;1:23.
- 114 Lieb S, Michaelis S, Plank N, Bernhardt G, Buschauer A, Wegener J. Label-free analysis of GPCR-stimulation: The critical impact of cell adhesion. *Pharmacol Res* 2016;108:65-74.
- 115 Tiefenthaler K, Lukosz W. Sensitivity of grating couplers as integrated-optical chemical sensors. *J Opt Soc Am B: Opt Phys* 1989;6:12.
- 116 Yu N, Atienza JM, Bernard J, Blanc S, Zhu J, Wang X, Xu X, Abassi YA. Real-Time monitoring of morphological changes in living cells by electronic cell sensor arrays: An approach to study G-Protein coupled receptors. *Anal Chem* 2006;78:35-43.
- 117 Wang SS, Moharam MG, Magnusson R, Bagby JS. Guided-mode resonances in planar dielectric-layer diffraction gratings. *J Opt Soc Am A* 1990;7:25.
- 118 Lee PH, Gao A, van Staden C, Ly J, Salon J, Xu A, Fang Y, Verkleeren R. Evaluation of dynamic mass redistribution technology for pharmacological studies of recombinant and endogenously expressed g protein-coupled receptors. *Assay Drug Dev Technol* 2008;6:83-94.
- 119 Steyer JA, Almers W. A real-time view of life within 100 nm of the plasma membrane. *Nat Rev Mol Cell Biol* 2001;2:268-275.
- 120 Otto A. Excitation of nonradiative surface plasma waves in silver by the method of frustrated total reflection. *Z Phys A: Hadrons Nucl* 1968;216:398-410.
- 121 Owen V. Real-time optical immunosensors — A commercial reality. *Biosens Bioelectron* 1997;12:i-ii.
- 122 Erb E-M, Chen X, Allen S, Roberts CJ, Tendler SJB, Davies MC, Forsén S. Characterization of the surfaces generated by liposome binding to the modified dextran matrix of a surface plasmon resonance sensor chip. *Anal Biochem* 2000;280:29-35.

- 123 Madeira A, Vikeved E, Nilsson A, Sjögren B, Andrén PE, Svenningsson P. Identification of protein-protein interactions by surface plasmon resonance followed by mass spectrometry. *Current Protocols in Protein Science*: John Wiley & Sons, Inc., 2001.
- 124 Salamon Z, Cowell S, Varga E, Yamamura HI, Hruby VJ, Tollin G. Plasmon resonance studies of agonist/antagonist binding to the human δ -opioid receptor: New structural insights into receptor-ligand interactions. *Biophys J* 2000;79:2463-2474.
- 125 Robelek R, Wegener J. Label-free and time-resolved measurements of cell volume changes by surface plasmon resonance (SPR) spectroscopy. *Biosens Bioelectron* 2010;25:1221-1224.
- 126 Olaru A, Bala C, Jaffrezic-Renault N, Aboul-Enein HY. Surface plasmon resonance (SPR) biosensors in pharmaceutical analysis. *Crit Rev Anal Chem* 2015;45:97-105.
- 127 R.B.M. S, Tudos AJ. *Handbook of Surface Plasmon Resonance*. RSC Adv 2008
- 128 Markey F. Principles of surface plasmon resonance. In: Nagata K, Handa H, eds. *Real-Time Analysis of Biomolecular Interactions: Applications of BIACORE*. Tokyo: Springer Japan, 2000: pp 13-22.
- 129 Stolwijk J. *Electric Manipulation and Impedance Analysis of Adherent Cells on Gold-Film Electrodes*. Faculty of Chemistry and Pharmacy: Regensburg, 2012.
- 130 Miyano K, Sudo Y, Yokoyama A, Hisaoka-Nakashima K, Morioka N, Takebayashi M, Nakata Y, Higami Y, Uezono Y. History of the G protein-coupled receptor (GPCR) assays from traditional to a state-of-the-art biosensor assay. *J Pharmacol Sci* 2014;126:302-309.
- 131 Giaever I, Keese CR. Micromotion of mammalian cells measured electrically. *Proc Natl Acad Sci U S A* 1991;88:7896-7900.
- 132 Wegener J, Hakvoort A, Galla H-J. Barrier function of porcine choroid plexus epithelial cells is modulated by cAMP-dependent pathways in vitro. *Brain Res* 2000;853:115-124.
- 133 Michaelis S, Wegener J, Robelek R. Label-free monitoring of cell-based assays: Combining impedance analysis with SPR for multiparametric cell profiling. *Biosens Bioelectron* 2013;49:63-70.
- 134 Shan X, Patel U, Wang S, Iglesias R, Tao N. Imaging local electrochemical current via surface plasmon resonance. *Science* 2010;327:1363-1366.
- 135 Abbas A, Linman MJ, Cheng Q. New trends in instrumental design for surface plasmon resonance-based biosensors. *Biosens Bioelectron* 2011;26:1815-1824.
- 136 Peters MF, Scott CW. Evaluating cellular impedance assays for detection of GPCR pleiotropic signaling and functional selectivity. *J Biomol Screening* 2009;14:246-255.
- 137 Schröder R, Janssen N, Schmidt J, Kebabian A, Merten N, Hennen S, Müller A, Blattermann S, Mohr-Andra M, Zahn S, Wenzel J, Smith NJ, Gomeza J, Drewke C, Milligan G, Mohr K, Kostenis E. Deconvolution of complex G protein-coupled receptor signaling in live cells using dynamic mass redistribution measurements. *Nat Biotechnol* 2010;28:943-949.
- 138 Stallaert W, Dorn JF, van der Westhuizen E, Audet M, Bouvier M. Impedance responses reveal β 2-adrenergic receptor signaling pluridimensionality and allow classification of ligands with distinct signaling profiles. *PLoS ONE* 2012;7:e29420.

3 The critical impact of cell adhesion in optical and impedance-based label-free assays

Note: Prior to the submission of this thesis, parts of this chapter were published in cooperation with partners:

Lieb, S.; Michaelis S.; Plank, N.; Bernhardt, G.; Buschauer, A.; Wegener, J.

Label-free analysis of GPCR-stimulation: The critical impact of cell adhesion

Pharmacol. Res. **2016**, *108*, 65-74

The following experiments were performed by co-authors:

S.M.: Performed ECIS-SPR measurements with U-373 MG and BAE cells

N.P.: Generated HEK293T-CRE-Luc-hH₁R cells (cf. N.P., PhD thesis, University of Regensburg, 2016).

3.1 Introduction

G-protein-coupled receptors (GPCRs) constitute the largest family of membrane-bound signaling proteins, which transmit extracellular stimuli across the cell membrane into the cytoplasm by activating heterotrimeric G-proteins [1,2]. GPCRs are involved in a plethora of diseases, including inflammation, pain, cardiovascular diseases and neurological disorders [3-6]. They represent the biological targets of more than 30% of all marketed drugs [7]. In addition to those GPCRs addressed by approved drugs, the discovery and characterization of orphan receptors still holds a great therapeutic potential [8].

Various functional assays have been designed and successfully applied to determine the ligand-dependent, GPCR-mediated activation or inhibition of cellular signaling cascades, e. g. by quantification of second messengers such as cyclic AMP, inositol trisphosphate or calcium ions [9]. These assays require specific molecular probes (e.g. Fura-2/AM), and the analytical readout is most often based on fluorescence or luminescence. By contrast, label-free technologies provide a holistic, unbiased and time-resolved approach to monitor the cellular response to a compound of interest (agonist/antagonist). These techniques are becoming more and more accepted and appreciated in drug discovery [10], in particular, due to their applicability to orphan GPCRs, for which the endogenous ligands and the physiological signaling pathways are still to be identified.

The most widely applied devices to perform label-free cell-based assays rely on measuring (i) the electrochemical impedance Z of cell-covered planar electrodes (Fig. 1A) [11-13] or (ii) the resonance wavelength λ of cell-covered optical waveguides (resonance waveguide = RWG) during experimental stimulation of the cells (Fig. 1B) [14-17]. Although the surface plasmon resonance (SPR) technique (Fig. 1C) was developed earlier, it has not yet received the same attention for the analysis of cell-based assays as RWG- or impedance-based approaches.

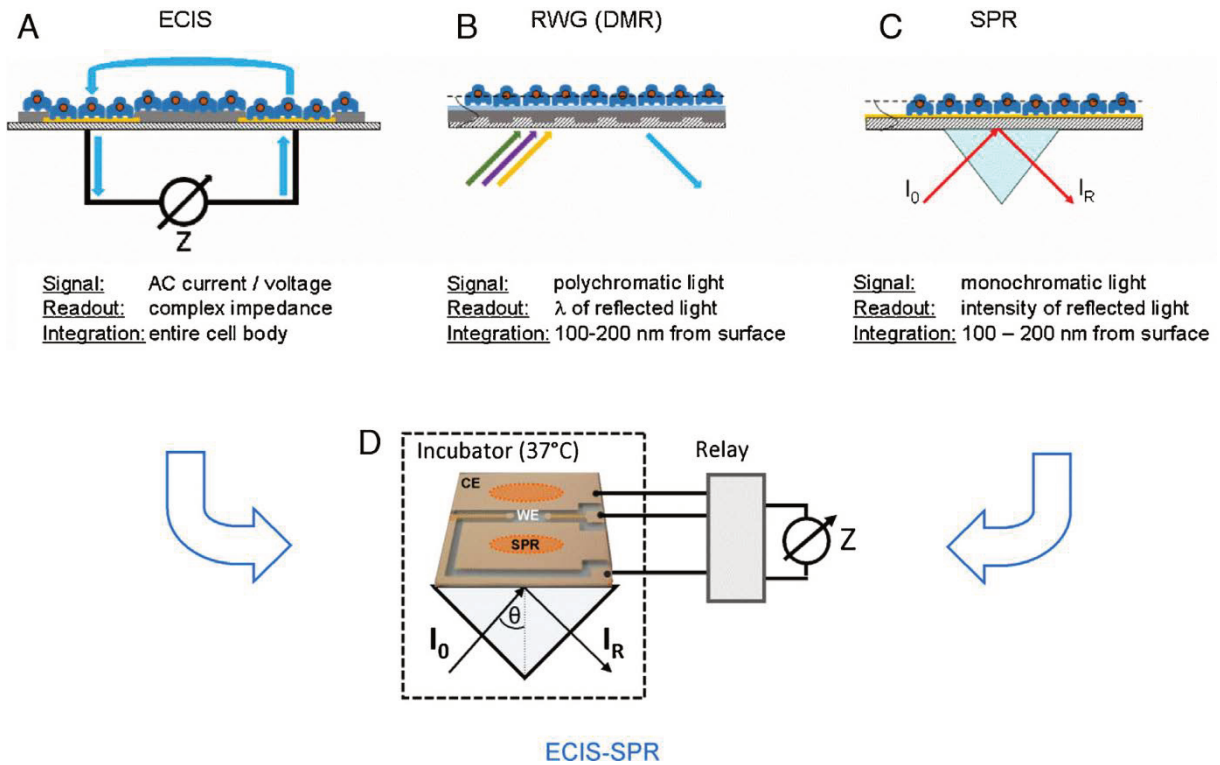


Fig. 1: Schematic overview of the most widely applied label-free approaches to monitor cell-based assays. (A) *Electric Cell-Substrate Impedance Sensing* (ECIS) reads the electrical impedance of cell-covered electrodes with non-invasive AC currents and voltages. The impedance signal Z is sensitive to coverage of the electrode with cells and the geometric shape of the cells on the electrode. (B) Surfaces that hold a *resonant waveguide grating* (RWG) reflect monochromatic light of wavelength λ when exposed to polychromatic incident light. The resonance wavelength of the reflected light is determined by the refractive index close to the surface, making the device sensitive to any change in mass distribution in the lower part of the cell body. (C) Monochromatic incident light excites *surface plasmons* under *resonance* (SPR) conditions along a gold-covered surface. The intensity of the reflected light – not dissipated into plasmonic energy – is determined by the refractive index close to the surface. Thus, SPR provides very similar information as RWG. (D) Setup for simultaneous monitoring of the cellular response by ECIS and SPR. The sensor surface holds two elliptical fields for SPR sensing and two much smaller working electrodes for ECIS recordings. The relay allows switching between the individual electrodes. RWG = resonance wave guide; ECIS = electric cell-substrate impedance sensing; SPR = surface plasmon resonance; I_0 = intensity of the incident light; I_R = intensity of the reflected light; Z = impedance; CE = counter electrode; WE = working electrode.

In SPR the intensity of the reflected light is measured. Intensity readings report on the generation of surface plasmons along a gold-coated growth surface. Whereas ECIS is sensitive to the dielectric properties of the cell bodies on the electrode, RWG and SPR report on the integral refractive index within a distance of 100 to 200 nm from the surface. The refractive index is affected by the cell bodies and the distribution of mass along the surface.

The basic concepts of all these approaches have been described in detail elsewhere [11,13,16]. Thus, we only give a short summary to emphasize those similarities and differences that are important for the main conclusion of this study.

The use of electrochemical impedance measurements to monitor cell-based assays was first described by Giaever and Keese [15] and is referred to as electric cell-substrate impedance sensing or short ECIS. In ECIS the cells are grown on the surface of thin gold-film electrodes deposited on the growth surface. When cells attach and spread on the electrode, the impedance increases since the dielectric cell bodies behave like insulating particles forcing the current to flow below, between or through the cells, depending on the AC frequency used for the measurement. Accordingly, the technique is sensitive to electrode coverage and cell morphology. When confluent cell layers are studied, cell morphology determines the impedance readout entirely. This phenomenon is based on the fact that cell size as well as the tightness of cell-cell and cell-substrate contacts determines the geometric and resistive properties of the ionic current pathways around the cell bodies. Any change in cell shape causes a corresponding change in the geometry of the current pathways and, thus, the measured impedance. Since it is well known that GPCR activation may lead to actin cytoskeleton remodeling [14], it is straightforward to apply ECIS as monitoring device in cell-based assays to investigate GPCR pharmacology.

In RWG devices [17] the surface for cell growth is manufactured with an optical grating. As a consequence polychromatic incident light is reflected as monochromatic light while an evanescent electric field is generated at the substrate surface. The evanescent electric field penetrates approximately 100 - 200 nm into the sample. The integral refractive index within this "sensitive sheet" affects the resonance condition and, thus, determines the wavelength of the reflected light. Since the plasma membrane of adherent mammalian cells can be as close as 25 nm to the surface (strongly dependent on cell type), the resonant wavelength is affected by any mass redistribution, provided that it is localized in the lower part of the cell body close to the membrane. With respect to this interpretation of refractive index changes the approach is often referred to as "DMR" for dynamic mass redistribution.

In SPR [16] a high quality glass slide is covered with a thin layer of gold. When the interface between glass and gold is hit by a monochromatic laser beam under resonance conditions

(wavelength, angle of incidence) the evanescent electric field couples into the conduction band electrons of the metal and excites surface plasmons (i.e. electron density fluctuations). These plasmons generate an evanescent electric field with a similar penetration depth as the one provided by the resonance waveguide grating in the range of 100 to 200 nm (dependent on wavelength). The refractive index within this sensitive “sheet” affects the resonance condition and thereby modulates the intensity of the refracted light. Accordingly, RWG and SPR approaches are both sensitive to the integrated refractive index within the evanescent field close to the surface. For any changes that occur on the apical side of the cells or more distant from the surface, both, RWG and SPR, are blind. It has been suggested that both techniques primarily record signals resulting from changes of the cortical cytoskeleton adjacent to the basal plasma membrane.

Whereas RWG and SPR readouts are closely related, impedance measurements are based on very different physics and the signal is integrated over the entire cell body. Thus, optical (RWG, SPR) and electrochemical approaches (ECIS) provide complementary information. Simultaneous application of these techniques might help to unravel the fine structure and patterns of time-resolved response profiles. To explore the potential of such a combination of approaches, recently, we developed an experimental setup that allows to apply ECIS and SPR [18] to one and the same cell population (Fig. 1D). Since the cells are grown on gold-films for either of the two approaches, the gold-film is structured by photolithography to provide electrodes for ECIS and measurement fields for SPR. Thus, the ECIS-SPR approach provides fully synchronized time course data for both readouts.

With this ensemble of label-free detection techniques, it was our objective to study the impact of cell adhesion on the different readouts. We examined two different cell types, human U-373 MG glioblastoma cells and bovine aortic endothelial cells (BAEC) that endogenously express prototypical class A GPCRs, the histamine H_1 receptor (H_1R) and the β_2 -adrenergic receptor (β_2 -AR), respectively. These receptors are well known and have been intensely studied on the cellular level with various methods. In addition we studied HEK-293 cells that were engineered to stably express (i) the human histamine receptor H_1R and (ii) the H_1R plus the human macrophage scavenger receptor 1 (hMSR1) [19]. The latter is known to support and enhance cell-matrix adhesion [20].

3.2 Materials and methods

3.2.1 Cells and culture conditions

The U-373 MG human glioblastoma cells, endogenously expressing the hH₁R, were purchased from the American Type Culture Collection (ATTC, Rockville, MD, USA). Cells were cultivated in Eagle's Minimum Essential Medium containing L-glutamine and 4.5 g/L D-glucose (Sigma, Munich, Germany), supplemented with 3.7 g/L NaHCO₃ (Merck, Darmstadt, Germany), 110 mg/L sodium pyruvate (Serva, Heidelberg, Germany) and 10 % fetal calf serum (FCS, Biochrom, Berlin, Germany). Bovine aortic endothelial cells (BAEC), endogenously expressing the β₂-adrenergic receptor, were kindly provided by Dr. S. Zink and Prof. Dr. P. Rösen (Deutsches Diabetes-Zentrum, Düsseldorf, Germany). These endothelial cells were originally isolated from aortae of freshly slaughtered calves as described elsewhere [13] and propagated by sequential subcultivation. Cells were cultivated in DMEM containing L-glutamine and 4.5 g/L D-glucose, supplemented with 3.7 g/L NaHCO₃, 110 mg/L sodium pyruvate and 10 % FCS. Routine cultures of both cell lines were maintained in 25-cm² culture flasks (Sarstedt, Nümbrecht, Germany) in a humidified incubator at 37 °C and 5 % CO₂. Cells were subcultivated (1:10) twice a week.

3.2.2 Transfections

Human embryonic kidney (HEK293T) cells were purchased from the German Collection of Microorganism and Cell Cultures (DSMZ, Braunschweig, Germany). HEK293T cells stably expressing the CRE controlled luciferase were established as previously described [21]. The HEK293T-CRE-Luc cells were stably co-transfected with pcDNA3.1(+)-hH₁R. Cells were detached from a 25 cm² culture flask by trypsinization one day before transfection. Cells were centrifuged (10 min, 300 g) and suspended in medium. Two mL of the cell suspension at a density of 5·10⁵ /mL were seeded into a 6-well flat bottom plate (Sarstedt, Nümbrecht, Germany). The plasmid was linearized with *PvuI* (New England Biolabs, Frankfurt am Main, Germany) for 2 h at 37 °C prior to transfection. The linearized vector was purified with the PCR purification KIT (Qiagen, Leipzig, Germany) according to the manufacturer's manual. DNA (2 µg) was diluted with DMEM without FCS, and 6 µL of the transfection reagent FuGene HD

(Roche Diagnostics, Mannheim, Germany) were added. The mixture was vortexed and incubated for 15 min before addition to the cells. The medium was removed 32 h later and the cells were transferred into a 25 cm² culture flask with DMEM 10 % FCS and hygromycin b (250 µg/ml) (A.G. Scientific, San Diego, USA). 24 h later the medium was replaced by fresh DMEM supplemented with 10% FCS, G418 (600 µg/ml) (Biochrom, Berlin, Germany) and hygromycin b (250 µg/mL). Co-transfected cells were cultured in Dulbecco's Modified Eagle Medium (Sigma, Munich, Germany) containing L-glutamine, 4.5 g/L glucose and 3.7 g/L NaHCO₃. The medium was supplemented with 110 mg/L sodium pyruvate, 10 % (v/v) fetal calf serum as well as the selection antibiotics G418 (600 µg/ml) and hygromycin b (250 µg/ml). This co-transfected cell line is referred to as HEK293T-CRE-Luc-hH₁R cells.

A second stable transfectant was generated from the HEK293T-CRE-Luc-hH₁R cells by co-transfection with pRESpuro3/hMSR1 (kindly provided by Dr. S. Krief, bioprojet Biotech, Saint-Grégoire, France) encoding the human macrophage scavenger receptor 1 (hMSR1) [19] and puromycin resistance. For transfection, the cells were seeded in a six-well-plate (Sarstedt, Nümbrecht, Germany) so that they reached approximately 60–70 % confluency on the next day. The transfection mixture containing 2 µg of pRESpuro3/hMSR1 DNA was diluted with serum free DMEM, and 6 µL of FuGeneHD transfection reagent were added. The selected stable transfectant (HEK293T-CRE-Luc-hH₁R-hMSR1 cells) was maintained in DMEM supplemented with 10 % FCS, 600 µg/mL of G418, 200 µg/mL of hygromycin b and 0.75 µg/mL of puromycin (InvivoGen, San Diego, USA) in a humidified atmosphere containing 5 % CO₂ at 37 °C. Expression of the hMSR1 receptor in HEK293T-CRE-Luc-hH₁R-hMSR1 cells was confirmed by western blot analysis (fig. A1, appendix).

3.2.3 Chemicals and test compounds

Chemicals of analytical grade were purchased from Merck (Darmstadt, Germany) unless otherwise stated. Stock solutions of histamine dihydrochloride (Acros Organics, Geel, Belgium) and (–)-isoprenaline hydrochloride (Sigma Aldrich, Munich, Germany) were prepared in Millipore water (Merck-Millipore, Darmstadt, Germany) and stored at -20 °C. Shortly before the experiments, aliquots were thawed and diluted with Leibovitz' L-15 medium (Thermo Scientific, Darmstadt, Germany) without FCS to the final concentration.

3.2.4 Impedimetric assay

Time-resolved impedimetric monitoring of cell-based assays was performed using the ECIS-Z device for 96-well electrode arrays of type 96W1E+. Hardware and disposable arrays were from Applied BioPhysics (Troy, NY, USA). Each well holds two circular electrodes of 350 μm diameter, which are electrically arranged in series. Thus, the device monitors 0.2 mm^2 of a confluent cell layer, corresponding to approximately $2.5 \cdot 10^3$ cells, assuming circular cells with an average diameter of 10 μm . Prior to seeding any of the four cell types, the electrode arrays were cleaned and decontaminated by three successive argon plasma exposures of 30 s each (Plasma Cleaner PDC-002, Harrick Plasma, New York, USA). Suspensions of the different cell types in their individual culture medium were prepared from close-to-confluent cell layers by standard trypsinization techniques. For the measurements 300 μL of culture medium containing approximately $9 \cdot 10^4$ HEK293T cells/well, $4.5 \cdot 10^4$ U-373 MG cells/well or $5 \cdot 10^4$ bovine aortic endothelial cells /well, respectively, were seeded into the individual wells of an electrode array. The cells were allowed to attach in a CO_2 incubator at 37 $^\circ\text{C}$ for 24 h. About 1 h before the assay was performed, the culture medium was aspirated and replaced by 150 μL of pre-warmed L-15 medium without FCS. The arrays were connected to the ECIS device inside an incubator (Galaxy 48S, New Brunswick, USA) in a humidified atmosphere (without additional CO_2) at 37 $^\circ\text{C}$ for continuous impedance monitoring. Data was recorded at an AC frequency of 4 kHz. After recording baseline data, the test compounds dissolved in L-15 medium were added, and the cellular response was monitored for approximately 40 min. Time course data is presented as the shift of impedance magnitude $\Delta|Z|(t)$ relative to the last data point before test compounds were added into the wells at time zero. Thus, $\Delta|Z|(t) = |Z|(t) - |Z|(0)$. The time courses for all test compounds were subsequently corrected for the corresponding values of untreated controls (buffer only).

To the best of our knowledge there is only one technique, fluorescence interference contrast microscopy (FLIC), recently developed by Braun and Fromherz [22] allowing the determination of the distance between the lower cell membrane and the electrode surface. HEK293T-CRE-Luc-hH₁R cells and HEK293T-CRE-Luc-hH₁R-hMSR1 cells were also studied by recording the impedance of the cell-covered electrodes along a frequency band from 10 Hz to 100 kHz (impedance spectroscopy). Frequency-resolved impedance data was analyzed according to a biophysical model that decomposes the overall impedance of a cell-covered electrode into

subcellular contributions as described earlier [23,24]. According to this model, which is schematically illustrated in Fig. 2, the overall impedance of the cell layer arises from current flow along trans- (dashed lines) and paracellular ionic pathways (solid lines). These pathways are further decomposed in (i) the resistance between adjacent cells (cell-cell junctions, '1' in Fig. 2), (ii) the impedance of the plasma membranes ('2' in Fig. 2) and (iii) the resistance in the cleft between basal cell membrane and electrode surface R_{cleft} ('3' in Fig. 2). This cleft resistance R_{cleft} is defined as: $R_{\text{cleft}} = r_c^2 \cdot (\rho / d)$ with the cell radius r_c , the specific resistivity in the cleft ρ and the distance between lower membrane and electrode surface d . When the cell radius and the specific resistivity of the medium in the cleft underneath the cells are constant, R_{cleft} is inversely proportional to the distance between cell and surface. We analyzed the two HEK293T transfectants with respect to their individual resistances in the cell-substrate junctions. The results are presented as the average resistance in the cleft between the basal cell membrane and the electrode R_{cleft} .

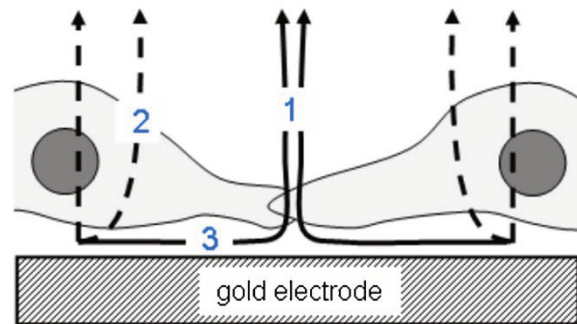


Fig. 2: Schematic illustrating the physical model that has been used to analyze impedance spectra of the two different HEK293T transfectants with respect to the cleft resistance R_{cleft} (3). R_{cleft} describes the resistance in the cell-substrate junction which is dependent on the distance between basal cell membrane and the electrode surface d . Besides R_{cleft} the model comprises the parameter R_b (1) to account for the resistance between cells and the membrane impedance Z_m (2). Solid arrows indicate paracellular current flow, whereas dashed arrows indicate transcellular current flow.

3.2.5 Dynamic mass redistribution assay

Label-free dynamic mass redistribution ('DMR') monitoring was carried out on an EnSpire (PerkinElmer, Waltham, USA) multimode reader, which is based on the EPIC optical biosensor technology using resonance waveguides (RWG). Prior to RWG-based assays, suspensions of cells under study were prepared in their individual culture medium from close-to-confluent cell layers by standard trypsinization. For the measurements 40 μL of cells suspended in cell culture medium were seeded into uncoated 384-well EnSpire cell assay microplates applying the individual densities: $2 \cdot 10^4$ genetically engineered HEK293T cells/well, $2.5 \cdot 10^3$ bovine aortic endothelial cells/well and $1.5 \cdot 10^4$ U-373 MG cells/well. The microplates were incubated in a humidified atmosphere containing 5% CO_2 at 37 °C for 24 h, providing cell layers of approximately 90 % confluency. Immediately before starting the experiments, the cells were washed four times with L-15 medium and were allowed to equilibrate inside the Enspire multimode reader at 37 °C for about one hour. After recording baseline data, 10 μL of the test substances dissolved in L-15 medium (concentration 4x) were added with a multichannel electronic finnpipette (Thermo Fisher Scientific, Waltham, MA, USA) and the cellular response was recorded continuously for 40 min. Time course data is presented as the shift of resonance wavelength $\Delta\lambda(t)$ relative to the last data point before test compounds were added into the wells at time zero. Thus, $\Delta\lambda(t) = \lambda(t) - \lambda(0)$. The time courses for all test compounds were subsequently corrected for the corresponding values of untreated controls (buffer only).

3.2.6 Experimental setup for ECIS-SPR assays

The dual sensor platform was set up by implementing both techniques, ECIS and SPR, on the same sensor chip. The ECIS-SPR chips were prepared from high-refractive-index glass slides (2.5cm x 2.5cm) covered with a 5 nm chromium bottom and a 45 nm top gold layer. The metal layers were subsequently structured by photolithography and wet etching as described previously [18], providing the goldfilm pattern as indicated in figure 1D. A PDMS spacer (Sylgard 184 silicone elastomer kit, Dow Corning, Michigan, USA) forming a cell culture compatible flow cell was glued on top of the sensor using a non-toxic silicone adhesive (Master fix Aquarium Silikon, Warenimport und Handels GmbH, Vienna, Austria). The silicone glue was allowed to cure for about 24h. The resulting sensor surface (Fig. 1D) featured two individually

addressable small circular ECIS working electrodes (diameter \approx 1mm) and one large counter electrode, which was approximately 100fold bigger in surface area. This counter electrode was used as SPR measurement spot at the same time. Electrodes and SPR sensor spots were housed in a common fluid volume of about 500 μ L. The individual readouts from both techniques provide the optical and electrical properties of the cells on the sensor chip simultaneously.

SPR measurements were recorded on a Biosuplar400TSPR system (MiviTec GmbH, Sinzing, Germany) at 37 °C. The sensor chip was mounted on top of an F61-glass prism of the Biosuplar system using appropriate immersion oil (refractive index: 1.61; Cargille, NJ, USA). The flow cell was covered with an acrylic glass lid equipped with in- and outlet ports. After mounting of the cell-covered sensor chip, a standard angle scan was performed to localize the angle of incidence providing the maximal sensitivity of reflectivity. Subsequently, the SPR system was run in kinetic measurement mode, during which changes in reflectivity (ΔR) were recorded over time (t) at this most sensitive angle of incidence. For ECIS measurements of the same cell population the impedance of the two individual working electrodes was alternately measured against the common counter electrode on the sensor chip using a Solartron SI-1260 Gain-Phase-Analyzer (Farnborough, UK). A relay allowed switching between the two working electrodes. The impedance magnitude at a sampling 16 kHz (BAEC) or 20 kHz (U-373 MG) is plotted as shift in impedance $\Delta|Z|$ as a function of time relative to the last value before compound addition. The different sampling frequencies used in these experiments are a consequence of the different electrodes size in ECIS-SPR compared to the commercial 96well ECIS electrode arrays and individual dielectric properties of the two cell types studied here.

Prior to the experiment, suspension of U-373 MG and bovine aortic endothelial cells were prepared from close-to-confluent cell layers by standard trypsinization and seeded at a final density of 10^5 U-373 MG cells/cm² or $9 \cdot 10^4$ bovine aortic endothelial cells/cm², respectively. This provided a complete coverage of the sensor surface by cell adhesion within 24 hours. Before starting the experiments the individual culture medium was replaced by L-15 medium and baseline data was recorded for one hour to allow the system to equilibrate before addition of pre-warmed solutions of the test compounds dissolved in L-15 medium. Time course data $|Z|(t)$ and $R(t)$ is presented as changes in impedance $\Delta|Z|(t)$ and reflectivity $\Delta R(t)$ relative to the last data point before compound addition at time zero.

3.2.7 Fura-2 calcium assay

The assay was performed as described elsewhere [25]. In brief, after trypsinization, the cells were centrifuged at 300 g for 10 min. Thereafter, the medium was discarded and the cells were counted in a hemocytometer. To three volumes of cell suspension in loading buffer (HEPES (Serva, Heidelberg, Germany) 25 mM; NaCl 120 mM, KCl 5 mM, MgCl₂ 2 mM, CaCl₂ 1.5 mM, glucose 10 mM; pH 7.4) one volume of loading dispersion (1 mL loading dispersion: 2 % BSA (Serva); 5 µL Pluronic (Sigma); 4 µL Fura-2 (VWR, Ismaning, Germany)) was added. Cell density was adjusted to 10⁶/mL. The prepared suspension was incubated in the dark for 30 min and subsequently centrifuged. Cells were resuspended in loading buffer and allowed to stand in the dark for another 30 min. The cells were washed twice with loading buffer and adjusted to a final density of 10⁶/mL. The assay was performed in acrylic cuvettes (VWR) using an LS50 B spectrofluorimeter (Perkin Elmer).

3.2.8 Data analysis

Concentration-response curves were constructed from the recorded time courses after correction for the time courses of untreated controls, by measuring the area-under-the curve (AUC) of individual response profiles $[\Delta|Z|(t)$ or $\Delta\lambda(t)$] from 0 – 40 min for each compound concentration. The concentration of half-maximum cell response EC₅₀ was determined by fitting a four-parameter sigmoidal transfer function (Eq. (1)) to the recorded data using GraphPad Prism 5.01 (GraphPad Software, San Diego, USA).

$$Y = Y_{min} + (Y_{max} - Y_{min}) / (1 + 10^{\log(EC_{50}-x) \cdot n}) \quad (1)$$

Herein Y denotes the signal response at a given concentration x, Y_{max} is the maximal response, Y_{min} is the minimal response, EC₅₀ is the concentration of half-maximal response with the Hill slope n.

3.3 Results and discussion

3.3.1 Impedance and DMR response of U-373 MG cells upon hH₁R stimulation

As the hH₁R is G $\alpha_{q/11}$ -coupled, activation of the receptor by the endogenous agonist histamine leads to an increase in cytosolic Ca²⁺, inositol-1,4,5-trisphosphate (IP₃) and diacylglycerol (DAG) concentrations. We studied the response of U-373 MG cells, endogenously expressing H₁ receptors, to histamine using impedimetric (ECIS) and optical (EnSpire) readouts. Both assays were performed under similar conditions. Neither the electrode surfaces (ECIS) nor the RWG substrates (EnSpire) were coated with extracellular matrix proteins prior to cell seeding. After 5 min of baseline recording, histamine was added at increasing concentrations to the individual wells, and the cellular response was studied with a time resolution of approximately one min for both methods.

Figure 3A shows the time course of the impedance change $\Delta|Z|$ at a sampling frequency of 4 kHz when U-373 MG cells were exposed to increasing concentrations of histamine in a typical experiment. The response is clearly concentration-dependent and shows a characteristic pattern with an initial dip of the signal followed by a pronounced rise. Figure 3B shows the same dataset after correcting for the time course of the control (L-15 only). At the highest agonist concentration applied, the dip of $\Delta|Z|$ amounted to approximately -200 Ω within the first two minutes, followed by an increase to more than 900 Ω within 20 min after addition of histamine. This impedimetric response profile $\Delta|Z|(t)$ is in agreement with those typically recorded for G $\alpha_{q/11}$ -mediated responses [12] in other labs. When the area-under-the-curve (AUC) for the pool of baseline-corrected time courses (fig. 3B) was calculated between 0 and 40 min and plotted as a function of the logarithm of the histamine concentration, we obtained a sigmoidal curve (Fig 3C) with a pEC₅₀ of 6.52 ± 0.08 .

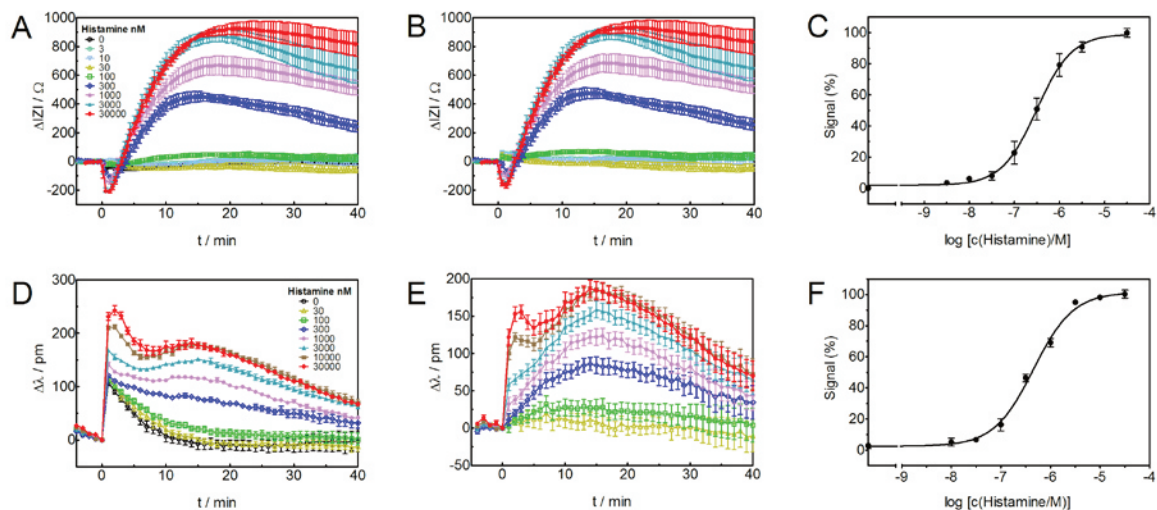


Fig. 3: Histamine induced response of U-373 MG cells monitored by ECIS (A-C) and RWG/DMR (D-F). (A, D) Representative time courses (performed in triplicate) of the change of impedance $\Delta|Z|$ recorded at 4 kHz (A) or resonance wavelength $\Delta\lambda$ (D). (B, E) Time courses of $\Delta|Z|$ and $\Delta\lambda$ were corrected for the signal upon addition of agonist-free L-15 medium by subtraction. (C, F) Concentration-response curves were derived from the area-under-the-curve (AUC) of baseline-corrected data integrated from 0 – 40 min for four independent experiments, each performed in triplicate.

As shown in figures 3D-F, in case of RWG monitoring, the histamine-induced response was concentration-dependent, too, but the pattern (Fig. 3D) was different from the impedimetric profile (Fig. 3A). The signal increased rapidly to a maximum within 2-3 min after histamine addition, followed by a decline and, in case of histamine concentrations >300 nM, a second rise of the signal within 15 - 16 min was observed. This phenomenon was highly reproducible. A monotonic fast increase of the signal within the first 5 min after stimulation and a slow decrease over the residual observation time (20 min) was reported in the literature when dynamic mass redistribution (EPIC) had been applied to $G\alpha_{q/11}$ -coupled GPCRs [26,27]. To the best of our knowledge, two relative maxima in the time-resolved response profile have not been reported for $G\alpha_{q/11}$ -stimulation so far [17,26]. For the normalized signals (Fig. 3E) the relative maximum after approximately 3 min became only visible at rather high histamine concentrations, suggesting that this effect might be, at least in part, unspecific, resulting from receptor-independent, interactions of the agonist (e.g. membrane interactions) or from a change in intracellular signaling. AUC analysis of the time profiles from 0 to 40 min revealed the S-shaped concentration-response relationship shown in Fig. 3F with a pEC_{50} of 6.12 ± 0.10 .

The pEC_{50} values determined with both techniques are in good agreement but significantly different from the pEC_{50} of 4.87 ± 0.14 ($N = 10$) determined by Ca^{2+} mobilization assays using Fura-2/AM. The significantly smaller pEC_{50} values returned by label-free methods may reflect the contribution of different signaling pathways to the holistic readouts. Interestingly, both time profiles show two extrema: two relative maxima in the RWG-based profile compared to a minimum and a subsequent maximum for the impedance-based readout. Whereas the impedance minimum and the first relative maximum of the RWG-signal appear approximately at the same time after addition of histamine, the impedance maximum and the second maximum in RWG-data are slightly shifted along the time axis. At this point we can only speculate about the reasons for these observations. Both techniques are sensitive to coverage of the surface with cells and changes in cell morphology [17]. But, whereas RWG-based recordings report on a dynamic mass redistribution within a short distance from the surface, impedance readings reflect changes in cell shape integrated over the entire cell body. Thus, individual changes at different positions of the cell body contribute to the two time profiles with very different individual weights. Moreover, ECIS-readings report on the geometry of ionic current pathways which are determined by the position of the cell membranes. In contrast, time course data recorded by RWG-based devices mirror a displacement of masses which may precede or follow changes in membrane morphology.

3.3.2 Impedance and DMR response of BAECs upon β_2 -adrenergic receptor stimulation

As β_2 -adrenergic receptors (β_2 -AR) are $G\alpha_s$ -coupled, activation results in stimulation of adenylyl cyclase and a subsequent increase in the concentration of the second messenger cAMP. When BAECs were exposed to increasing concentrations of isoprenaline, there was a sustained, monotonic and concentration-dependent increase in $\Delta|Z|$ (Fig. 4A). The maximal response was achieved within 10 min after agonist addition. After passing the maximum, the signal slowly decreased but did not return to basal values within the observation time of 40 min, as becomes most obvious from the baseline-corrected data in figure 4B. Whereas we found this time profile to be highly reproducible for many passages of BAECs, the literature is controversial with respect to impedimetric time-resolved response profiles for $G\alpha_s$ -coupled

receptors. Similar to our observations, Yu et al. also report on a monotonic impedance increase with subsequent decline to basal values within two hours [28]. Other authors describe a *decrease* in impedance below baseline values as a characteristic response to $G\alpha_s$ activation [17]. Quantitative analysis of the baseline-corrected time profiles by calculating the AUC from time 0 to 40 min gave the concentration-response curve shown in Fig. 4C. The corresponding pEC_{50} was calculated as 6.0 ± 0.4 . In previous impedimetric studies we found very similar pEC_{50} values of 6.5 ± 0.2 for the same cell type, using a different electrode size [11]. Radioligand binding studies on BAECs revealed a pK_D value of 6.97 ± 0.03 for isoprenaline [13]. Thus, with respect to potency the different assays – radioligand binding versus functional assays - provide a difference up to one order of magnitude for the half-maximum response.

RWG-based monitoring of BAECs upon isoprenaline stimulation is summarized in Fig. 4D-F. The time profiles showed an immediate steep increase to the maxima of the curves after addition of the agonist. This maximum is very similar at the highest isoprenaline concentration and the medium control. Although the signals appear to be weakly concentration-dependent in the baseline-corrected time courses (figure 4E), the AUC data plotted against the concentrations of isoprenaline cannot be fitted according by a sigmoidal concentration-response curve (figure 4F), precluding the calculation of a reliable pEC_{50} value. Obviously, the RWG-based time profiles do not primarily report on the agonist-induced cell response but may contain other signal contributions, for instance, perturbations from liquid handling. This interpretation is supported by the observation of a similar initial ‘jump’ of the signal in U-373 MG cells upon addition of histamine (cf. Fig. 3D). Compared to the histamine-induced response of U-373 MG cells, the maximum signal change of $\Delta\lambda \approx 70$ pm, as observed here, is markedly reduced.

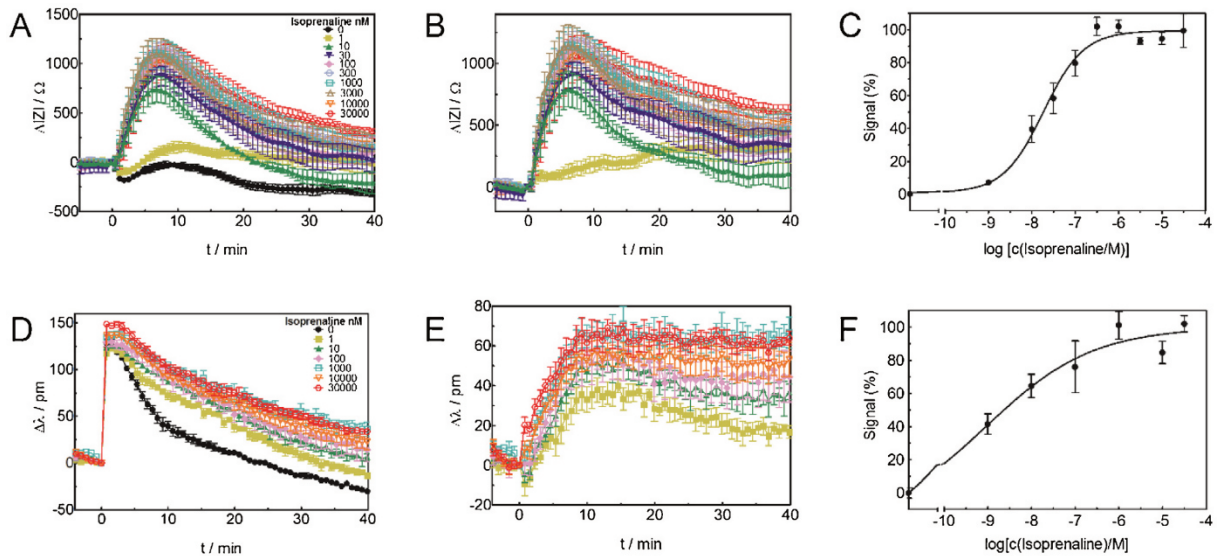


Fig. 4: Isoprenaline-induced response of BAE cells monitored by ECIS (A-C) and RWG/DMR (D-F). (A, D) Representative time courses (performed in triplicate) of the change of impedance $\Delta|Z|$ recorded at 4 kHz (A) or resonance wavelength $\Delta\lambda$ (D). (B, E) Time courses of $\Delta|Z|$ and $\Delta\lambda$ were corrected for the signal upon addition of agonist-free L-15 medium by subtraction. (C, F) Concentration-response curves were derived from the area-under-the-curve (AUC) of baseline-corrected data integrated from 0 – 40 min for four independent experiments, each performed in triplicate.

Based on the data shown in figure 4D-F the question arose, why the isoprenaline stimulation of β_2 -AR expressed on BAE cell surfaces is not as properly reported by resonance waveguide devices as the histamine response of U-373 MG cells. As the impedance data (Fig. 4A-C) provides a concentration-dependent response profile for the very same cell type and assay conditions, there is no doubt that the signal transduction machinery is operating. In order to exclude that the different supports used in electrochemical and optical analysis are the reason for the observed differences, we studied the U-373 MG and the BAEC cells by the combined ECIS-SPR technique. By ECIS-SPR analysis, cells from the same population were grown in the same medium on a surface covered with a thin gold film for both, the ECIS and the SPR readout.

3.3.3 Comparing U-373 MG (H_1R) and BAE cells (β_2 -AR) stimulation by ECIS-SPR analysis

Both cell types, U-373 MG and BAEC, were grown to confluency on ECIS-SPR sensor chips as shown in Fig. 1D. These supports provided a structured gold-film for performing both, ECIS and SPR monitoring on the same sensor surface. As the sensor surface holds only two individually addressable ECIS working electrodes and two readout fields for SPR detection, the throughput in this experimental setup was limited. Fig. 5A and 5B show typical time course data for confluent U-373 MG cells stimulated by 100 μ M histamine. Fig. 5A shows the ECIS profile and Fig. 5B the SPR profile of the same cell population. The time profiles were very similar to those depicted in Fig. 3. The ECIS signal showed a minimum after addition of the agonist, followed by a maximum and a slight decrease along the observation period. The SPR-profile showed two relative maxima, similar to the RWG signals at very high concentrations of histamine (cf. Fig. 3D). Thus, in case of stimulation by histamine, the time-resolved ECIS-SPR profiles (Fig. 5A, B) were in good agreement with the curves from ECIS and RWG-based experiments for U-373 MG cells when recorded separately (Fig. 3).

When BAECs were studied by ECIS-SPR upon exposure to 10 μ M of isoprenaline (Fig. 5C), ECIS recordings revealed the same characteristic time course as shown in Fig. 4A. Thus, the cell population was responsive to isoprenaline and the impedimetric profile was reproducible. By contrast, there was no significant response detectable by simultaneous SPR analysis of the very same cell population under identical conditions (Fig. 5D). Thus, both optical methods, the RWG and the SPR analysis, failed to determine the agonist potency of isoprenaline on BAECs. In contrast to the RWG-based time profiles (cf. Fig. 4E), there are no indications for unspecific cell responses due to liquid handling in SPR-based time courses (Fig. 5D). Please note that the cell-covered SPR-chip is not removed from the temperature controlled housing for agonist addition. Instead, liquid exchange was performed via inlet/outlet ports so that the cells are always covered by liquid, reducing unspecific perturbations.

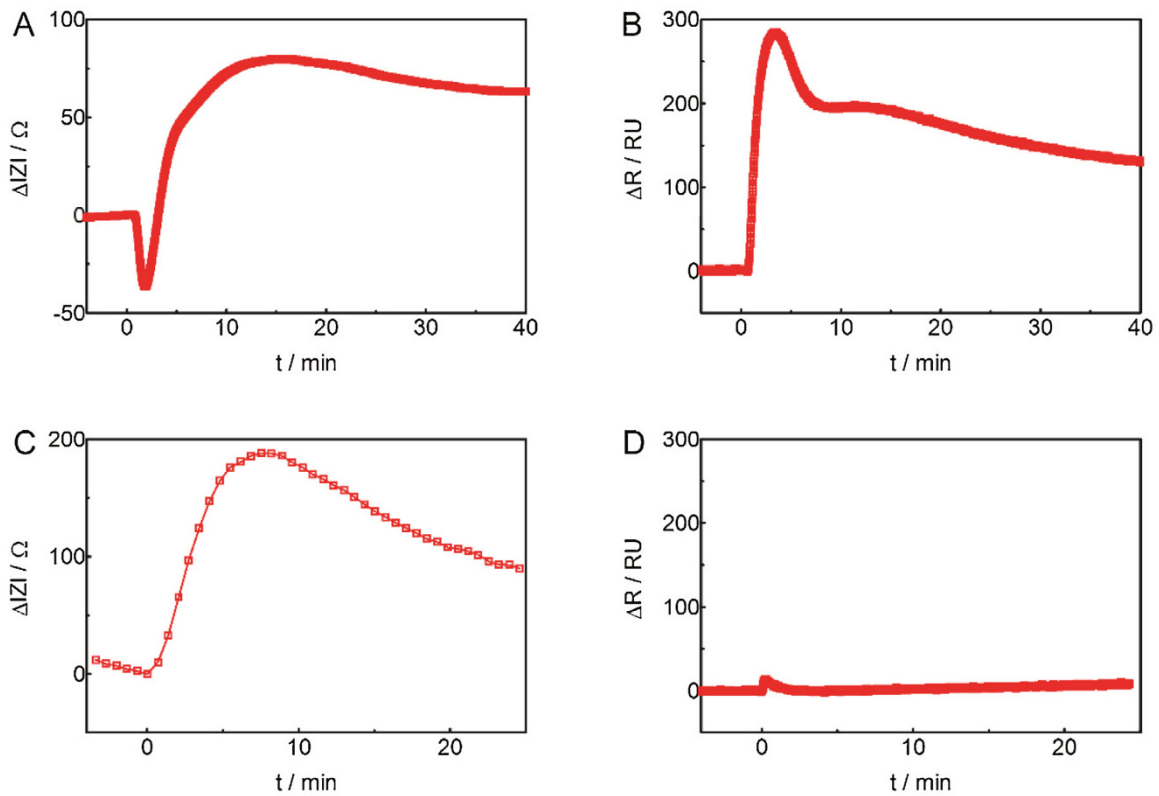


Fig. 5: Representative time-resolved response profiles of U-373 MG cells (A, B) and BAE cells (C, D) upon exposure to 100 μM histamine or 10 μM isoprenaline, respectively. (A) and (C) present the change in impedance $\Delta|Z|$ as a function of time. (B) and (D) show the time course of the reflectivity change ΔR . ECIS and SPR data were recorded for the same cell population on the same sensor chip. Due to limited throughput of the ECIS-SPR device, we present typical time courses from single registrations. The results were highly reproducible ($N = 10$ independent experiments, each performed in duplicate).

From an earlier study, performing an in-depth analysis of the impedimetric response of BAECs upon stimulation with isoprenaline, we learned that BAECs attach rather weakly to their growth substrate [11]. At the time we estimated the average distance between basal cell membrane and growth support to be larger than 500 nm from optical xz -sections recorded by confocal laser scanning microscopy (extracellular space labeled by fluorophore) [11]. Therefore, analysis by SPR is illusive, considering that the penetration depth of the evanescent electric field (Fig. 6) is in the range of 100 – 200 nm. Thus, the absence of any change in reflectivity or resonance wavelength in case of the BAECs is most likely due to an unsuitable distance of the cells to the surface. Accordingly, the adhesion of cells to the surface must be considered as a factor that potentially affects and modulates the sensor response.

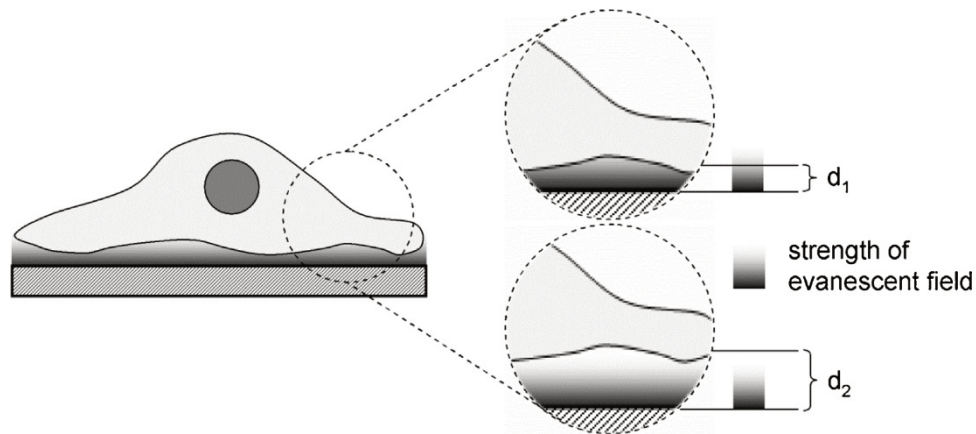


Fig. 6: Schematic illustrating the average distance between basal cell membrane and growth support d_1 or d_2 ($d_1 < d_2$) with respect to the penetration depth of the evanescent electric field (100 – 200 nm) indicated by the gray coded bar. When the distance d becomes larger than the penetration depth of the evanescent field, cellular responses are not detectable.

Compounds such as cytochalasin D, which are frequently used to assess the role of the actin cytoskeleton in signal transduction [29], are capable of significantly affecting the cell-substrate distance and to alter the sensitivity of the optical readout before or during an experiment which makes data interpretation rather complex.

3.3.4 Comparison of HEK293T-CRE-Luc-hH₁R with and without hMSR1 co-transfection

To explore the dependence of the optical signal on cell adhesion, we performed studies with HEK293T-CRE-Luc cells engineered to express either the human histamine H₁ receptor alone or in combination with the human macrophage scavenger receptor 1 (hMSR1). The latter is known to act as a cell adhesion molecule binding to the extracellular matrix (ECM). Scavenger receptors were first described by Brown and Goldstein [30]. The macrophage scavenger receptor 1 is a trimeric class A membrane glycoprotein with a single cytoplasmic domain, a single transmembrane region and a huge extracellular domain which mediates recognition of polyanionic ligands, such as modified forms of low density lipoprotein (LDL) [20,31,32]. It has been reported that cells expressing the human class A scavenger receptor show improved adhesion to the ECM [20]. In agreement to this, HEK cells expressing either hH₁R alone (HEK293T-CRE-Luc-hH₁R) or hH₁R *and* hMSR1 (HEK293T-CRE-Luc-hH₁R-hMSR1) behaved very

differently during routine trypsinization. Whereas those cells not expressing hMSR1 were completely detached from the surface within less than one minute, it took more than ten minutes to detach HEK cells co-expressing hMSR1. This observation indicates an improved adhesion of the HEK293T-CRE-Luc-hH₁R-hMSR1 cells to the growth support as it has been reported before [20]. Co-expressing hMSR1 has become an accepted [33] and commercialized strategy ('GripTite™293MSR cells') to render HEK293T cells more adhesive and thereby improve their resistance to detachment in robot-based high throughput drug screening assays with automated plate-washing protocols. Both transfectants were studied by ECIS- and RWG-monitoring with respect to their responsiveness to 1 μM histamine. The results are summarized in figure 7. Whereas Fig. 7A presents the ECIS profile of HEK293T-CRE-Luc-hH₁R to 1 μM histamine, Fig. 7B shows the RWG profile for the same stimulus. ECIS- and RWG-based time courses mirror the stimulation of the hH₁ receptor, but the cellular response was rather weak, in particular, when monitored by RWG. In contrast, under the same conditions, HEK293T-CRE-Luc-hH₁R-hMSR1 cells revealed signals of higher intensity in both assays, especially pronounced and with higher signal-to-noise ratio in the RWG/DMR assay (Fig. 7C, D).

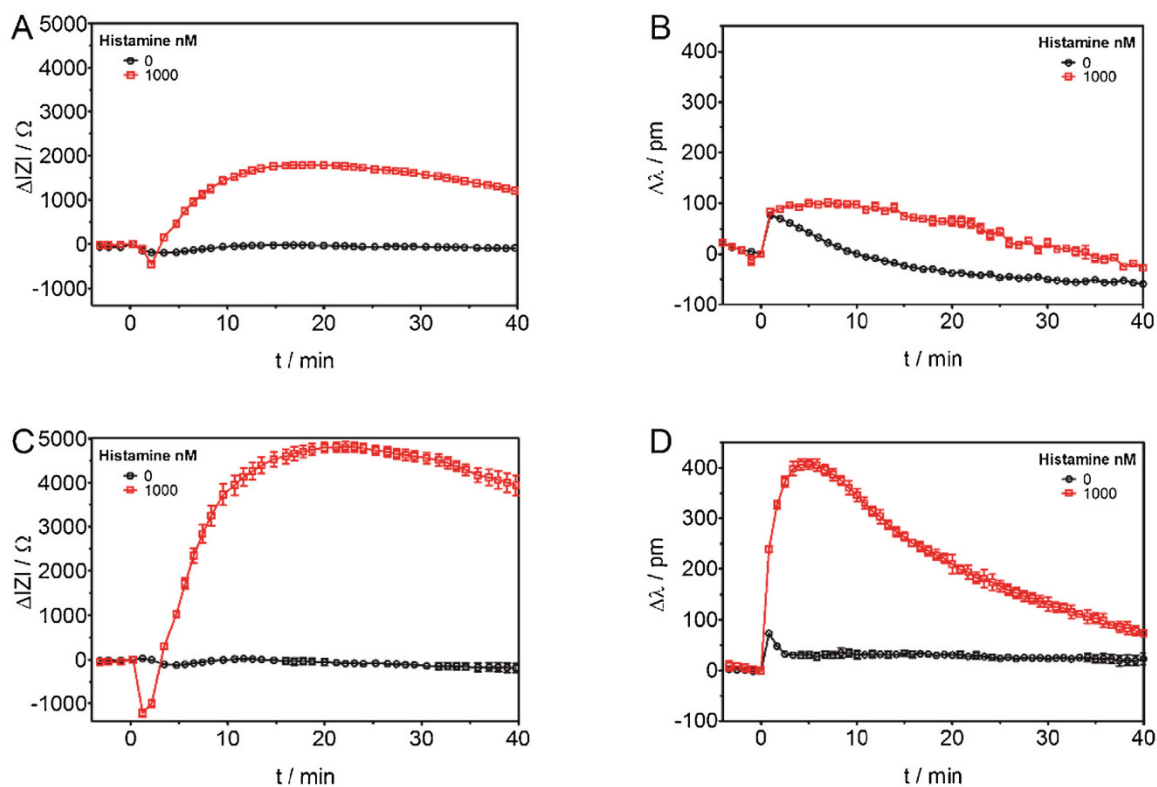


Fig. 7: (A, B) Representative response traces of HEK293T-CRE-Luc-H1R cells expressing the histamine H_1 receptor during exposure to $1 \mu\text{M}$ histamine (red) relative to a medium control (black). The time-resolved impedance profile $\Delta|Z|(t)$ is plotted in (A), the RWG/DMR profile in (B). (C, D) Response of HEK293T-CRE-Luc-H1R-hMSR1 cells co-expressing the histamine H_1 and hMSR1 receptor during exposure to $1 \mu\text{M}$ histamine (red) relative to a medium control (black). The time-resolved impedance profile $\Delta|Z|(t)$ is plotted in (C), the RWG/DMR profile in (D). The impedance was recorded at a sampling frequency of 4 kHz. Experiments were performed in triplicate.

This result suggests that expression of hMSR1 improves adhesion and reduces the distance between cell and substrate for these cells which strongly increases the height of the signal. It is noteworthy that, unlike the RWG-based time courses, the shape of the impedance profile (Fig. 7A) was very similar to that of U-373 MG (Fig. 3A) and HEK293T-CRE-Luc-hH₁R-hMSR1 cells (Fig. 7C) upon histamine stimulation. The absence of a second maximum in the time course of the resonance wavelength $\Delta\lambda$ suggests that the cellular background contributes to the observed response profiles apart from the type of GPCR under study and the signaling pathways involved.

In addition to the optical methods, the critical role of cell adhesion becomes obvious from analyzing impedance spectra. When the impedance of cell-covered gold-film electrodes is recorded along an extended frequency range from 10 Hz to 100 kHz, the resulting impedance

spectra are analyzed by a physical model illustrated in Fig. 2, decomposing the integral impedance of the cell layer into three major contributors: (i) the resistance between adjacent cells R_b as a measure of cell-cell junctions; (ii) the impedance of the cell membranes Z_m and (iii) the resistance of the electrolyte-filled cleft underneath the cells between the basal cell membrane and the electrode surface, R_{cleft} . According to its definition, $R_{\text{cleft}} = r_c^2 \cdot (\rho / d)$, the cleft resistance R_{cleft} is inversely proportional to the distance d between cell and substrate with r_c representing the cell radius and ρ abbreviating the specific electrolyte resistance in the cleft between cell and substrate with thickness d . More detailed information on this model is given elsewhere [23].

Analyzing the impedance spectra of both HEK293T transfectants according to this model provides a cleft resistance of R_{cleft} of $(16 \pm 4) \Omega \cdot \text{cm}^2$ for the HEK293T-CRE-Luc-hH₁R cells devoid of the adhesion protein hMSR1. For the co-transfected cells expressing hMSR1, the calculation revealed a cleft resistance R_{cleft} of $(31 \pm 6) \Omega \cdot \text{cm}^2$. Under the plausible assumption that r_c and ρ are constant for both cell types (same cellular background, same culture medium), this difference in R_{cleft} translates in a reduction of the distance between cell membrane and surface d by approximately 50 %. Although this calculation is based on assumptions, the results further support the hypothesis of a shorter distance between the HEK293T-CRE-Luc-hH₁R-hMSR1 cells and the surface, improving RWG-based and to a minor degree impedance-based cellular assays.

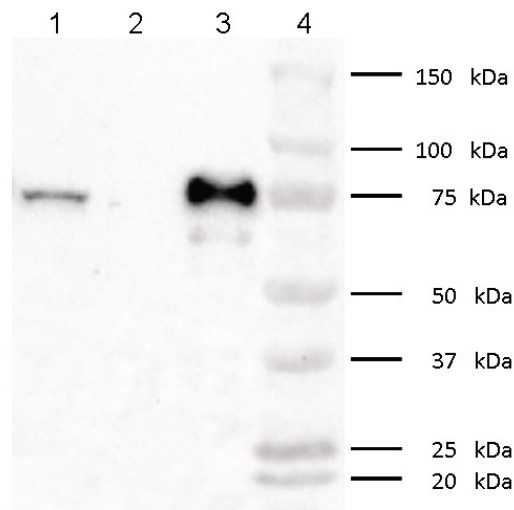
3.4 Conclusion

The present study has shown that the distance between cell and surface of the sensing devices directly affects the sensitivity of both, optical and impedance-based readouts. RWG- and SPR-based cell monitoring is particularly affected as measurements rely on dynamic mass redistribution within a few hundred nanometers away from the surface. In case that the distance between cell membrane and the growth surface exceeds the penetration depth of the evanescent field, the method becomes insensitive and eventually blind. Therefore, it is mandatory to control and, if necessary, to improve cell adhesion to the surface, as demonstrated by comparing HEK-293 cells expressing the H₁R alone or in combination with the adhesion protein hMSR₁. The results suggest that impedimetric and optical readouts are complementary. The combination of ECIS and SPR may be helpful in this respect as broadband impedance analysis allows deconvolution of the individual impedance contributions, providing indirect *in situ* information about the adhesion of the cells upon the sensor surface.

3.5 Appendix

3.5.1 Detection of hMSR1 expression in HEK293T-CRE-Luc-hH₁R-hMSR1 cells by immunoblotting

Figure A1 shows the result of an immunoblot analysis of cell lysates using an antibody against the human macrophage scavenger receptor 1 (hMSR1). As positive control, cell lysates were prepared from human epithelial cells derived from pancreas carcinoma PANC-1 which are known to express the hMSR1 receptor (lane 1). Lane 2 and 3 represent the immunoblot of cell lysates prepared from HEK293T-CRE-Luc-hH₁R (2) and HEK293T-CRE-Luc-hH₁R-hMSR1 cells (3). The band at 75 kDa clearly indicates that hMSR1 is strongly expressed by HEK293T-CRE-Luc-hH₁R-hMSR1, but not by HEK293T-CRE-Luc-hH₁R cells. This is in accordance with the fact that HEK293T-CRE-Luc-hH₁R-hMSR1 show improved adhesion to the growth surface compared to HEK293T-CRE-Luc-hH₁R.



- 1: PANC-1 (positive control)
- 2: HEK293T CRE Luc hH₁R
- 3: HEK293T CRE Luc hH₁R hMSR1
- 4: Mw marker

Figure A1: Immunodetection of hMSR1. Cell lysates prepared from PANC-1 (positive control, lane 1), HEK293T-CRE-Luc-hH₁R (lane 2) and HEK293T-CRE-Luc-hH₁R-hMSR1 cells (lane 3) were immunoblotted after SDS-PAGE using an anti-hMSR1 monoclonal antibody and a secondary detection antibody together with a molecular weight marker (right lane). hMSR1 is expressed by HEK293T-CRE-Luc-hH₁R-hMSR1 and PANC-1 cells but not by HEK293T-CRE-Luc-hH₁R cells.

3.5.2 SDS-PAGE and western blot

The expression of the human macrophage scavenger receptor (hMSR1) by HEK293T-CRE-Luc-hH₁R-hMSR1 cells was verified by immunoblotting. HEK293T-CRE Luc hH₁R hMSR1, HEK293T-CRE Luc hH₁R and PANC-1 cells (ATCC no. CRL-1469), grown in 75-cm² culture flasks (Sarstedt) to 80% confluency, were washed twice with ice-cold PBS and harvested by scraping after addition of ice-cold RIPA lysis buffer (20 mM TRIS pH=7.8; 200 mM NaCl; 1 mM EDTA; 1 mM EGTA; 1% Triton-X-100; 5 mM K₂HPO₄; 10 mM glycerol phosphate, supplemented with protease inhibitor mix (SIGMAFAST Protease Inhibitor cocktail tablets, Sigma)), and the samples were vortexed and centrifuged (13000 g, 4 °C, 10 min). The concentration of soluble protein was determined according to Bradford (Protein Assay from Bio-Rad Laboratories, Munich, Germany). An amount of 10 µg of total protein in sample buffer or 5 µL of a ready-to-use stained protein marker (Precision Plus Protein Dual Color Standard (BioRad)) were loaded per lane onto a SDS gradient gel (Novex 8–16% Tris-Glycine Gel, Fisher Scientific). The SDS-PAGE was performed at 140 V for about 1.5 h. The separated proteins were electroblotted to a nitrocellulose membrane (pore size 0.2 µm, Peqlab Biotechnologie, Erlangen, Germany) at 200 mA for 40 min (blotting buffer: Tris (0.3 g), glycine (1.4 g) ad 100 mL of water/MeOH (8:2 v/v)). To prevent unspecific binding, the membrane was incubated with Tris-buffered saline (20 mM Tris and 150 mM NaCl in water, pH 7.6) containing 1% of Tween-20 (in the following referred to as "TBST") and 5% skimmed milk powder at rt for 2 h. Subsequently, the membrane was incubated with the primary antibody (rabbit monoclonal anti-macrophage scavenger receptor 1 antibody (ab151707); abcam, Cambridge, UK), diluted 1:2500 with TBST + 2% (w/v) BSA (SERVA, Heidelberg, Germany) under rotation at 4 °C over night. The membrane was washed with TBST (4 × 20 min, rt) followed by incubation with the secondary antibody (donkey anti-rabbit IgG-HRP (sc-2313, Santa Cruz Biotechnology, Dallas, TX), diluted 1:10000 with TBST + 2% BSA, under shaking at rt for 1 h. Subsequently the membrane was washed with TBST (4 × 20 min, rt), and incubated with the substrate (Clarity Western ECI Substrate, BioRad) at rt for 1 min. The bioluminescence was detected with a ChemiDoc MP Imaging System (BioRad).

3.6 References

- 1 Jacoby E, Bouhelal R, Gerspacher M, Seuwen K. The 7 TM G-Protein-Coupled Receptor Target Family. *ChemMedChem* 2006;1:760-782.
- 2 Lagerstrom MC, Schioth HB. Structural diversity of G protein-coupled receptors and significance for drug discovery. *Nat Rev Drug Discov* 2008;7:339-357.
- 3 Penela P, Murga C, Ribas C, Tutor AS, Peregrín S, Mayor F. Mechanisms of regulation of G protein-coupled receptor kinases (GRKs) and cardiovascular disease. *Cardiovasc Res* 2006;69:46-56.
- 4 Albizu L, Moreno JL, González-Maeso J, Sealfon SC. Heteromerization of G Protein-coupled receptors: Relevance to neurological disorders and neurotherapeutics. *CNS Neurol Disord: Drug Targets* 2010;9:636-650.
- 5 Stone LS, Molliver DC. In search of analgesia: Emerging poles of GPCRs in pain. *Mol Interventions* 2009;9:234-251.
- 6 Sun L, Ye RD. Role of G protein-coupled receptors in inflammation. *Acta Pharmacol Sin* 2012;33:342-350.
- 7 Garland SL. Are GPCRs Still a Source of New Targets? *Journal of Biomolecular Screening* 2013;18:947-966.
- 8 Tautermann CS. GPCR structures in drug design, emerging opportunities with new structures. *Bioorg Med Chem Lett* 2014;24:4073-4079.
- 9 Kenakin TP. Cellular assays as portals to seven-transmembrane receptor-based drug discovery. *Nat Rev Drug Discov* 2009;8:617-626.
- 10 Schroder R, Janssen N, Schmidt J, Kebig A, Merten N, Hennen S, Muller A, Blattermann S, Mohr-Andra M, Zahn S, Wenzel J, Smith NJ, Gomeza J, Drewke C, Milligan G, Mohr K, Kostenis E. Deconvolution of complex G protein-coupled receptor signaling in live cells using dynamic mass redistribution measurements. *Nat Biotech* 2010;28:943-949.
- 11 Wegener J, Zink S, Roesen P, Galla H-J. Use of electrochemical impedance measurements to monitor b-adrenergic stimulation of bovine aortic endothelial cells. *Pfluegers Archiv - Eur J of Physiol* 1999;437:925-934.
- 12 Ciambone GJ, Liu VF, Lin DC, McGuinness RP, Leung GK, Pitchford S. Cellular dielectric spectroscopy: A powerful new approach to label-free cellular analysis. *J Biomol Screening* 2004;9:467-480.
- 13 Zink S, Rösen P, Sackmann B, Lemoine H. Regulation of endothelial permeability by β -adrenoceptor agonists: Contribution of β 1- and β 2-adrenoceptors. *Biochim Biophys Acta, Mol Cell Res* 1993;1178:286-298.
- 14 Cotton M, Claing A. G protein-coupled receptors stimulation and the control of cell migration. *Cellular Signalling* 2009;21:1045-1053.
- 15 Giaever I, Keese CR. Monitoring fibroblast behavior in tissue culture with an applied electric field. *Proc Natl Acad Sci U S A* 1984;81:3761-3764.
- 16 Robelek R, Wegener J. Label-free and time-resolved measurements of cell volume changes by surface plasmon resonance (SPR) spectroscopy. *Biosensors and Bioelectronics* 2010;25:1221-1224.
- 17 Scott CW, Peters MF. Label-free whole-cell assays: expanding the scope of GPCR screening. *Drug Discovery Today* 2010;15:704-716.
- 18 Michaelis S, Wegener J, Robelek R. Label-free monitoring of cell-based assays: Combining impedance analysis with SPR for multiparametric cell profiling. *Biosensors and Bioelectronics* 2013;49:63-70.

- 19 Matsumoto A, Naito M, Itakura H, Ikemoto S, Asaoka H, Hayakawa I, Kanamori H, Aburatani H, Takaku F, Suzuki H. Human macrophage scavenger receptors: primary structure, expression, and localization in atherosclerotic lesions. *Proc Natl Acad Sci U S A* 1990;87:9133-9137.
- 20 Robbins AK, Horlick RA. Macrophage scavenger receptor confers an adherent phenotype to cells in culture. *BioTechniques* 1998;25:240-244.
- 21 Nordemann U, Wifling D, Schnell D, Bernhardt G, Stark H, Seifert R, Buschauer A. Luciferase reporter gene assay on human, murine and rat histamine H₄ receptor orthologs: Correlations and discrepancies between distal and proximal readouts. *PLoS ONE* 2013;8:e73961.
- 22 Braun D, Fromherz P. Fluorescence interference-contrast microscopy of cell adhesion on oxidized silicon. *Appl Phys A* 1997;65:341-348.
- 23 Giaever I, Keese CR. Micromotion of mammalian cells measured electrically. *Proc Natl Acad Sci U S A* 1991;88:7896-7900.
- 24 Wegener J, Hakvoort A, Galla H-J. Barrier function of porcine choroid plexus epithelial cells is modulated by cAMP-dependent pathways in vitro. *Brain Research* 2000;853:115-124.
- 25 Müller M, Knieps S, Geßele K, Dove S, Bernhardt G, Buschauer A. Synthesis and Neuropeptide YY1 Receptor Antagonistic Activity of N,N-Disubstituted ω -Guanidino- and ω -Aminoalkanoic Acid Amides. *Arch Pharm (Weinheim)* 1997;330:333-342.
- 26 Fang Y. Non-Invasive Optical Biosensor for Probing Cell Signaling. *Sensors (Basel, Switzerland)* 2007;7:2316-2329.
- 27 Schrage R, Schmitz A-L, Gaffal E, Annala S, Kehraus S, Wenzel D, Büllsbach KM, Bald T, Inoue A, Shinjo Y, Galandrin S, Shridhar N, Hesse M, Grundmann M, Merten N, Charpentier TH, Martz M, Butcher AJ, Slodczyk T, Armando S, Efferm M, Namkung Y, Jenkins L, Horn V, Stöbel A, Dargatz H, Tietze D, Imhof D, Galés C, Drewke C, Müller CE, Hölzel M, Milligan G, Tobin AB, Gomeza J, Dohlman HG, Sondek J, Harden TK, Bouvier M, Laporte SA, Aoki J, Fleischmann BK, Mohr K, König GM, Tüting T, Kostenis E. The experimental power of FR900359 to study Gq-regulated biological processes. *Nature Communications* 2015;6:10156.
- 28 Yu N, Atienza JM, Bernard J, Blanc S, Zhu J, Wang X, Xu X, Abassi YA. Real-Time Monitoring of Morphological Changes in Living Cells by Electronic Cell Sensor Arrays: An Approach To Study G Protein-Coupled Receptors. *Analytical Chemistry* 2006;78:35-43.
- 29 Peters MF, Vaillancourt F, Heroux M, Valiquette M, Scott CW. Comparing label-free biosensors for pharmacological screening with cell-based functional assays. *Assay Drug Dev Technol* 2010;8:219-227.
- 30 Goldstein JL, Ho YK, Basu SK, Brown MS. Binding site on macrophages that mediates uptake and degradation of acetylated low density lipoprotein, producing massive cholesterol deposition. *Proceedings of the National Academy of Sciences of the United States of America* 1979;76:333-337.
- 31 Fraser I, Hughes D, Gordon S. Divalent cation-independent macrophage adhesion inhibited by monoclonal antibody to murine scavenger receptor. *Nature* 1993;364:343-346.
- 32 Greaves DR, Gordon S. The macrophage scavenger receptor at 30 years of age: current knowledge and future challenges. *Journal of Lipid Research* 2009;50:S282-S286.
- 33 Frenzel R, Voigt C, Paschke R. The human thyrotropin receptor is predominantly internalized by beta-arrestin 2. *Endocrinology* 2006;147:3114-3122.

4 Label-free versus conventional cellular assays: Functional investigations on the human histamine H₁ receptor

Note: Prior to submission of the thesis, parts of this chapter had been submitted for publication in cooperation with partners:

Lieb, S.; Littmann, T.; Plank, N.; Felixberger, J.; Tanaka, M.; Krief, S.; Elz, S.; Bernhardt, G.; Wegener, J.; Ozawa, T.; Buschauer, A.

Label-free versus conventional cellular assays: Functional investigations on the human histamine H₁ receptor

The following experiments were performed by co-authors:

M.T.: Generated hH₁R-split-luciferase and β -arrestin-split-luciferase constructs for the β -arrestin recruitment assay

J.F.: Established and performed β -arrestin recruitment assays (cf. J.F., PhD thesis, University of Regensburg, 2016)

T.L.: Performed β -arrestin recruitment assays with hH₁R agonists and antagonists

N.P.: Established luciferase gene reporter assay and performed gene reporter, aequorin calcium and radioligand competition binding assays.

4.1 Introduction

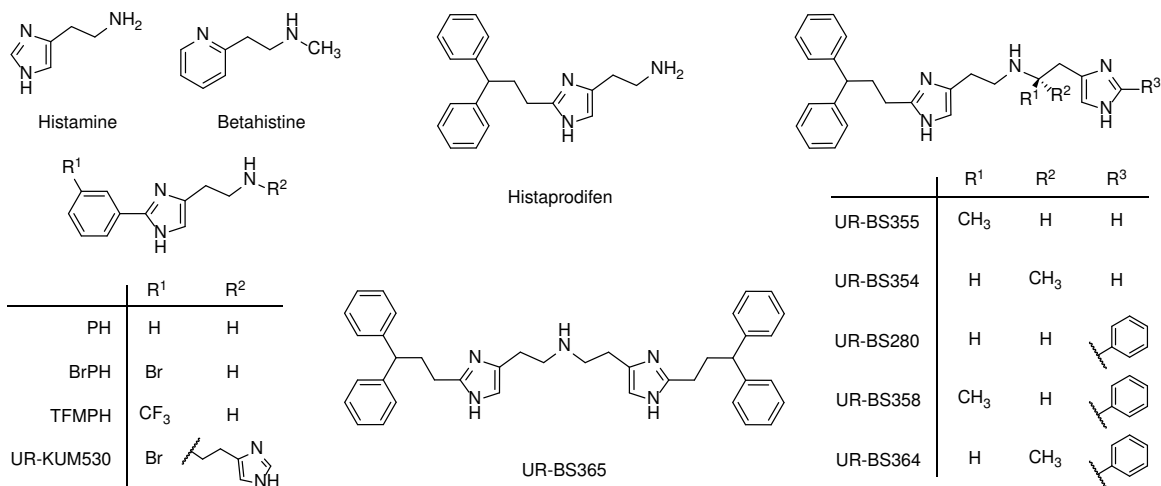
The discovery of the first ‘antihistamines’, later designated as histamine H₁ receptor (H₁R) [1] antagonists, in 1937 and the introduction of first generation antihistaminic drugs for the treatment of allergic conditions in the 1940s represent milestones in medicinal chemistry and drug research [2,3]. The success story of this well-established class of drugs was continued by the development of second generation H₁R antagonists with low central effects and reduced affinity to off-targets (for a recent review on histamine receptors and ligands cf. [4]). The identification and preclinical characterization of the first generation H₁R antagonists was based on holistic approaches, i. e., pharmacological investigations on isolated organs and proof-of-principle studies in experimental animals, e. g., guinea-pigs. Beginning with the feasibility of radioligand binding studies more than 30 years ago, there was increasing preference for reductionist over holistic approaches in the search for ligands of G protein-coupled receptors (GPCRs). Nowadays, appropriate techniques of biochemistry and molecular biology, e. g., the cloning and expression of receptors, methods for the identification and quantification of intracellular signals as well as the resolution of three-dimensional structures of the biological targets, enable the study of GPCRs at the cellular and even the molecular level. Functional assays are mainly performed on the human orthologue of the respective protein expressed in appropriate cells. However, receptor activation may not always result in a uniform cellular response [5]. Due to the complexity of signaling networks, the selection of an individual pathway, for example, the calcium or the cyclic AMP response, even though being considered characteristic of a given receptor, may be insufficient as a readout to describe the overall cellular effect. GPCRs can activate or inhibit different effectors in a ligand-specific manner, known as “functional selectivity” or “biased signaling” [6-12]. Being aware of the limitations of the assays relying on specific readouts, holistic cellular approaches should provide a more realistic picture of the overall response to a ligand-specific receptor-mediated stimulus. Optical and impedimetric methods such as dynamic mass redistribution (DMR; resonant waveguide grating, RWG) and electric cell-substrate impedance sensing (ECIS) are based on changes of the refractive index close to the surface or the electrochemical impedance of cell-covered electrodes, respectively [6,13-21]. As label-free techniques, DMR and ECIS are of special value for investigations on orphan receptors, but may also be very useful in case of well-known GPCRs such as the H₁R [22], for example, with respect to the

identification of multiple signaling pathways, i. e., responses beyond those considered in conventional assays [6,15-17,19,23-26].

The canonical signaling of the human H₁R implies mainly G_{q/11} protein mediated activation of phospholipase C, resulting in increased inositol-1,4,5-trisphosphate (IP3) and 1,2-diacylglycerol (DAG) levels, the mobilization of calcium ions from intracellular stores and multiple downstream effects depending on phosphorylation processes [4,27-30]. However, the H₁R was also reported to be capable of coupling to G-proteins other than G_{q/11}, i. e., to G_{i/o} [31-33] or G_s [34], and to induce cellular responses such as the activation of nuclear factor κB (NFκB) [35] via Gα_{q/11} and Gβγ. Moreover, the recruitment of β-arrestins and receptor internalization upon H₁R activation [36,37] as well as H₁R/arrestin mediated cellular signalling processes, e.g. MAPK activation [38,39] were described.

Taking into consideration the possible ligand-dependent functional selectivity, the complexity of the signaling machinery and the crosstalk within biochemical networks, the characterization of ligands in focused functional assays seems incomplete. To compare the the cellular effects of H₁R ligands depending on the type of readout using genetically engineered HEK293T cells, i. e., cells of an identical genetic background, we investigated a set of agonists and antagonists (Fig. 1) by DMR and ECIS in comparison to gene reporter (luciferase) assay, calcium assays (Fura-2 and aequorin), β-arrestin recruitment and radioligand competition binding.

Agonists



Antagonists

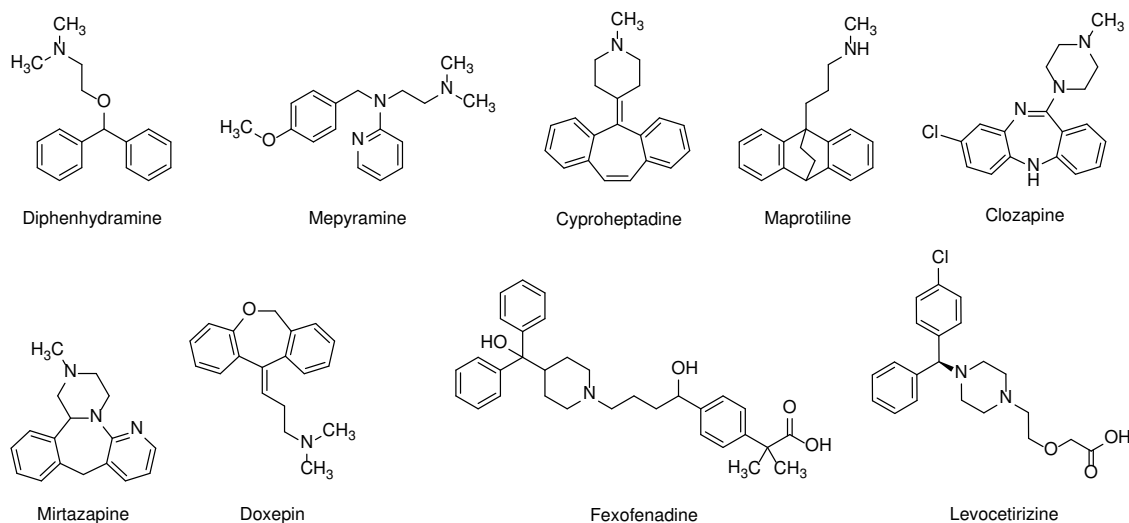


Fig. 1: Structures of compounds investigated at the human histamine H₁ receptor.

4.2 Materials and methods

4.2.1 Histamine receptor ligands

Histamine dihydrochloride was from Acros Organics (Geel, Belgium), betahistine dihydrochloride, diphenhydramine hydrochloride, cyproheptadine hydrochloride, maprotiline hydrochloride, fexofenadine hydrochloride and clozapine were from Sigma Aldrich (Taufkirchen, Germany), mepyramine maleate was from Tocris Bioscience (Ellisville, MO, USA), levocetirizine dihydrochloride and mirtazapine were from Biotrend (Cologne, Germany). UR-KUM530 [40], 2-phenylhistamine (PH), 2-(3-bromophenyl)histamine (BrPH) and 2-(3-trifluoromethylphenyl)histamine (TFMPH) [41,42], histaprodifen [43] and the analogues UR-BS280, -BS354, -BS355, -BS358, -BS364 and -BS365 [44] were synthesized as reported

previously. The stock solutions of agonists (10 mM) were prepared with Millipore water, except for the histaprodifen derivatives (30% DMSO). The stock solutions for antagonists (10 mM) were prepared in Millipore water, except for clozapine (stock solution in 0.1 M HCl) and fexofenadine (50% DMSO). In case that compound solutions were prepared with DMSO, the final DMSO concentration was kept below 0.5% in all assays. All stock solutions were stored at -20 °C. For label-free measurements, aliquots were thawed and diluted with Leibovitz' L-15 medium (Thermo Scientific, Darmstadt, Germany) without FCS. For Fura-2, aequorin Ca²⁺ and luciferase assay, aliquots were diluted with Millipore water.

4.2.2 Genetically engineered cells and culture conditions

4.2.2.1 HEK293T-CRE-Luc-hH1R and HEK293T-CRE-Luc-hH1R-hMSR1 cells

Human embryonic kidney (HEK293T) cells stably expressing the firefly luciferase under the control of the cyclic AMP response element (CRE) [45] were stably co-transfected with pcDNA3.1(+)-hH₁R, encoding the human H₁R, and pIRESpuro3/hMSR1, encoding the human macrophage scavenger receptor [46], and maintained as published recently (HEK293T-CRE-Luc-hH1R-hMSR1 cells) [20].

4.2.2.2 HEK293T-CRE-Luc-hH1R-mtAEQ cells

To obtain cells expressing mitochondrially tagged aequorin (HEK293T-CRE-Luc-hH₁R-mtAEQ cells), HEK293T-CRE-Luc-hH₁R cells were stably co-transfected with the pcDNA3.1/zeo-mtAEQ plasmid. The medium was removed 24 h after transfection, and the cells were transferred in a 75-cm² culture flask with DMEM supplemented with 10 % FCS. Selection was started the next day by adding medium containing hygromycin (250 µg/mL), G418 (600 µg/mL) and zeocin (40 µg/mL) (Thermo Fisher Scientific, Rockford, IL, USA).

4.2.2.3 HEK293T-ARRB1-H1R and HEK293T-ARRB2-H1R cells for the hH1R-β-arrestin luciferase fragment complementation assay

The fusion construct of the human H₁R (the hH₁R cDNA was from cDNA Resource Center, Bloomsburg, PA, USA) and the C-terminal luciferase fragment (H1R-ELucC) was generated using the previously described construct SSTR2-ELucC [47] by replacing the cDNA of SSTR2 by the cDNA of the H₁R. HEK293T cells were stably transfected with the pcDNA3.1/myc-HIS (B)

vector encoding a β -arrestin isoform (1 or 2) N-terminally fused with the N-terminus of a green click-beetle luciferase (ELucN-ARRB1 or ELucN-ARRB2, respectively) [47], and the pcDNA4/V5-HIS (B) vector encoding H1R-ELucC (Fig. S1, Supporting Information). Cells transfected with pcDNA3.1/myc-HIS (B) were cultivated in the presence of 600 $\mu\text{g}/\text{mL}$ G418 for up to 3 weeks until stable growth was observed. For the cells co-transfected with the pcDNA4/V5-HIS (B) vector encoding H1R-ELucC, 40 $\mu\text{g}/\text{mL}$ zeocin was used. To determine the H1R-ELucC expression, western blot analyses (cf. Fig. S1, Supporting Information) and saturation binding studies were performed with both HEK293T-ARRB1-H₁R cells and HEK293T-ARRB2-H₁R cells using [³H]mepyramine (cf. Fig. S2, Supporting Information).

4.2.3 Radioligand competition binding assay

HEK293T-CRE-Luc-hH₁R cells were grown in a 75-cm² flask to a confluency of around 80%. The cells were detached with 5 mL of trypsin and resuspended in 5 mL Leibovitz' L-15 medium. After centrifugation, the cells were resuspended in L-15 medium. The assays were performed in the presence of 5 nM [³H]mepyramine (Hartmann Analytic, Braunschweig, Germany), specific activity 20 Ci/mmol, $K_d = 4.5$ nM, $c = 5$ nM; nonspecific binding was determined in the presence of 10 μM of diphenhydramine hydrochloride (Sigma, Deisenhofen, Germany). Samples containing Leibovitz' L-15 medium, test compound (final concentration in the range from 0.1 nM to 10 μM), radioligand, and HEK293T-CRE-Luc-hH₁R cells (at a density of 1 million cells/mL), were incubated at room temperature and shaken at 250 rpm for 60 min. Filtration through glass microfiber filters (Whatman GF/C), pretreated with poly(ethylenimine) (0.3%, w/v), using a Brandel 96 sample harvester, separated unbound from cell-associated [³H]mepyramine. After three washing steps with buffer (Tris, 75 mM, adjusted to pH 7.4 with HCl; MgCl₂, 12.5 mM; EDTA, 1 mM), filter pieces were punched and transferred into 96-well sample plates 1450-401 (PerkinElmer, Rodgau, Germany). A volume of 200 μL of scintillation cocktail (Rotiscint Ecoplus, Roth, Karlsruhe, Germany) was added per well before incubation in the dark under shaking at 200 rpm. Radioactivity was measured with a Micro Beta2 1450 scintillation counter. Ligands were tested in at least three independent experiments each performed in triplicate.

4.2.4 Aequorin calcium assay

The assay was essentially performed as described previously for neuropeptide Y (NPY) Y₄ receptor ligands [48]. HEK293T-CRE-Luc-hH₁R-mtAEQ cells were detached with trypsin/EDTA and DMEM without phenol red and centrifuged at 300 g for 10 min. The cell suspension was adjusted to a density of 10 million cells/mL in DMEM without phenol red, and coelenterazin (Biotrend) was added, so that the final concentration was 2 μM. The suspension was incubated in the dark for 2 h. The cell suspension was diluted 1:20 with loading buffer (HEPES (Serva, Heidelberg, Germany), 25 mM; NaCl, 120 mM; KCl, 5 mM; MgCl₂, 2 mM; CaCl₂, 1.5 mM; glucose 10 mM; pH was adjusted to 7.4), and the suspension was incubated in the dark under gentle stirring for additional 3 h. In the agonist mode, 18 μL of a 10-fold concentrated solution of the test compound in loading buffer were added per well of a white 96-well plate (Greiner, Frickenhausen, Germany), and luminescence was measured for 43 s with a GENios Pro microplate reader after injecting 162 μL of the cell suspension. Subsequently, 20 μL of a 1 % Triton 100-X solution were injected, and light emission was recorded for additional 22 s. In the antagonist mode, 2 μL (100-fold concentrated) of the respective antagonist solution were incubated with 178 μL of the cell suspension for 15 min. Luminescence was measured after injecting 20 μL of agonist solution (10-fold concentrated) for 43 s and, subsequently, after addition of 20 μL of a 1 % Triton X-100 for additional 22 s. The fractional luminescence was calculated by dividing the area of the first peak (injection of the cell suspension, respectively agonist solution) by the sum of the areas of peak 1 and peak 2 (Triton X-100 injection) using Sigma Plot 11.0 software.

4.2.5 Fura-2 calcium assay

The assay was essentially performed as described for NPY Y₁ receptor ligands [49]. After detachment of the cells with trypsin/EDTA, the cells were suspended in DMEM containing 5% FCS and centrifuged at 300 g for 10 min. The medium was discarded, and the cells were resuspended in DMEM and counted. To three volumes of the cell suspension, prepared in loading buffer (HEPES (Serva), 25 mM; NaCl, 120 mM; KCl, 5 mM; MgCl₂, 2 mM; CaCl₂, 1.5 mM; glucose 10 mM; pH was adjusted to 7.4), one volume of loading dispersion (1 mL of loading dispersion contained: 2 % BSA (Serva); 5 μL of Pluronic (Sigma); 4 μL of Fura-2 (VWR, Ismaning, Germany) was added, so that the final cell density was 1.0 mio cells per mL. The suspension

was incubated in the dark for 30 min. Thereafter, the suspension was centrifuged, the cells were resuspended in loading buffer and allowed to stand in the dark for another 30 min. The cells were washed twice with loading buffer and adjusted to a final density of 1.0 mio cells per mL. The assay was performed either in acrylic cuvettes (VWR) using an LS50 B spectrofluorimeter (Perkin Elmer) [49] or in transparent 96-well microplates (Greiner) using a GENios Pro microplate reader [50]. Assays in the antagonist mode were always performed in cuvettes, and the cells were preincubated with the respective antagonist for 15 min.

4.2.6 Luciferase gene reporter assay

The assay was essentially performed as previously described for the histamine H₄ receptor [45]. One day prior to the experiments, the HEK293T-CRE-Luc-hH₁R cells were adjusted to a density of approximately 800,000 per mL in DMEM without phenol red (Sigma Aldrich) supplemented with 5 % FCS. 160 µL of the cell suspension were seeded into flat bottom 96-well plates (Greiner) per well. The cells were allowed to attach overnight. In the antagonist mode, the hH₁R was stimulated by 300 nM histamine in the presence of the test compound. In the agonist mode, the H₁R was activated by 20 µL of a 10 fold concentration of the respective compound. To obtain a volume of 200 µL per well 20 µL of DMEM were added. All wells contained the same amount of DMSO or water. The medium was discarded, and 80 µL of lysis buffer (25 mM Tricine (Sigma Aldrich); Glycerol 10 % (v/v) (Merck); EGTA, 2 mM (Sigma Aldrich); 1 % (v/v) Triton™ X-100 (Serva); MgSO₄ × 7 H₂O, 5 mM (Merck); DTT, 1 mM (Sigma), the pH was adjusted to 7.8 with HCl) were added to each well. The plates were shaken at 600 rpm for 15 min. Afterwards, 40 µL of the lysate were transferred into white 96-well plates (Greiner). Luminescence was measured with a GENios Pro microplate reader (Tecan, Salzburg, Austria). Light emission was induced by injecting 80 µL of the assay buffer (25 mM Gly-Gly, (Sigma Aldrich); MgSO₄ × 7 H₂O, 15 mM; KH₂PO₄, 15 mM (Merck); EGTA, 4 mM; ATP disodium salt, 2 mM (Sigma Aldrich); DTT, 2 mM; D-luciferin potassium salt, 0.2 mg/mL (Synchem, Felsberg, Germany); pH was adjusted to 7.8 with HCl). Luminescence [51] was measured for 10 s. To determine the effect of pertussis toxin (PTX) cells were seeded in medium containing 0.5 µg/mL PTX. For experiments in the presence of FR900359 (1 µM and 10 µM) or gallein (Santa Cruz Biotechnology, Heidelberg, Germany) (20 µM, stock solution: 10 mM in DMSO), cells were pre-incubated with the Gα_q inhibitor or the Gβγ inhibitor for 2 h.

4.2.7 β -Arrestin recruitment assay

One day before the experiment, HEK293T-ARRB1-H₁R and HEK293T-ARRB2-H₁R cells were trypsinized (0.05% trypsin, 0.02% EDTA in PBS) and centrifuged (400 g, 5 min). The cells were resuspended in DMEM without phenol red (Sigma, Steinheim, Germany) supplemented with 5% FCS, and 90 μ L of the cell suspension were seeded in white, TC-treated, flat bottom 96-well microtiter plates (VWR, Ismaning, Germany) at a density of approximately 100,000 cells/well. The cells were cultivated at 37 °C overnight in a water-saturated atmosphere containing 5% CO₂. Shortly before the experiment, the cells were removed from the incubator and allowed to equilibrate to room temperature, and 10 μ L of agonist solution were added per well. The plates were shaken at 25 °C for 60 min. In the antagonist mode, prior to addition of the agonist, cells were incubated with the respective antagonist for 15 min. At the end of the incubation period, 50 μ L of medium were replaced by 50 μ L of Bright-Glo luciferase assay reagent (Promega, Mannheim, Germany). The plates were vigorously shaken (800 rpm) for 5 min. Bioluminescence was recorded for 1 s per well using the GENios Pro microplate reader (Tecan, Salzburg, Austria).

4.2.8 Impedimetric assay

For the investigation of H₁R agonists on HEK293T-CRE-Luc-hH₁R-hMSR1 cells, the assay was performed as recently described for histamine [20] using an ECIS-Z device for 96-well electrode arrays (type 96W1E+) from Applied BioPhysics (Troy, NY, USA). A volume of 300 μ L of cell suspension, prepared in DMEM containing 10% FCS from close-to-confluent cell layers by standard trypsinization techniques, was dispensed at a density of $9 \cdot 10^4$ cells per well. The cells were allowed to attach in a CO₂ incubator at 37 °C for 24 h. About 1 h before the assay the culture medium was replaced by 150 μ L of serum-free L-15 medium. Data were recorded with the ECIS device inside an incubator (Galaxy 48S, New Brunswick, USA) in a humidified atmosphere (without additional CO₂) at 37 °C at an AC frequency of 4 kHz for 1 h until the baseline was constant (equilibration), and for another 40 min after addition of the agonist at various concentrations. For data handling cf. [20].

For the determination of H₁R antagonist activities, after equilibration for 1 h, 150 μ L a solution of the respective antagonist was added to the cells for an incubation period of about 20 min. Subsequently 150 μ L of the antagonist containing solution was replaced by the same volume

of L-15 medium containing the antagonist at the same concentration and 60 nM of histamine to obtain a final agonist concentration of 30 nM, which is known to elicit 80% of the maximal response in the absence of an antagonist.

The effect of pertussis toxin (PTX) was determined in the agonist mode using cells pretreated with 1, 10 or 100 ng/mL PTX in DMEM supplemented with 10% FCS for about 20 h. About 1 h before the assay the culture medium was replaced by 150 μ L of serum-free L-15 medium and the assay was performed as described above. To investigate the effect of UBO-QIC, by analogy with the antagonist mode, cells were preincubated in the presence of the $G\alpha_q$ inhibitor at final concentrations of 0.1, 1 or 10 μ M for 20 min.

4.2.9 Dynamic mass redistribution assay

The assay was performed in the agonist mode as previously described for histamine on HEK293T-CRE-Luc-hH₁R-hMSR1 cells [20] using an EnSpire (PerkinElmer, Waltham, USA) multimode reader. A volume of 40 μ L of cell suspension, prepared from close-to-confluent cell layers by standard trypsinization, in DMEM containing 10% FCS was dispensed at a density of $2 \cdot 10^4$ cells per well into uncoated 384-well EnSpire microplates. Incubation in a humidified atmosphere containing 5% CO₂ at 37 °C for 24 h provided cell layers of approximately 90 % confluency. The cells were washed four times with serum-free L-15 medium and allowed to equilibrate in a volume of 30 μ L of the same medium per well in the multimode reader at 37 °C for about 1 h. After recording the baseline, the agonist of interest, dissolved in L-15 medium (10 μ L) was added, the cellular response was recorded for 40 min and data analysis was performed as described [20].

In the antagonist mode, after equilibration in 30 μ L of medium per well for 1 h, a solution of the respective antagonist in 10 μ L of serum-free L15 medium was added, and the incubation was continued for 20 min. Subsequently, another 10 μ L of antagonist at the same concentration containing additionally 500 nM of histamine to obtain a final agonist concentration of 100 nM, which is known to elicit 80% of the maximal response in the absence of an antagonist.

The effect of pertussis toxin (PTX) was determined in the agonist mode using cells pretreated with 1, 10 or 100 ng/mL PTX in DMEM supplemented with 10% FCS for about 20 h. The cells

were washed four times with serum-free L-15 medium and the assay was performed as described above. Experiments in the presence of FR900359 (UBO-QIC) were performed according to the antagonist mode with the exception that instead of antagonist the $G\alpha_q$ inhibitor was added at final concentrations of 0.1, 1 or 10 μM .

4.2.10 Data analysis

The data were analyzed with GraphPad Prism 5.01 (GraphPad Software, San Diego, USA) and fitted to four-parameter sigmoidal concentration-response curves providing EC_{50} values of agonists and IC_{50} values of antagonists. For antagonists, pK_b values were calculated from IC_{50} values according to the Cheng-Prusoff equation [52].

4.3 Results and discussion

4.3.1 Functional characterization of H_1 receptor agonists

Changes of the resonance wavelength of cell-covered optical waveguides (resonance waveguide = RWG), recorded in DMR, or of the impedance of cell-covered electrodes, measured in ECIS, reflect alterations in the cytoskeletal framework [53-55]. As demonstrated in a recent study, cell adhesion to the surface is a critical issue in such label-free assays [20]. The DMR assay reports on changes in mass distribution *inside* the cell close to the growth surface or *outside* the cell in the narrow cleft between cell and substrate. Mass redistribution and cell shape changes may be connected in the way that mass redistribution induces cell shape changes or vice versa, although difficult to prove or disprove. It is reasonable to assume that the signal is dominated by dynamic processes that occur *in* the actin cortex or by remodeling *of* the actin cortex at the membrane in the vicinity of the growth support [53-55]. It is noteworthy in this context that the actin cortex is 100 to 1000 nm thick dependent on cell-type but DMR is only sensitive within 200-300 nm from the substrate surface. The actin cortex is not necessarily the exclusive origin for any DMR signal since relocation of other (even extracellular) (macro)molecules that are not linked to the actin cortex or the membrane can cause similar DMR signals. This is different from ECIS which is insensitive to mass redistribution but reflects changes in the ionic current pathways around or across the dielectric lipid bilayer, primarily associated with alterations in cell morphology. Due to the intimate molecular

contact between the plasma membrane lipid bilayer and the adjacent actin cortex, changes in the position of the membrane are invariably associated with a concomitant relocation of the actin cortex so that both readout techniques often but not always report on similar phenomena. Thus, some cellular responses leading to mass redistribution but not to changes in the position of the membrane relative to the growth support are visible in DMR but not in ECIS and the information gained from both readouts is not identical but complementary .

Therefore, we performed both, DMR and ECIS, with HEK293T-CRE-Luc cells engineered to co-express the human histamine H₁ receptor and the human macrophage scavenger receptor 1 (hMSR1) [56], to improve adhesion as described previously [20]. Both label-free assays were performed under similar conditions, e. g., with respect to temperature, cell-culture medium and equilibration-time. Typical time courses and the resulting concentration-response curves are shown in Fig. 2 for histamine as an example. The transient dip of the impedimetric signal observed immediately after addition of the agonist is considered characteristic of G_q coupling [29] allowing for a discrimination from G_i coupling.

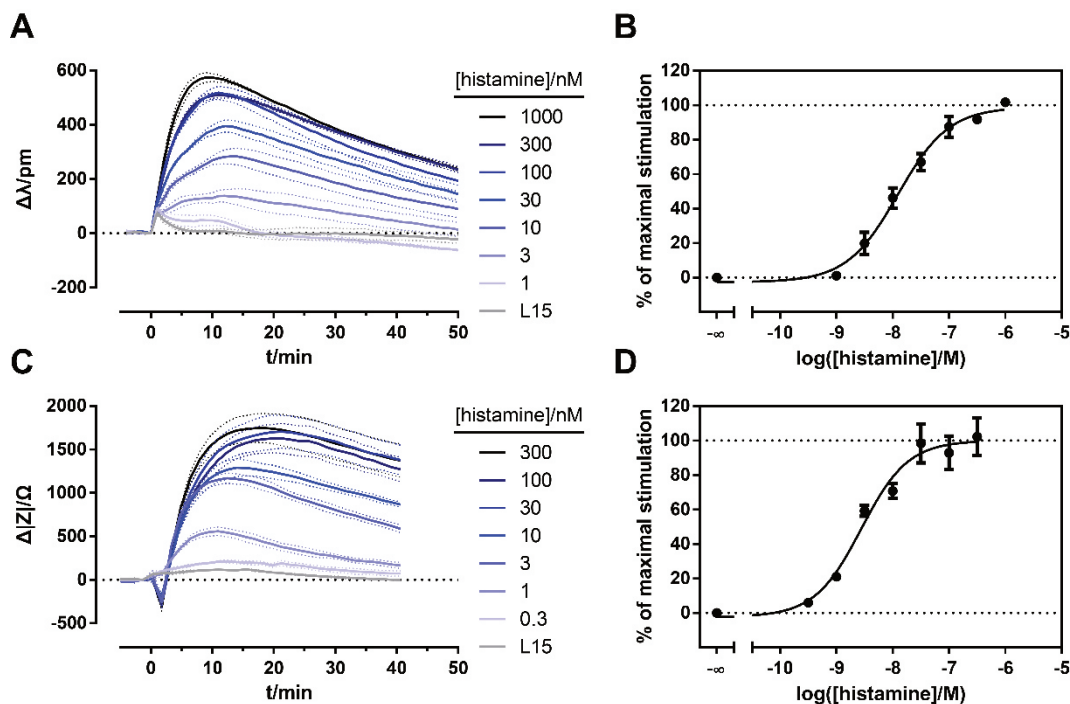


Fig. 2: Histamine induced response of HEK293T-CRE-Luc-hH₁R-hMSR1 cells monitored by DMR (A, B) and ECIS (C, D). Typical time courses (triplicates) of the change of the resonance wavelength (A) and the change in impedance $\Delta|Z|$ recorded at 4 kHz (C). Concentration-response curves (B, D) were derived from the corresponding area-under-the-curve (AUC) of baseline-corrected data integrated from 0 to 40 min.

The DMR signal at the highest histamine concentration peaks after an exposure time of approximately 10 min, whereas the ECIS signal is retarded and peaks between 15 and 20 min after histamine addition. Moreover, the time needed for a maximum response decreases with concentration in DMR but increases with concentration in ECIS. This may be interpreted as a hint that an agonist-induced mass redistribution precedes cell shape changes, at least at higher histamine concentrations. Alternatively, both signals imply different processes downstream from receptor activation according to individual kinetics.

The construction of concentration-response curves revealed pEC₅₀ values of 7.49 ± 0.08 and 7.92 ± 0.16 for histamine in the DMR assay and ECIS, respectively. Comparing the data summarized in Table 1 and visualized in Fig. 3, the apparent potencies of histamine differ by up to a factor of approximately 10, depending on the type of assay. The highest pEC₅₀ values of histamine was determined in the impedance-based (7.92) and the β -arrestin2 recruitment assay (7.74), whereas the luciferase gene reporter and the Fura-2 calcium assay yielded the lowest potency (pEC₅₀ = 6.87).

4.3 Results and discussion

Table 1.: hH1R agonism determined in different functional assays using genetically engineered HEK293T cells^{a,b}. For comparison published functional data from [32P]GTPase assays^c are included.

	gene reporter (luciferase)		β-arrestin1 recruitment		β-arrestin2 recruitment		Ca ²⁺ (Fura-2 AM)		Ca ²⁺ (aequorin)		DMR		impedimetry		GTPase [40,57,58]	
	<i>pEC</i> ₅₀	<i>E</i> _{max}	<i>pEC</i> ₅₀	<i>E</i> _{max}	<i>pEC</i> ₅₀	<i>E</i> _{max}	<i>pEC</i> ₅₀	<i>E</i> _{max}	<i>pEC</i> ₅₀	<i>E</i> _{max}	<i>pEC</i> ₅₀	<i>E</i> _{max}	<i>pEC</i> ₅₀	<i>E</i> _{max}	<i>pEC</i> ₅₀	<i>E</i> _{max}
histamine	6.87 ± 0.06	1.00	7.11 ± 0.1	1.00	7.74 ± 0.08	1.00	6.87 ± 0.06	1.00	6.94 ± 0.15	1.00	7.49 ± 0.08	1.00	7.92 ± 0.16	1.00	6.92 [57]	1.00
UR-KUM530	7.49 ± 0.08	1.05 ± 0.03	7.46 ± 0.03	0.91 ± 0.08	7.97 ± 0.23	0.99 ± 0.06	6.94 ± 0.02	0.99	7.61 ± 0.06	1.03 ± 0.01	7.99 ± 0.09	1.12 ± 0.03	8.60 ± 0.11	1.15 ± 0.05	7.75 [40]	0.94
betahistine	6.56 ± 0.25	0.96 ± 0.02			7.48 ± 0.04	0.80 ± 0.01	n.d.	-	6.69 ± 0.13	0.96 ± 0.02	6.29 ± 0.17	0.71 ± 0.06	7.59 ± 0.08	0.25 ± 0.03	5.85 [58]	0.86
PH	5.12 ± 0.15	0.56 ± 0.01	5.25 ± 0.10	0.51 ± 0.03	6.15 ± 0.09	0.67 ± 0.04	n.d.	-	n.d.		6.39 ± 0.17	0.50 ± 0.03	7.59 ± 0.33	0.11 ± 0.03	6.14 [40]	0.72
BrPH	5.46 ± 0.17	0.56 ± 0.05	5.99 ± 0.03	0.43 ± 0.01	6.49 ± 0.01	0.63 ± 0.02	5.90 ± 0.07	0.66	n.d.		n.d.		n.d.		6.75 [40]	0.62
TFMPH	5.81 ± 0.06	0.62 ± 0.02	5.68 ± 0.06	0.38 ± 0.01	6.73 ± 0.10	0.55 ± 0.06	n.d.	-	n.d.		6.56 ± 0.15	0.71 ± 0.03	7.16 ± 0.18	0.62 ± 0.12	6.71 [40]	0.61
histaprodiven			5.85 ± 0.02	0.46 ± 0.01	6.48 ± 0.12	0.47 ± 0.06	n.d.	-	n.d.		n.d.		n.d.		6.95 [57]	0.62

^a Experiments were performed using HEK293T cells expressing hH₁R and additional constructs: luciferase gene reporter: HEK293T-CRE-Luc-hH₁R cells; β-arrestin recruitment assay: HEK293T-ARRB1-H₁R and HEK293T-ARRB2-H₁R cell; Fura-2 calcium assay: HEK293T hH₁R CRE-Luc cells; aequorin calcium assay: HEK293T-CRE-Luc-hH₁R-mtAEQ cells; DMR and impedimetry (ECIS): HEK293T-CRE-Luc-hH₁R-hMSR1 cells.

^b Data represent mean values ± SEM from at least three independent experiments performed in triplicate, except for UR-KUM530 and BrPH in the Fura-2 AM Ca²⁺-assay and BrPH and TFMPH in the gene reporter assay, which were analyzed in two independent experiments performed in triplicate; n.d., not determined; n.a., not applicable.

^c Determined on membranes of hH₁R expressing Sf9 cells. For hH₁R binding data determined on membranes of Sf9 cells cf. [40,57].

4.3.2 Cellular response to H₁R agonists in various assays

To investigate, whether activation of the H₁R by ligands other than histamine provides different assay-related pEC₅₀ values as well, we selected the agonists shown in Fig. 1 for functional studies. All agonists included in this study preferentially induced the recruitment of β -arrestin2 over the β -arrestin1 isoform as generally observed for class A GPCRs [59]. Unfortunately, it turned out that not all of these compounds are compatible with the different assay conditions. In particular, the histaprodifen analogues [57], designated UR-BS compounds in the present study, caused cytotoxic effects at concentrations >1 μ M (for cytotoxicity of selected compounds cf. Figure S3, Supporting Information), most probably due to their amphiphilic nature. Although the β -arrestin recruitment assays revealed partial agonism in the expected concentration range (cf. Table S1, Supporting Information), attempts to characterize such compounds in ECIS and in the Fura-2 calcium assay using U373 MG cells [20] as well as in the luciferase gene reporter assays failed (data not shown). In contrast to the UR-BS compounds, the phenylhistamine derivative UR-KUM530 [40] proved to be non-toxic up to a concentration of 100 μ M (cf. Figure S3A, Supporting Information), allowing for the determination of pEC₅₀ values in both, the label-free and the conventional assays. As becomes obvious from Fig. 3 and Table 1, UR-KUM530 is more potent than histamine in all assays and seems to be a superagonist in both, the impedimetric and the DMR assay. Interestingly, the concentration-response curve from ECIS is exceptionally steep, resulting in about 30-fold higher potency than in the Fura2 assay. The time course of the impedimetric signal was similar to that of histamine with regard to the initial dip and the subsequent rise, suggesting G_q coupling (data not shown) for this compound, too. By contrast, the investigation of betahistine revealed completely different concentration-response curves (Fig. 3): full agonism in the aequorin calcium and the luciferase gene reporter assay (E_{\max} : 0.96), but only partial agonism in β -arrestin2 recruitment (E_{\max} : 0.80), DMR (E_{\max} : 0.71) and, in particular, in the impedimetric assay (E_{\max} : 0.25). The extremely low intrinsic activity observed in the ECIS assay cannot be explained. Regardless of the weak increase in $\Delta|Z|$, a transient dip of the signal was observed (data not shown). The agonist potency of betahistine was lowest in the DMR and highest in the arrestin recruitment assay.

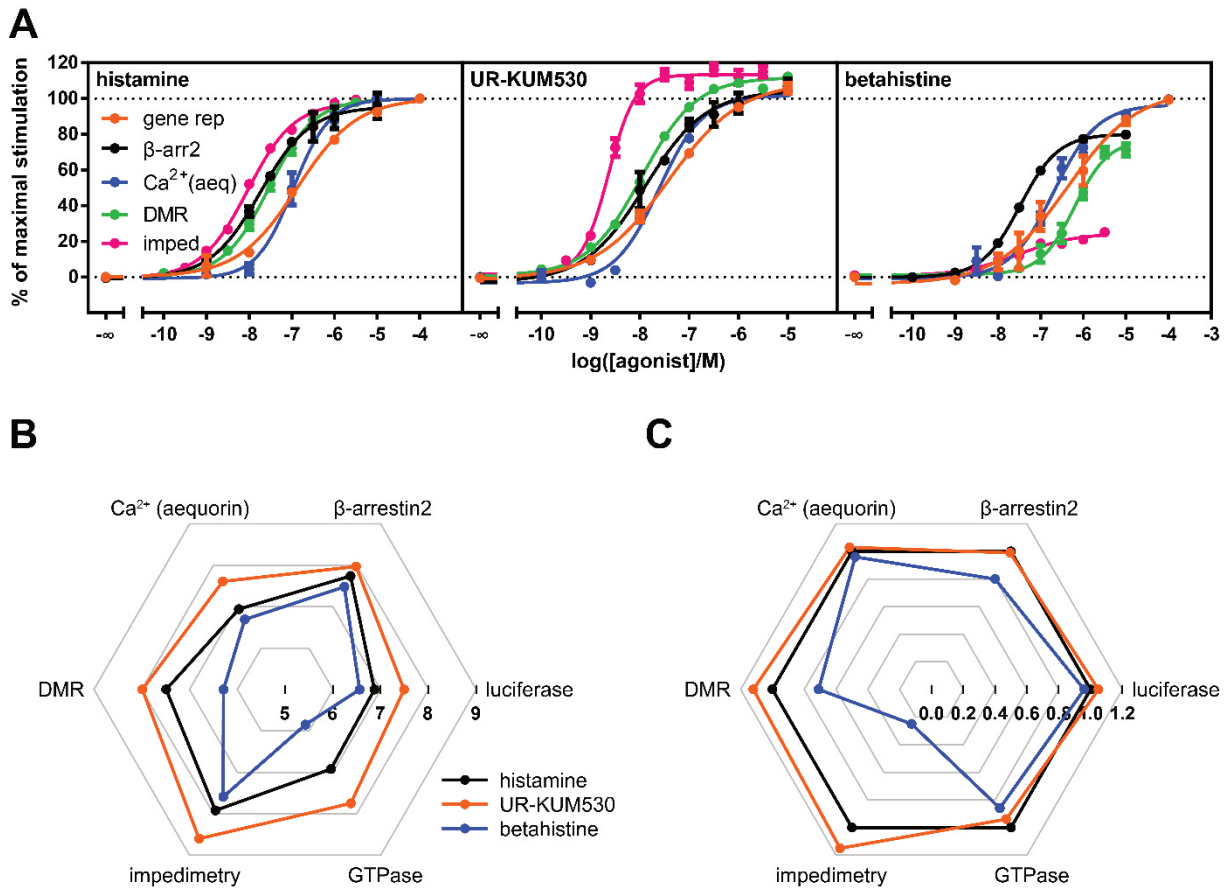


Fig. 3: Assay-dependent concentration-response curves of histamine, UR-KUM530 and betahistine (A). Radar plots representing pEC₅₀ values (B) and efficacies (C). Experiments were performed using HEK293T cells expressing the hH₁R and additional constructs: gene rep (luciferase gene reporter assay): HEK293T-CRE-Luc-hH₁R cells; β arr2: (β -arrestin2 recruitment assay): HEK293T-ARRB2-H₁R cells; Ca²⁺(aeq) (aequorin calcium assays): HEK293T-CRE-Luc-hH₁R-mtAEQ cells; DMR and ECIS: HEK293T-CRE-Luc-hH₁R-hMSR1 cells. Data were normalized to a solvent control and the maximal response to the endogenous ligand histamine in the respective assay. Data represent mean \pm SEM from at least three independent experiments performed in triplicate.

Potencies and intrinsic activities can increase as a function of receptor density [60]. In cells of one and the same genetic background (HEK293T-CRE-Luc-hH₁R for calcium, luciferase gene reporter, DMR and impedance-based functional assays) our data illustrate that the measured potencies and maximal responses vary depending on both, the readout and the chemical structure of the agonist. This becomes obvious from concentration-response curves and, in particular, from the radar plot in Fig. 3. The potencies of histamine and UR-KUM530 in the luciferase gene reporter assay were similar to those obtained in assays exploiting the GTPase activity as a proximal readout (Table 1). The efficacy of UR-KUM530 was the same as that of histamine except for both label-free assays, which gave a slightly higher maximal response

(Fig. 3). This might be interpreted as “superagonism” [61] related to different binding modes of histamine and UR-KUM530 [40], resulting in a differential activation of signaling pathways. The response to UR-KUM530 was completely inhibited by diphenhydramine (100 μ M) or mepyramine (10 μ M) in both assays, DMR and ECIS, confirming that the effects were H₁R mediated (data not shown). The pK_b values determined from the corresponding inhibition curves were 7.68 ± 0.24 and 8.48 ± 0.44 in ECIS and 7.07 ± 0.11 and 8.64 ± 0.32 in DMR for diphenhydramine and mepyramine, respectively, which is comparable to the respective values determined versus histamine as agonist (Table 1).

The assay-dependent differences regarding pEC₅₀ and E_{max} values observed for all agonists under study are difficult to explain, as not all assays can be performed under identical conditions. However, the order of potency of agonists was consistent between the noninvasive and the canonical assays.

4.3.3 Investigation of G protein coupling

To investigate the contribution of G_{i/o} and G_{q/11} proteins we constructed concentration-response curves of histamine and UR-KUM530 in the presence of pertussis toxin (PTX) [31] or the cyclic depsipeptide FR900359 (UBO-QIC) [62,63], respectively.

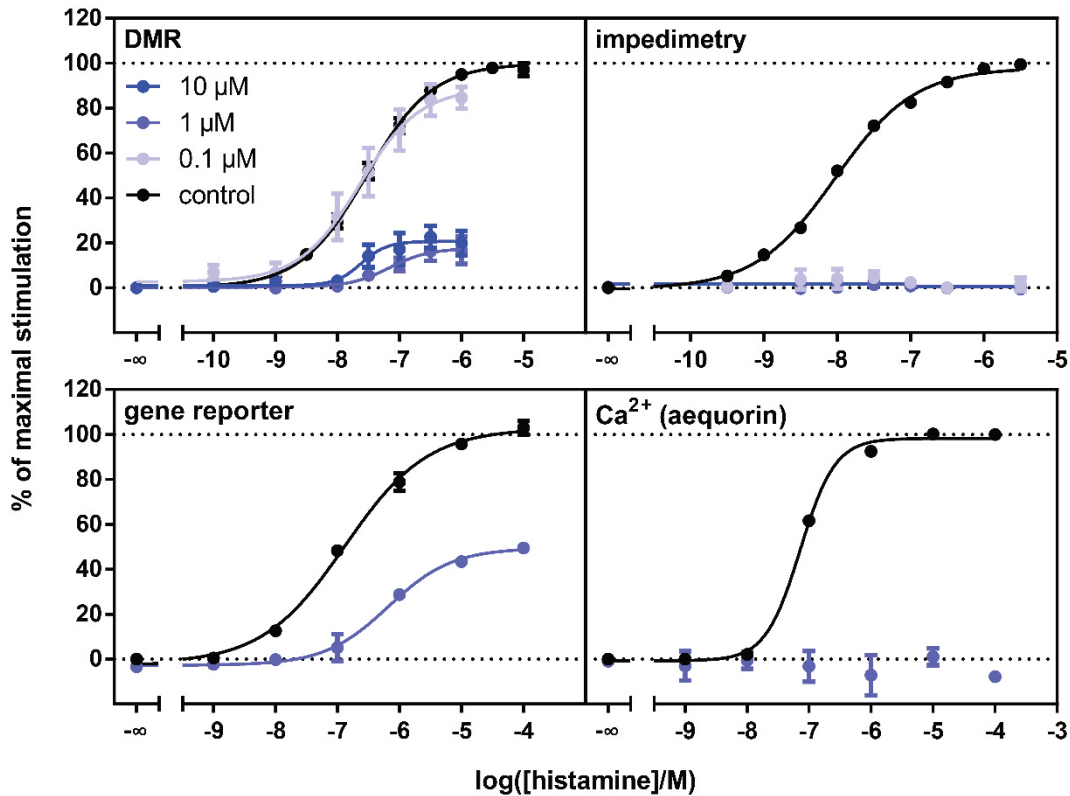


Fig. 4: Effect of the G_q -inhibitor FR900359 on the histamine-induced response in DMR, ECIS, gene reporter and Ca^{2+} (aequorin) assays. Experiments were performed using HEK293T cells expressing hH₁R and additional constructs: DMR and ECIS: HEK293T-CRE-Luc-hH₁R-hMSR1 cells; luciferase gene reporter: HEK293T-CRE-Luc-hH₁R cells; aequorin calcium assay: HEK293T-CRE-Luc-hH₁R-mtAEQ cells. Data were normalized to a solvent control and the maximal activation of each system by the endogenous ligand histamine, respectively. Data represent mean \pm SEM from at least two independent experiments performed in triplicate.

As becomes obvious from Fig. 4, the histamine response was reduced to a different extent by the $G_{q/11}$ inhibitor FR900359 depending on the assay. The impedance-based readout as well as the aequorin calcium assay revealed a complete lack of response to histamine in the presence of FR900359 at concentrations of 0.1 and 1 μ M, respectively. By contrast, the DMR signal was reduced by approximately 80% and the luciferase activity (gene reporter assay) was lowered by about 50% in the presence of FR900359 at a concentration of 1 μ M, and the maximal responses could not be further suppressed by FR900359 at a concentration of 10 μ M (not shown for gene reporter assay). Whereas the blockade of the calcium signal was expected due to $G_{q/11}$ inhibition, the differential effects of FR900359 on the two holistic assays (impedimetry vs. DMR) and on the luciferase activity suggested additional signaling pathways to contribute to the respective readouts (DMR and gene reporter assay) upon H₁R stimulation.

In the presence of pertussis toxin at concentrations from 1 to 100 ng/mL, the impedance of the histamine-stimulated cells signal remained almost unaffected (Fig. 5), i. e., there is no indication of a contribution of G_i to the impedimetric response. This observation is in agreement with the complete blockade by the G_q inhibitor FR900359. On the contrary, PTX decreased the response in DMR in a concentration-dependent manner resulting in complete blockade at a concentration of 100 ng/mL (Fig. 5). Although the DMR response was also strongly suppressed by FR900359, the results demonstrate that G_i is involved, too. This phenomenon is reminiscent of promiscuous GPCRs, capable of coupling to G_q and G_i , as reported for the free fatty acid receptor FFA1 [63], and depending on the cell type, the H_1R was described to couple to G_q and/or G_i [31,34,64]. This is supported by the effect of PTX and the histamine-induced luciferase activity in the gene reporter assay (Fig. 5). Inhibition of G_i by PTX (500 ng/mL) resulted in an increase in bioluminescence by approximately 20%. The HEK293T-CRE-Luc-hH1R cells were engineered to detect the cyclic AMP dependent expression of luciferase. However, in case of H_1R stimulation the cAMP cascade is not required, as the increase in luciferase activity is elicited by G_q -coupling resulting in an increase in intracellular $[Ca^{2+}]$ and subsequent calmodulin dependent phosphorylation of the CRE binding protein (CREB) [65-67]. The increase in bioluminescence in the presence of PTX confirms the contribution of G_i as an inhibitory component in this assay.

Generally, the $G\beta\gamma$ dimer is also capable of interacting with effector proteins. For instance, $G\beta\gamma$ can interfere with the cAMP pathway [68-70] and can trigger an intracellular increase in intracellular Ca^{2+} by interacting with phospholipase C and Ca^{2+} channels [71]. Very recently, regardless of its selectivity for $G\alpha_q$ over $G\alpha_i$ and $G\alpha_s$ [63], FR900359 was reported to inhibit $G\beta\gamma$ -mediated signaling, too [72]. In this context, we investigated the influence of gallein, which is supposed to be a reversible inhibitor of $G\beta\gamma$ with a K_d value of 422 nM [73,74]. In the presence of gallein at a concentration of 20 μ M, the concentration-response curve of histamine in the luciferase gene reporter assay on HEK293T-CRE-Luc-hH₁R cells remained unaffected (data not shown), suggesting that the $G\beta\gamma$ dimer is not involved.

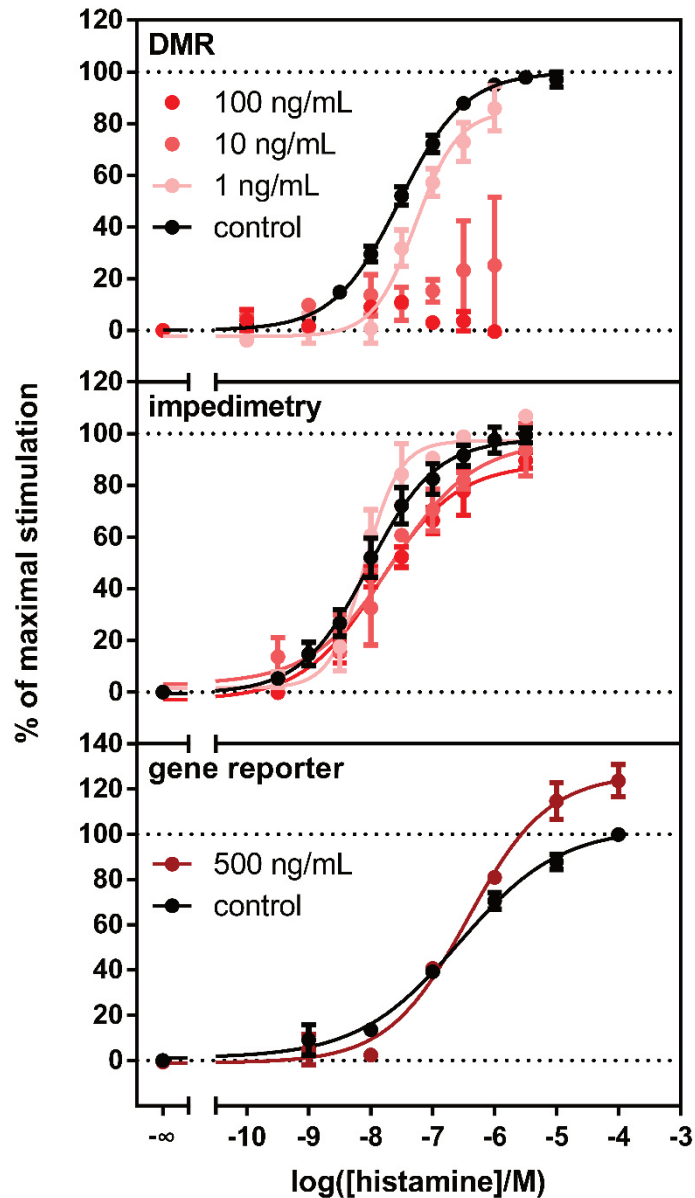


Fig. 5: Effect of the G_{α_i} -inhibitor pertussis toxin on the histamine-induced responses in DMR, impedimetric (ECIS) and gene reporter assays. Experiments were performed using HEK293T cells expressing hH_1R and additional constructs: DMR and ECIS: HEK293T-CRE-Luc- hH_1R -hMSR1 cells; luciferase gene reporter: HEK293T-CRE-Luc- hH_1R cells. Data were normalized to a solvent control and the maximal activation of each system by the endogenous ligand histamine, respectively. Data represent mean \pm SEM from at least three independent experiments performed in triplicate.

With respect to the two label-free approaches, it is noteworthy that ECIS reads primarily G_{α_q} -mediated cell shape changes upon histamine stimulation, as FR900359 completely inhibits the cellular response. Consistent with the inhibition of the calcium signal in the aequorin assay, experiments with a calcium ionophore using U-373 MG cells, constitutively expressing the H_1R revealed that an increase in intracellular Ca^{2+} alone was sufficient to produce very similar ECIS traces to those upon histamine stimulation (data not shown). The dependence of the ECIS

signal on the increase in $[Ca^{2+}]_i$ is plausible due to (i) the predominant influence of the actin cortex on membrane topography/cell shape and (ii) the fact that $[Ca^{2+}]_i$ is a well-known modulator of cortical actin (in concert with myosin). Other signaling pathways that are potentially triggered by histamine are not mirrored in the signal, when they are not linked to cortical actin or reorientation of the membrane.

In DMR assays, the G_q inhibitor FR900359 could not entirely block the agonist induced response, whereas the G_i inhibitor PTX almost entirely reduced the signal. Thus, DMR records a response integrating both G_q and G_i -mediated signaling.

As demonstrated for DMR in Fig. 6, the inhibition of the cellular signal by FR900359 and PTX upon stimulation with UR-KUM530 was qualitatively the same as in case of histamine (cf. Fig. 4 and Fig. 5). There is no indication of a differential activation of signaling pathways, when comparing both H_1R agonists.

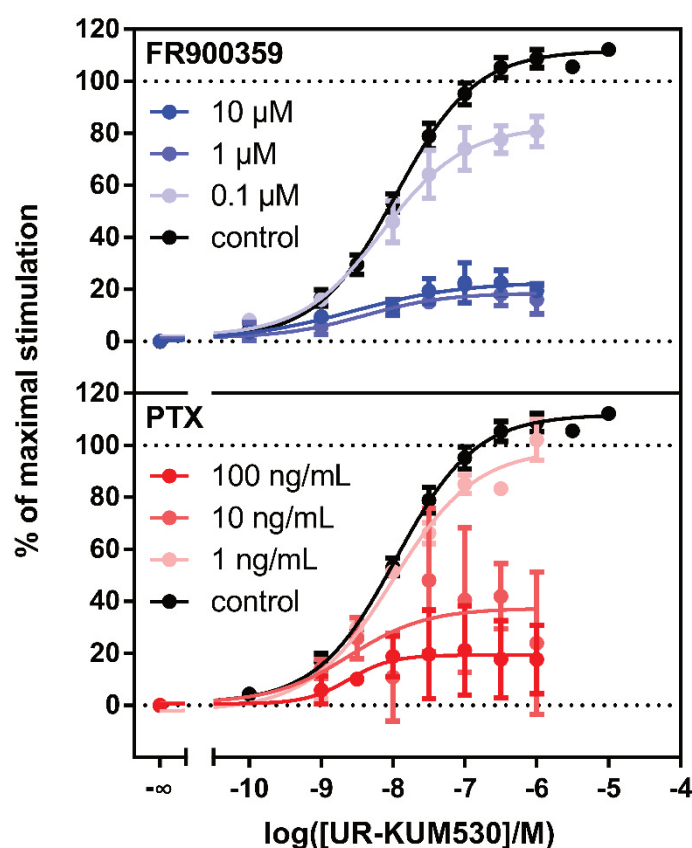


Fig. 6: Effect of the G_q inhibitor FR900359 on the response to the H_1R agonist UR-KUM530 in the DMR assay. Data were determined on HEK293T-CRE-Luc-h H_1R -hMSR1 cells and represent mean \pm SEM from at least three independent experiments performed in triplicate.

4.3.4 Functional characterization of H₁ receptor antagonists

For most of the hH₁R antagonists under study, the pK_B values were in the same range as the functional data (GTPase assay, Sf9 cell membranes) from the literature [58,75] and the binding data from our laboratory (Table 2). However, there were some discrepancies, as becomes obvious from the inhibition curves and the radar plot in Fig. 7, in particular, in case of fexofenadine, when studied in the aequorin assay, and for diphenhydramine, cyproheptadine and maprotiline in the impedimetric assay. The data gained from the impedimetric assay suggested 10- to 30-fold higher apparent affinity compared to the values determined by radioligand competition binding. Except for impedimetric readouts, experiments in the antagonist mode do not display a similarly strong assay-dependence for a given antagonist as observed in case of agonists (cf. radar plot in Fig. 7). However, there is a trend towards higher pK_b values in ECIS.

Table 2: pK_b-values for hH1R antagonists determined in different functional assays and pK_i-values determined in radioligand competition binding studies.

	gene reporter (luciferase)	β-arrestin2 recruitment ^a	Ca ²⁺ (Fura-2 AM)	Ca ²⁺ (aequorin)	DMR ^b	impedimetry ^c	GTPase ^d	competition binding
diphenhydramine	7.66 ± 0.24	7.96 ± 0.04	7.43 ± 0.08	7.62 ± 0.05	7.55 ± 0.05	7.59 ± 0.10	7.81 [58]	7.40 ± 0.03
mepyramine	8.13 ± 0.10	8.08 ± 0.09	8.85 ± 0.01	8.39 ± 0.12	8.43 ± 0.11	8.70 ± 0.14	8.25 [58]	8.39 ± 0.04
cyproheptadine	8.55 ± 0.11	8.60 ± 0.06	8.60 ± 0.03	7.99 ± 0.13	8.01 ± 0.14	10.15 ± 0.28	8.72 [58]	8.63 ± 0.05
maprotiline	8.47 ± 0.12	8.38 ± 0.03	8.58 ± 0.08	8.00 ± 0.05	8.19 ± 0.13	8.84 ± 0.53	8.54 [75]	8.50 ± 0.05
fexofenadine	7.47 ± 0.03	6.95 ± 0.03	6.85 ± 0.09	6.29 ± 0.03	7.01 ± 0.03	8.23 ± 0.30	6.65 [58]	6.70 ± 0.06

Functional studies were performed using genetically engineered HEK293T cells (cf. Table 1, footnote) and binding data were determined on HEK293T-CRE-Luc-hH₁R cells. Data represent mean ± SEM from at least three independent experiments performed in triplicate. Functional and binding data of additional H₁R antagonists investigated in the respective assay, pK_b values: ^a levocetirizine, 7.16 ± 0.07; mirtazapine, 8.71 ± 0.07, clozapine, 7.64 ± 0.05. ^b mirtazapine, 8.46 ± 0.10; doxepine, 9.35 ± 0.19; clozapine, 8.21 ± 0.22. ^c levocetirizine, 8.72 ± 0.14; doxepine, 9.11 ± 0.28; clozapine, 9.60 ± 0.08. ^d mirtazapine 8.59 [75]; doxepine, 8.90 [75]; clozapine, 8.36 [75].

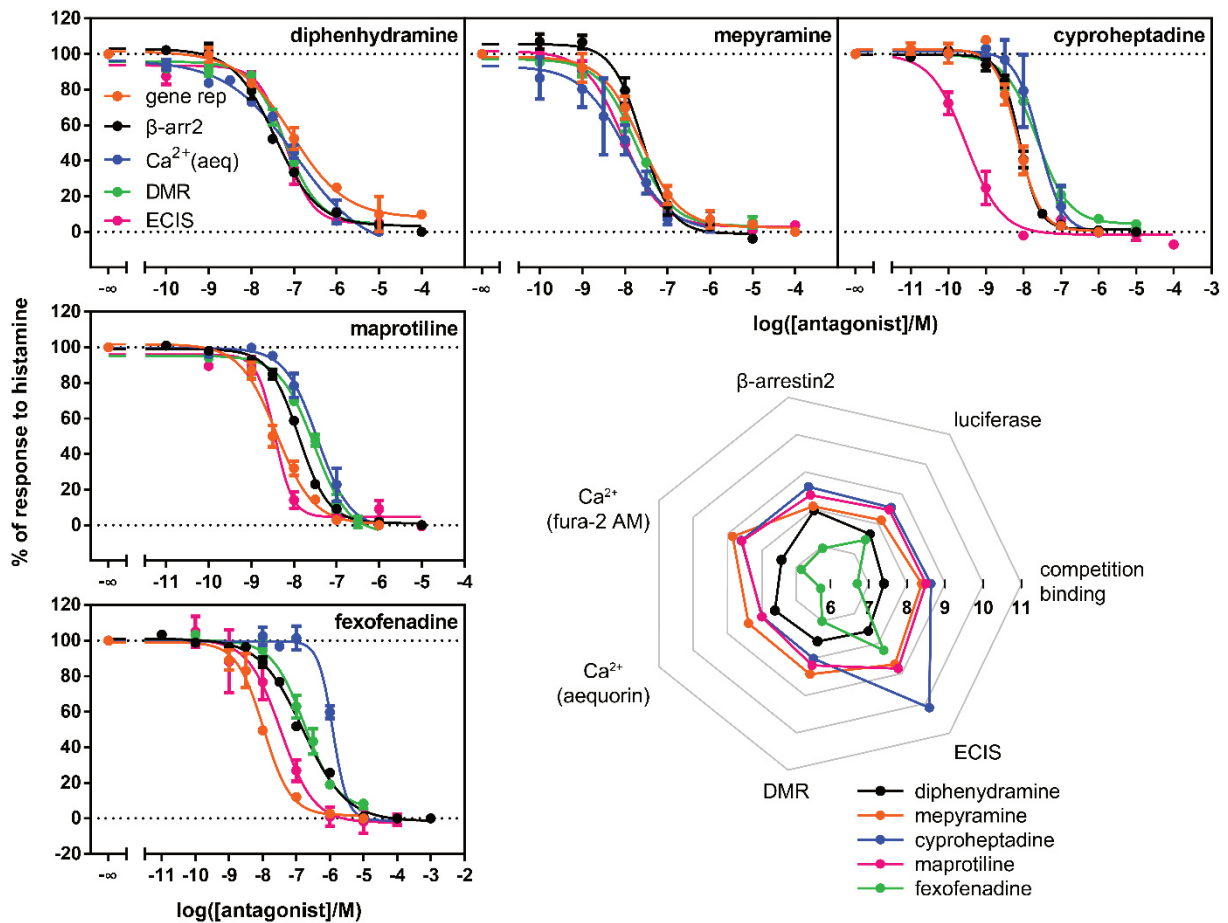


Fig. 7: Histamine H₁R antagonism of diphenhydramine, mepyramine, cyproheptadine, maprotiline and fexofenadine in five different assays. Inhibition curves and radar plot. Experiments were performed using genetically engineered HEK293T cells expressing the hH₁R and additional constructs; gene rep (luciferase gene reporter assay): HEK293T-CRE-Luc-hH₁R cells; β arr2: (β -arrestin2 recruitment assay): HEK293T-ARRB2-H₁R cells; Ca^{2+} (aeq) (aequorin calcium assay): HEK293T-CRE-Luc-hH₁R-mtAEQ cells; DMR and impeded (impedimetry): HEK293T-CRE-Luc-hH₁R-hMSR1 cells. Histamine was used at a concentration producing approximately 80% of the maximal response in the respective assay. Data were normalized to a solvent control and the EC₈₀-activation of histamine in each system. Data represent mean \pm SEM from at least three independent experiments performed in triplicate.

4.4 Conclusion

Label-free methods (DMR and impedimetry) and various signaling pathway specific readouts were used for the characterization of H₁R agonists and antagonists on genetically engineered HEK293T cells, i. e., cells of an identical genetic background. For antagonists, the results from DMR were compatible with those from conventional readouts, whereas the impedance-based data were inconsistent in some cases. Most pronounced differences became obvious for agonists regarding both, potencies and efficacies, depending on the chemical structure of the ligand and the type of readout, reflecting the complexity of the assays performed in the agonist mode. These differences can be explained only in part. The DMR appears to integrate both, G_q and G_i mediated signaling (Fig.4 and Fig. 5), the main two pathways described for the H₁R, as does the gene reporter assay. By contrast, ECIS and calcium assays apparently only to reflect G_q signaling. DMR, impedimetry and the Fura-2 assays allow the investigation of cellular effects in real time, whereas gene reporter, aequorin, β -arrestin recruitment, GTPase and GTP γ S assays are endpoint measurements. Distinct histamine H₁R ligands did not effect the different functional readouts in a uniform way, a phenomenon, which may indicate “functional selectivity” or “biased signaling”, provided that off-targets are not involved. As the latter cannot be excluded, in addition to different readouts, selective receptor agonists and antagonists as well as specific inhibitors of signaling pathways are required as pharmacological tools to reduce the risk of misinterpretation and pitfalls. In so far, label-free holistic methods such as DMR and impedimetry are reminiscent of investigations on isolated organs and may be considered as “integrative pharmacology” at the cellular level. The question arises whether human cells constitutively expressing the receptor of interest and originating from the organ to be targetted should serve as more appropriate models than genetically engineered cells.

4.5 Appendix

4.5.1 H₁R-ELucC/ELucN-ARRB expression in HEK293T cells

The HEK293 cells were seeded in 75 cm² tissue culture flasks and cultivated for 2 to 3 days in DMEM + 10% FCS to a confluency of about 60-90 %. The cells were then washed 3 times with ice cold PBS and subsequently lysed with 1 mL of RIPA buffer (20 mM Tris/HCl pH 7.8, 200 mM NaCl, 1 mM EGTA, 1 mM, 1% w/v Triton X-100, 5 mM K₂HPO₄, 1 x protease inhibitor mix (Sigma, Steinheim, Germany)). The crude mixture was transferred to 1.5 ml reaction vessels and incubated on ice for 20 min. During this period, the vessels were vigorously vortexed several times. The cell debris was removed by centrifugation (13000 x g, 5 min). The supernatant was mixed with 10% (v/v) glycerol, and aliquots were frozen and stored at -80 °C. The protein content of the samples was determined using the DC protein assay kit (Bio-Rad Laboratories, Munich, Germany) according to manufacturer's instructions.

The protein samples were analyzed by SDS-PAGE on a 12% acrylamide gel according to the general procedure established by Laemmli et al. [76]. For gel electrophoresis, 20 µg of protein per sample were loaded onto each lane. The samples for the detection of the V5-tagged receptor fusion constructs were mixed with 1 volume of 2x sample buffer containing 8 M urea and incubated for 30 min at room temperature. The samples for the detection of the c-myc-tagged arrestin fusion constructs were mixed with 1 volume of 2x sample buffer (Sigma, Steinheim, Germany) and incubated for 10 min at 98 °C. The precision plus dual color and biotinylated protein ladder (Bio-Rad Laboratories, Munich, Germany) were used as molecular weight markers. Electrophoresis was performed at 150 V for approx. 2 h.

For western blotting, the gels were placed on top of a nitrocellulose membrane between filter papers soaked in blotting buffer (25 mM Tris/HCl pH 8.3, 0.2 M glycine, 20% (v/v) methanol). Blotting was performed for 45 min at 250 mA. Afterwards, the membranes were incubated for at least 1 h in blocking solution (20 mM Tris/HCl pH 7.6, 0.14 M NaCl, 0.1% (v/v) Tween 20, 5% (w/v) fat free milk powder). After blocking, the membranes were cut closely above the 50 kDa band of the prestained protein marker. The lower part of the blots were developed using the anti β-actin antibody, the upper part using the Pierce anti c-myc antibody (Thermo Fisher, Darmstadt, Germany) for detecting the arrestin constructs or the anti V5 antibody (Thermo Fisher, Darmstadt, Germany) for the receptor constructs, respectively. Incubations with the

primary antibodies were performed using a 1:1000 dilution of the respective AB in blocking solution at 4 °C overnight. After 3 washing steps in TBST (20 mM Tris/HCl pH 7.6, 0.14 M NaCl, 0.1% (v/v) Tween 20) for 10 min each, the membranes were incubated with the secondary HRP-coupled antibodies, at a 1:1000 dilution in blocking solution for 1 h at RT. After 3 additional washing steps, the immunoreactive bands were detected using ECL western blotting substrate (Thermo Fisher, Darmstadt, Germany) and the ChemiDoc MP imaging system (Bio-Rad Laboratories, Munich, Germany). The scans of the blots were analyzed using the Image Lab 5.0 software (Bio-Rad Laboratories, Munich, Germany).

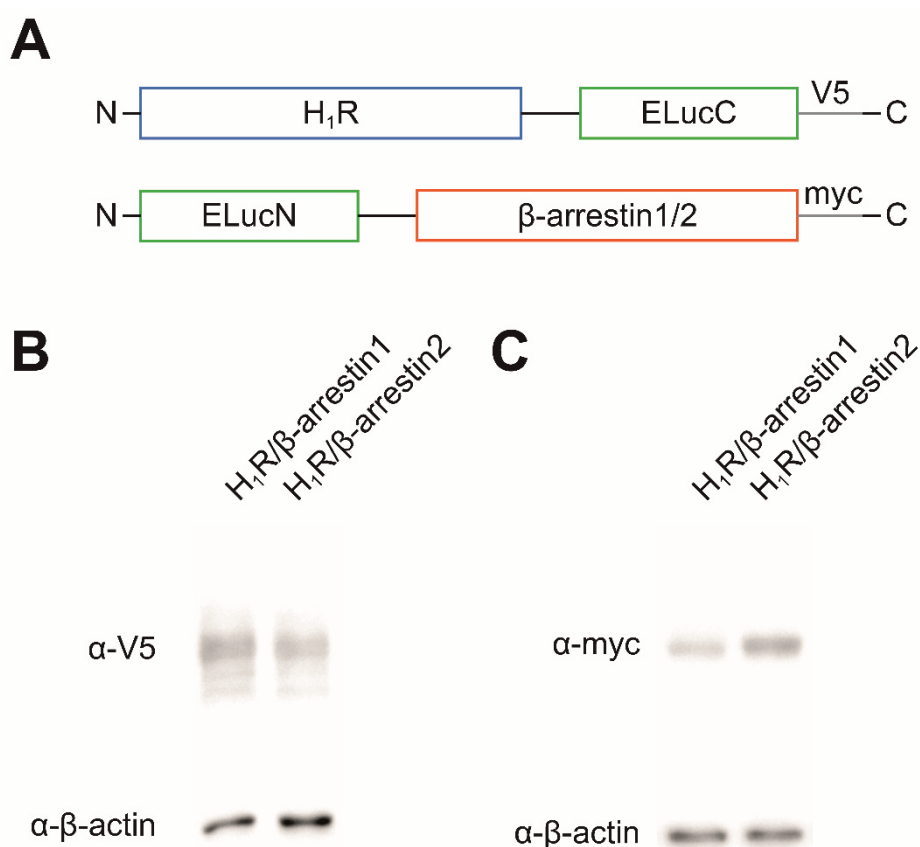


Fig S1: Schematic illustration of the fusion constructs used for the β-arrestin recruitment assay and the verification of their expression in HEK293T cells via western blot. **A:** The split-luciferase-based β-arrestin recruitment assay consists of two fusion proteins containing luciferase fragments of a green light-emitting luciferase from the click-beetle *Pyrophorus plagiophthalmus* (*ELuc*). The H₁R was fused C-terminally to the C-terminal fragment of ELuc (ELucC) and either one of the two β-arrestins (ARRB) was fused N-terminally to the N-terminal fragment of ELuc (ELucN). The receptor construct possesses C-terminally a V5-tag, whereas the β-arrestin constructs feature myc-tags. **B:** α-V5 antibody detection of H₁R fusion proteins in lysate of HEK293T cells transfected with H₁R-ELucC and either ELucN-ARRB1 or ELucN-ARRB2. **C:** α-myc antibody detection of β-arrestin fusion proteins in same HEK293T lysate as in B.

4.5.2 Radioligand saturation binding on HEK293T cells, expressing the H₁R-ELucC and ELucN-ARRB constructs

The radioligand saturation binding assays to determine the receptor expression was performed using whole cells. The HEK293T cells, expressing the hH₁R-ELucC and ELucN-ARRB constructs, were cultivated in DMEM +10% FCS in a 75 cm² cell culture flask to a confluence of about 70 – 90%. The cells were detached by treatment with 0.05% trypsin, 0.02% EDTA in PBS. After addition of 1/10 volume FCS, cells were harvested by centrifugation (400 x g, 5 min), subsequently resuspended in Leibovitz L-15 medium + 1% FCS and adjusted to a cell density of 2 million cells/mL. The binding assay was performed in flat bottom, polypropylene 96-well microtiter plates. The reaction mixture contained 10 µL of up to 80 nM mepyramine, 55 µL of Leibovitz + 1% FCS and 25 µL of cell suspension, giving a concentration of 50000 cells/well. In order to save radioligand, 1 part of mepyramine was diluted with 1 part of unlabeled mepyramine. The wells for the determination of the total binding contained additional 10 µL of Leibovitz, while, for the unspecific binding, 10 µL diphenhydramine at a concentration of 10 µM dissolved in Leibovitz were added. The mixture was incubated for 60 to 90 min at RT under shaking at 300 rpm. Afterwards, the cells were harvested by filtration through GF/C filters using a Brandel 96 sample harvester (Brandel, Gaithersburg, MD). After 3 washing steps with ice cold PBS, the filter bound radioactivity was measured by liquid scintillation counting using the *Micro Beta² 1450* scintillation counter (Perkin Elmer, Rodgau, Germany).

Data analysis was performed using *GraphPad Prism 5* software (GraphPad Software, La Jolla, CA). Specific binding values were calculated by subtraction of the unspecific binding from the respective total binding values. Data was plotted against the corresponding radioligand concentration and fitted by nonlinear regression using the one site saturation binding model. From the extrapolated B_{max} values, the binding sites per cell were calculated using the specific activity of the radioligand.

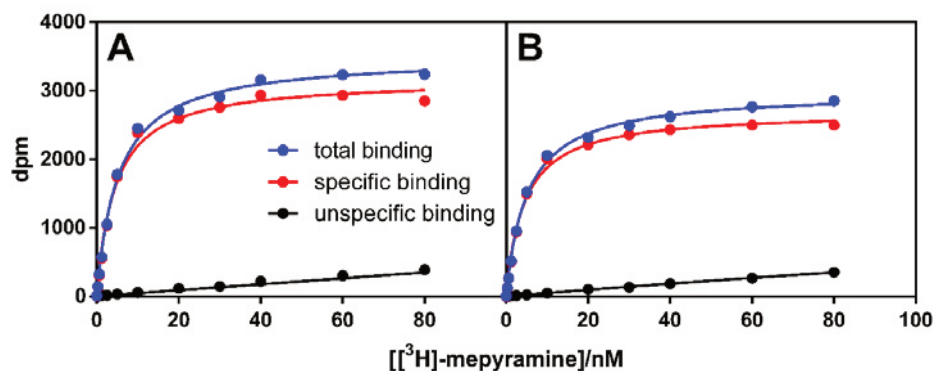


Fig S2: Radioligand saturation binding conducted with [³H]-mepyramine on HEK293T cells expressing H₁R-ELucC and either ELucN-ARRB1 (A) or ELucN-ARRB2 (B). Non-specific binding was determined in the presence of 10 μM diphenhydramine and was subtracted from total binding. Resulting specific binding was best fitted to a one-site saturation binding equation. K_D-values are as follows: 4.5 nM (H₁R-ELucC + ELucN-ARRB1) and 4.4 nM (H₁R-ELucC + ELucN-ARRB2) and are in good agreement with reference data [57]. Both cell lines show comparable receptor amounts per cell with 5.5 * 10⁵ receptors/cell for the β-arrestin1 cell line and 4.7 * 10⁵ receptors/cell for the β-arrestin2 cell line. Data ± SEM from one experiment performed in triplicate.

4.5.3 Cytotoxicity of selected H1R agonists in the crystal violet chemosensitivity assay

The assay was performed as previously described [77]. Accordingly, HEK293T-CRE-Luc-hH1R cells in DMEM were seeded into 96 well plates (Greiner, Frickenhausen, Germany) at a density of 15 cells per microscopic field (magnification: 320-fold). The cells were allowed to attach overnight, and the test compounds were added at the desired concentrations. As a control, cells were treated with medium containing only the respective solvent. After various incubation periods the cells were fixed with 1 % glutardialdehyde solution and stored at 4 °C. At the end of the assay, cells were stained with crystal violet. Prior to measurement, excess dye was removed by washing the cells with water, and cell-bound dye was extracted with 70 % EtOH. Absorbance was measured at 580 nm using a GENios Pro microplate reader (Tecan, Salzburg, Austria). Drug effects were expressed as corrected T/C- values, according to following equation:

$$\frac{T}{C} \text{ corr. (\%)} = \frac{T - C_0}{C - C_0} \times 100$$

where T = mean absorbance of treated cells, C = mean absorbance of controls and C₀ = mean absorbance of the cells when the test compounds were added (t = 0).

When the absorbance was less than that at $t = 0$, the cytotoxic effect was calculated according to following equation:

$$\text{cytotoxic effect (\%)} = \frac{C_0 - T}{C_0} \times 100$$

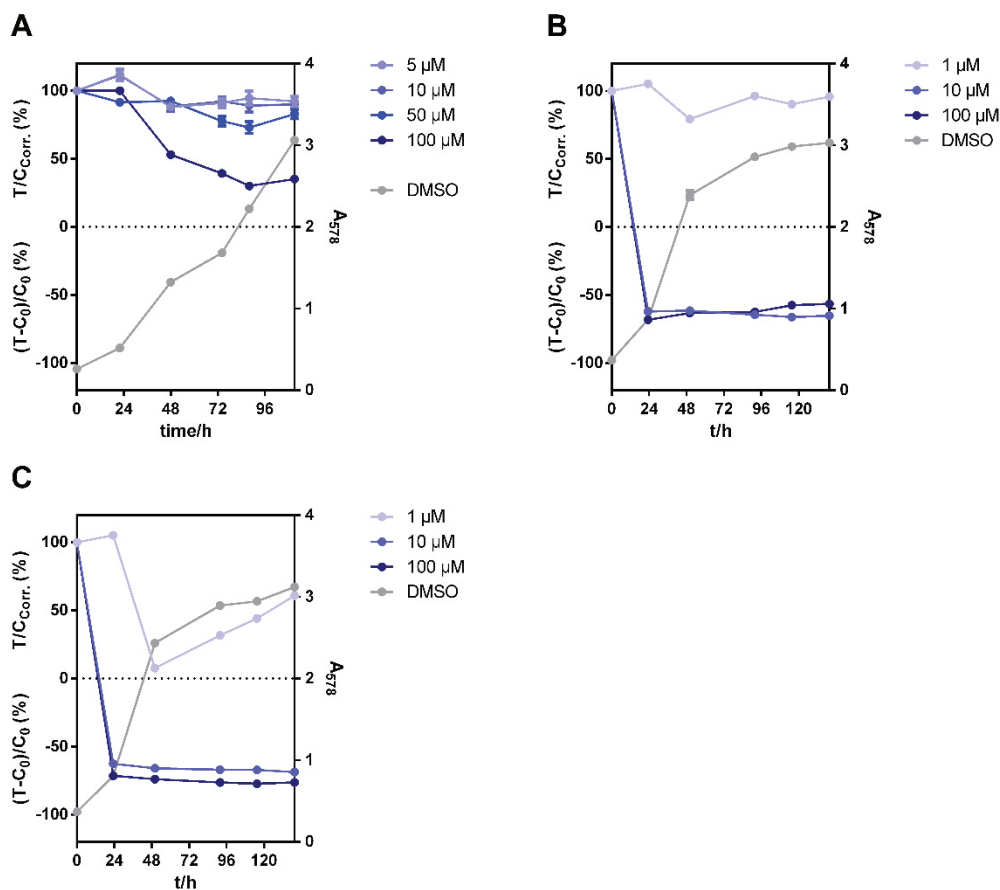


Fig. S3: Cytotoxicity assays performed on HEK293T-CRE-Luc-hH1R cells for the compounds UR-KUM530 (A), UR-BS280 (B) and UR-BS365 (C). Cytotoxicity of each compound was analysed over a time-period of at least four days. (Data \pm SEM from 16 experiments).

4.5.4 H₁R agonism of histaprodifen-derived hH₁R ligands in the β -arrestin recruitment assay

Table S1: pEC₅₀ and E_{max} values for histaprodifen-derived hH₁R ligands in the β -arrestin recruitment assay (HEK293T-ARRB1-H₁R and HEK293T-ARRB2-H₁R cells) and reference data from [³²P]GTPase assay using membranes of hH1R expressing Sf9 cells.^{a,b}

	β -arrestin1 recruitment		β -arrestin2 recruitment		GTPase (ref. [57])	
	pEC ₅₀	E _{max}	pEC ₅₀	E _{max}	pEC ₅₀ or (pK _B)	E _{max}
UR-BS280	5.77 ± 0.06	0.50 ± 0.02	6.01 ± 0.11	0.58 ± 0.10	6.67	0.52
UR-BS354	n.a.	0.03 ± 0.00	4.99 ± 0.19	0.22 ± 0.04	(6.00)	-
UR-BS355	5.85 ± 0.07	0.26 ± 0.02	6.16 ± 0.14	0.48 ± 0.05	6.65	0.47
UR-BS358	5.30 ± 0.25	0.09 ± 0.02	5.48 ± 0.08	0.43 ± 0.03	(6.56)	-
UR-BS364	n.a.	0.04 ± 0.01	5.49 ± 0.13	0.37 ± 0.08	(6.61)	-
UR-BS365	6.19 ± 0.10	0.33 ± 0.01	6.56 ± 0.18	0.54 ± 0.05	6.18	0.65

^a Data represent mean values ± SEM of three independent experiments performed in triplicate. n. a. = not applicable due to lack of intrinsic activity.

^b For hH₁R binding data determined on membranes of Sf9 cells cf. [57]

4.6 References

- 1 Ash AS, Schild HO. Receptors mediating some actions of histamine. *Br J Pharmacol Chemother* 1966;27:427-439.
- 2 Church MK, Maurer M. Antihistamines. *Chem Immunol Allergy* 2014;100:302-310.
- 3 Emanuel MB. Histamine and the antiallergic antihistamines: a history of their discoveries. *Clin Exp Allergy* 1999;29 Suppl 3:1-11.
- 4 Panula P, Chazot PL, Cowart M, Gutzmer R, Leurs R, Liu WL, Stark H, Thurmond RL, Haas HL. International union of basic and clinical pharmacology. XC VIII. Histamine receptors. *Pharmacol Rev* 2015;67:601-655.
- 5 Kenakin T, Watson C, Muniz-Medina V, Christopoulos A, Novick S. A simple method for quantifying functional selectivity and agonist bias. *ACS Chem Neurosci* 2012;3:193-203.
- 6 Ferrie AM, Goral V, Wang C, Fang Y. Label-free functional selectivity assays. *Methods Mol Biol* 2015;1272:227-246.
- 7 Kenakin T. Functional selectivity and biased receptor signaling. *J Pharmacol Exp Ther* 2011;336:296-302.
- 8 Kenakin T, Miller LJ. Seven transmembrane receptors as shapeshifting proteins: the impact of allosteric modulation and functional selectivity on new drug discovery. *Pharmacol Rev* 2010;62:265-304.
- 9 Marti-Solano M, Sanz F, Pastor M, Selent J. A dynamic view of molecular switch behavior at serotonin receptors: implications for functional selectivity. *PLoS One* 2014;9:e109312.
- 10 Seifert R. Functional selectivity of G-protein-coupled receptors: from recombinant systems to native human cells. *Biochem Pharmacol* 2013;86:853-861.
- 11 Stallaert W, Christopoulos A, Bouvier M. Ligand functional selectivity and quantitative pharmacology at G protein-coupled receptors. *Expert Opin Drug Discovery* 2011;6:811-825.
- 12 Zhou L, Bohn LM. Functional selectivity of GPCR signaling in animals. *Curr Opin Cell Biol* 2014;27:102-108.
- 13 Aristotelous T, Hopkins AL, Navratilova I. Surface plasmon resonance analysis of seven-transmembrane receptors. *Methods Enzymol* 2015;556:499-525.
- 14 Deng H, Sun H, Fang Y. Label-free cell phenotypic assessment of the biased agonism and efficacy of agonists at the endogenous muscarinic M3 receptors. *J Pharmacol Toxicol Methods* 2013;68:323-333.
- 15 Fang Y, Ferrie AM, Tran E. Resonant waveguide grating biosensor for whole-cell GPCR assays. *Methods Mol Biol* 2009;552:239-252.
- 16 Fang Y, Frutos AG, Verklereen R. Label-free cell-based assays for GPCR screening. *Comb Chem High Throughput Screen* 2008;11:357-369.
- 17 Grundmann M, Kostenis E. Label-free biosensor assays in GPCR screening. *Methods Mol Biol* 2015;1272:199-213.
- 18 McGuinness RP, Proctor JM, Gallant DL, van Staden CJ, Ly JT, Tang FL, Lee PH. Enhanced selectivity screening of GPCR ligands using a label-free cell based assay technology. *Comb Chem High Throughput Screen* 2009;12:812-823.
- 19 Miyano K, Sudo Y, Yokoyama A, Hisaoka-Nakashima K, Morioka N, Takebayashi M, Nakata Y, Higami Y, Uezono Y. History of the G protein-coupled receptor (GPCR) assays from traditional to a state-of-the-art biosensor assay. *J Pharmacol Sci* 2014;126:302-309.
- 20 Lieb S, Michaelis S, Plank N, Bernhardt G, Buschauer A, Wegener J. Label-free analysis of GPCR-stimulation: The critical impact of cell adhesion. *Pharmacol Res* 2016;108:65-74.
- 21 Fang Y. Label-free biosensors for cell biology. *Int J Electrochem* 2011:Article ID 460850.

- 22 Yu N, Atienza JM, Bernard J, Blanc S, Zhu J, Wang X, Xu X, Abassi YA. Real-Time monitoring of morphological changes in living cells by electronic cell sensor arrays: An approach to study G-Protein coupled receptors. *Anal Chem* 2006;78:35-43.
- 23 Halai R, Croker DE, Suen JY, Fairlie DP, Cooper MA. A Comparative Study of Impedance versus Optical Label-Free Systems Relative to Labelled Assays in a Predominantly Gi Coupled GPCR (C5aR) Signalling. *Biosens Bioelectron* 2012;2:273-290.
- 24 Ke N, Nguyen K, Irelan J, Abassi YA. Multidimensional GPCR profiling and screening using impedance-based label-free and real-time assay. *Methods Mol Biol* 2015;1272:215-226.
- 25 Peters MF, Vaillancourt F, Heroux M, Valiquette M, Scott CW. Comparing label-free biosensors for pharmacological screening with cell-based functional assays. *Assay Drug Dev Technol* 2010;8:219-227.
- 26 Schröder R, Janssen N, Schmidt J, Kebig A, Merten N, Hennen S, Muller A, Blattermann S, Mohr-Andra M, Zahn S, Wenzel J, Smith NJ, Gomeza J, Drewke C, Milligan G, Mohr K, Kostenis E. Deconvolution of complex G protein-coupled receptor signaling in live cells using dynamic mass redistribution measurements. *Nat Biotechnol* 2010;28:943-949.
- 27 Adjobo-Hermans MJ, Goedhart J, van Weeren L, Nijmeijer S, Manders EM, Offermanns S, Gadella TW, Jr. Real-time visualization of heterotrimeric G protein Gq activation in living cells. *BMC Biol* 2011;9:32.
- 28 Gutowski S, Smrcka A, Nowak L, Wu DG, Simon M, Sternweis PC. Antibodies to the alpha q subfamily of guanine nucleotide-binding regulatory protein alpha subunits attenuate activation of phosphatidylinositol 4,5-bisphosphate hydrolysis by hormones. *J Biol Chem* 1991;266:20519-20524.
- 29 Verdonk E, Johnson K, McGuinness R, Leung G, Chen Y-W, Tang HR, Michelotti JM, Liu VF. Cellular Dielectric Spectroscopy: A Label-Free Comprehensive Platform for Functional Evaluation of Endogenous Receptors. *Assay Drug Dev Technol* 2006;4:609-619.
- 30 Lu J, Li J. Label-free imaging of dynamic and transient calcium signaling in single cells. *Angew Chem Int Ed* 2015;54
- 31 Seifert R, Grünbaum L, Schultz G. Histamine H1-receptors in HL-60 monocytes are coupled to Gi-proteins and pertussis toxin-insensitive G-proteins and mediate activation of Ca²⁺ influx without concomitant Ca²⁺ mobilization from intracellular stores. *Naunyn Schmiedebergs Arch Pharmacol* 1994;349:355-361.
- 32 Wang YX, Kotlikoff MI. Signalling pathway for histamine activation of non-selective cation channels in equine tracheal myocytes. *J Physiol* 2000;523 Pt 1:131-138.
- 33 Robinson AJ, Dickenson JM. Activation of the p38 and p42/p44 mitogen-activated protein kinase families by the histamine H(1) receptor in DDT(1)MF-2 cells. *Br J Pharmacol* 2001;133:1378-1386.
- 34 Esbenshade TA, Kang CH, Krueger KM, Miller TR, Witte DG, Roch JM, Masters JN, Hancock AA. Differential activation of dual signaling responses by human H1 and H2 histamine receptors. *J Recept Signal Transduct Res* 2003;23:17-31.
- 35 Bakker RA, Schoonus SB, Smit MJ, Timmerman H, Leurs R. Histamine H1-receptor activation of nuclear factor-kappa B: roles for G beta gamma- and G alpha(q/11)-subunits in constitutive and agonist-mediated signaling. *Mol Pharmacol* 2001;60:1133-1142.
- 36 Brighton PJ, Rana S, Challiss RJ, Konje JC, Willets JM. Arrestins differentially regulate histamine- and oxytocin-evoked phospholipase C and mitogen-activated protein kinase signalling in myometrial cells. *Br J Pharmacol* 2011;162:1603-1617.
- 37 Willets JM, Taylor AH, Shaw H, Konje JC, Challiss RA. Selective regulation of H1 histamine receptor signaling by G protein-coupled receptor kinase 2 in uterine smooth muscle cells. *Mol Endocrinol* 2008;22:1893-1907.

- 38 Khoury E, Nikolajev L, Simaan M, Namkung Y, Laporte SA. Differential regulation of endosomal GPCR/beta-arrestin complexes and trafficking by MAPK. *J Biol Chem* 2014;289:23302-23317.
- 39 Paradis JS, Ly S, Blondel-Tepaz E, Galan JA, Beautrait A, Scott MG, Enslin H, Marullo S, Roux PP, Bouvier M. Receptor sequestration in response to beta-arrestin-2 phosphorylation by ERK1/2 governs steady-state levels of GPCR cell-surface expression. *Proc Natl Acad Sci U S A* 2015;112:E5160-5168.
- 40 Straßer A, Wittmann H-J, Kunze M, Elz S, Seifert R. Molecular basis for the selective interaction of synthetic agonists with the human histamine H1-receptor compared with the guinea pig H1-receptor. *Mol Pharmacol* 2009;75:454-465.
- 41 Leschke C, Elz S, Garbarg M, Schunack W. Synthesis and histamine H1 receptor agonist activity of a series of 2-phenylhistamines, 2-heteroarylhistamines, and analogues. *J Med Chem* 1995;38:1287-1294.
- 42 Zingel V, Leschke C, Schunack W. Developments in histamine H1-receptor agonists. *Prog Drug Res* 1995;44:49-85.
- 43 Elz S, Kramer K, Pertz HH, Detert H, ter Laak AM, Kuhne R, Schunack W. Histaprodifens: synthesis, pharmacological in vitro evaluation, and molecular modeling of a new class of highly active and selective histamine H1-receptor agonists. *J Med Chem* 2000;43:1071-1084.
- 44 Striegl B. Synthese und funktionelle in-vitro-Pharmakologie neuer Histamin-H1-Rezeptoragonisten aus der Suprahistaprodifen-Reihe. Faculty of Chemistry and Pharmacy: Regensburg, 2007.
- 45 Nordemann U, Wifling D, Schnell D, Bernhardt G, Stark H, Seifert R, Buschauer A. Luciferase reporter gene assay on human, murine and rat histamine H₄ receptor orthologs: correlations and discrepancies between distal and proximal readouts. *PLoS One* 2013;8:e73961.
- 46 Matsumoto A, Naito M, Itakura H, Ikemoto S, Asaoka H, Hayakawa I, Kanamori H, Aburatani H, Takaku F, Suzuki H. Human macrophage scavenger receptors: primary structure, expression, and localization in atherosclerotic lesions. *Proc Natl Acad Sci U S A* 1990;87:9133-9137.
- 47 Misawa N, Kafi AK, Hattori M, Miura K, Masuda K, Ozawa T. Rapid and high-sensitivity cell-based assays of protein-protein interactions using split click beetle luciferase complementation: an approach to the study of G-protein-coupled receptors. *Anal Chem* 2010;82:2552-2560.
- 48 Ziemek R, Schneider E, Kraus A, Cabrele C, Beck-Sickinger AG, Bernhardt G, Buschauer A. Determination of affinity and activity of ligands at the human neuropeptide Y Y4 receptor by flow cytometry and aequorin luminescence. *J Recept Signal Transduct Res* 2007;27:217-233.
- 49 Müller M, Knieps S, Gessele K, Dove S, Bernhardt G, Buschauer A. Synthesis and neuropeptide Y Y1 receptor antagonistic activity of N,N-disubstituted omega-guanidino- and omega-aminoalkanoic acid amides. *Arch Pharm (Weinheim)* 1997;330:333-342.
- 50 Mosandl J. Radiochemical and luminescence-based binding and functional assays for human histamine receptors using genetically engineered cells Faculty of Chemistry and Pharmacy: Regensburg, 2009.
- 51 Gupta A, Gillard M, Christophe B, Chatelain P, Massingham R, Hammarlund-Udenaes M. Peripheral and central H1 histamine receptor occupancy by levocetirizine, a non-sedating antihistamine; a time course study in the guinea pig. *Br J Pharmacol* 2007;151:1129-1136.

- 52 Cheng Y, Prusoff WH. Relationship between the inhibition constant (K_i) and the concentration of inhibitor which causes 50 per cent inhibition (I_{50}) of an enzymatic reaction. *Biochem Pharmacol* 1973;22:3099-3108.
- 53 Schröder R, Schmidt J, Blattermann S, Peters L, Janssen N, Grundmann M, Seemann W, Kaufel D, Merten N, Drewke C, Gomeza J, Milligan G, Mohr K, Kostenis E. Applying label-free dynamic mass redistribution technology to frame signaling of G protein-coupled receptors noninvasively in living cells. *Nat Protocols* 2011;6:1748-1760.
- 54 Stolwijk J, Matrougui K, Renken C, Trebak M. Impedance analysis of GPCR-mediated changes in endothelial barrier function: overview and fundamental considerations for stable and reproducible measurements. *Pflugers Arch - Eur J Physiol* 2015;467:2193-2218.
- 55 Cotton M, Claing A. G protein-coupled receptors stimulation and the control of cell migration. *Cellular Signalling* 2009;21:1045-1053.
- 56 Robbins AK, Horlick RA. Macrophage scavenger receptor confers an adherent phenotype to cells in culture. *BioTechniques* 1998;25:240-244.
- 57 Strasser A, Striegl B, Wittmann HJ, Seifert R. Pharmacological profile of histaprodifens at four recombinant histamine H1 receptor species isoforms. *J Pharmacol Exp Ther* 2008;324:60-71.
- 58 Seifert R, Wenzel-Seifert K, Bürckstümmer T, Pertz HH, Schunack W, Dove S, Buschauer A, Elz S. Multiple differences in agonist and antagonist pharmacology between human and guinea pig histamine H1-receptor. *J Pharmacol Exp Ther* 2003;305:1104-1115.
- 59 Oakley RH, Laporte SA, Holt JA, Caron MG, Barak LS. Differential affinities of visual arrestin, beta arrestin1, and beta arrestin2 for G protein-coupled receptors delineate two major classes of receptors. *J Biol Chem* 2000;275:17201-17210.
- 60 Wilson S, Chambers JK, Park JE, Ladurner A, Cronk DW, Chapman CG, Kallender H, Browne MJ, Murphy GJ, Young PW. Agonist potency at the cloned human beta-3 adrenoceptor depends on receptor expression level and nature of assay. *J Pharmacol Exp Ther* 1996;279:214-221.
- 61 Schrage R, De Min A, Hochheiser K, Kostenis E, Mohr K. Superagonism at G protein-coupled receptors and beyond. *Br J Pharmacol* 2015;doi: 10.1111/bph.13278.
- 62 Fujioka M, Koda S, Morimoto Y, Biemann K. Structure of Fr900359, a Cyclic Depsipeptide from *Ardisia-Crenata* Sims. *J Org Chem* 1988;53:2820-2825.
- 63 Schrage R, Schmitz A-L, Gaffal E, Annala S, Kehraus S, Wenzel D, Büllsbach KM, Bald T, Inoue A, Shinjo Y, Galandrin S, Shridhar N, Hesse M, Grundmann M, Merten N, Charpentier TH, Martz M, Butcher AJ, Slodczyk T, Armando S, Efferm M, Namkung Y, Jenkins L, Horn V, Stößel A, Dargatz H, Tietze D, Imhof D, Galés C, Drewke C, Müller CE, Hölzel M, Milligan G, Tobin AB, Gomeza J, Dohlman HG, Sondek J, Harden TK, Bouvier M, Laporte SA, Aoki J, Fleischmann BK, Mohr K, König GM, Tüting T, Kostenis E. The experimental power of FR900359 to study Gq-regulated biological processes. *Nat Commun* 2015;6:10156.
- 64 Seifert R, Hoer A, Offermanns S, Buschauer A, Schunack W. Histamine increases cytosolic Ca^{2+} in dibutyryl-cAMP-differentiated HL-60 cells via H1 receptors and is an incomplete secretagogue. *Mol Pharmacol* 1992;42:227-234.
- 65 Enslin H, Sun P, Brickey D, Soderling SH, Klamo E, Soderling TR. Characterization of Ca^{2+} /calmodulin-dependent protein kinase IV. Role in transcriptional regulation. *J Biol Chem* 1994;269:15520-15527.
- 66 Hardingham GE, Cruzalegui FH, Chawla S, Bading H. Mechanisms controlling gene expression by nuclear calcium signals. *Cell Calcium* 1998;23:131-134.

- 67 Ma H, Groth RD, Cohen SM, Emery JF, Li B, Hoedt E, Zhang G, Neubert TA, Tsien RW. gammaCaMKII shuttles Ca(2)(+)/CaM to the nucleus to trigger CREB phosphorylation and gene expression. *Cell* 2014;159:281-294.
- 68 Federman AD, Conklin BR, Schrader KA, Reed RR, Bourne HR. Hormonal stimulation of adenylyl cyclase through Gi-protein beta gamma subunits. *Nature* 1992;356:159-161.
- 69 Cabrera-Vera TM, Vanhauwe J, Thomas TO, Medkova M, Preinerger A, Mazzoni MR, Hamm HE. Insights into G-Protein structure, function, and regulation. *Endocr Rev* 2003;24:765-781.
- 70 Müller S, Lohse MJ. The role of G-protein beta gamma subunits in signal transduction. *Biochem Soc Trans* 1995;23:141-148.
- 71 Wettschureck N, Offermanns S. Mammalian G proteins and their cell type specific functions. *Physiol Rev* 2005;85:1159-1204.
- 72 Gao Z-G, Jacobson KA. On the selectivity of the Gαq inhibitor UBO-QIC: A comparison with the Gαi inhibitor pertussis toxin. *Biochem Pharmacol* 2016;107:59-66.
- 73 Lehmann DM, Seneviratne AM, Smrcka AV. Small molecule disruption of G protein beta gamma subunit signaling inhibits neutrophil chemotaxis and inflammation. *Mol Pharmacol* 2008;73:410-418.
- 74 Bonacci TM, Mathews JL, Yuan C, Lehmann DM, Malik S, Wu D, Font JL, Bidlack JM, Smrcka AV. Differential targeting of Gbetagamma-subunit signaling with small molecules. *Science* 2006;312:443-446.
- 75 Appl H, Holzammer T, Dove S, Haen E, Strasser A, Seifert R. Interactions of recombinant human histamine H(1)R, H(2)R, H(3)R, and H(4)R receptors with 34 antidepressants and antipsychotics. *Naunyn Schmiedebergs Arch Pharmacol* 2012;385:145-170.
- 76 Laemmli UK. Cleavage of structural proteins during the assembly of the head of bacteriophage T4. *Nature* 1970;227:680-685.
- 77 Bernhardt G, Reile H, Birnböck H, Spruß T, Schönenberger H. Standardized kinetic microassay to quantify differential chemosensitivity on the basis of proliferative activity. *J Cancer Res Clin Oncol* 1992;118:35-43.

5 Functional investigations of human NPY Y₂ and Y₄ receptors: Comparison of label-free and calcium-based methods

5.1 Introduction

The neuropeptide Y family comprises neuropeptide Y (NPY), peptide YY (PYY) and pancreatic polypeptide (PP) [1-3]. The peptides are composed of 36 amino acids and are structurally closely related [4,5]. In humans, NPY, PYY and PP differentially prefer four functional subtypes of the NPY receptor family, GPCRs referred to as Y₁R, Y₂R, Y₄R and Y₅R [3]. This multireceptor system influences several important physiological key functions and is associated with multiple diseases like epilepsy or depression [6-8]. A fifth receptor (y₆) was cloned from mouse genomic DNA [9], but up to now, no physiological correlate of the cloned y₆ receptor has been described [3,10]. After agonist-induced NPY receptor activation, the receptor is coupling to G-proteins of the pertussis toxin sensitive G $\alpha_{i/o}$ family [3,11]. Receptor activation results in the inhibition of adenylyl cyclases and, therefore, in a decrease in cyclic adenosine monophosphate (cAMP) formation [3]. Depending on the cell type, additional signaling pathways are reported, including the modulation of calcium and potassium channels [3,12,13]. The inhibition of the cAMP response has been a standard assay for the functional characterization of ligands on all NPY receptor subtypes [14-18]. Another method for the functional investigation of NPY Y₂ and Y₄ receptor ligands is based on the use the chimeric G-protein G_{qi5}, redirecting the cellular response to a calcium signal, which can be measured with classical fluorescence dyes (e. g. fura-2) or by bioluminescence as, for example, described for mitochondrially targeted apoaequorin [19,20].

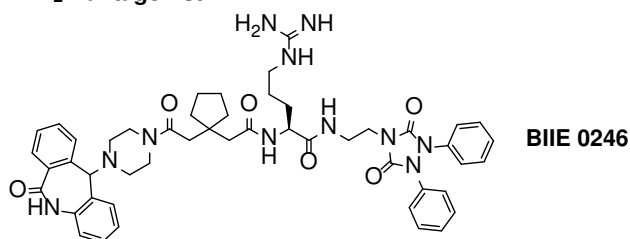
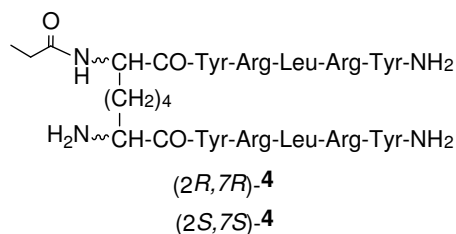
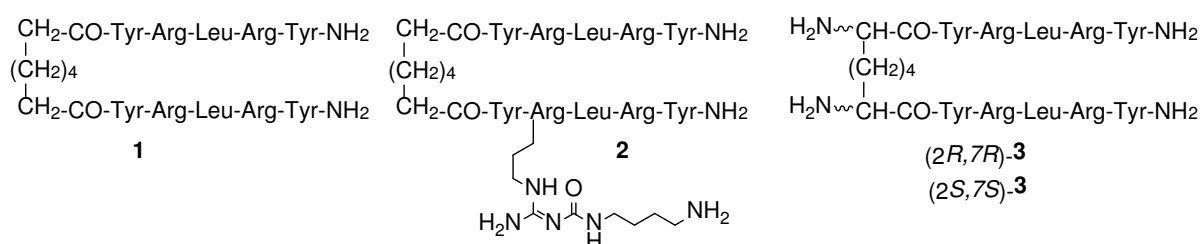
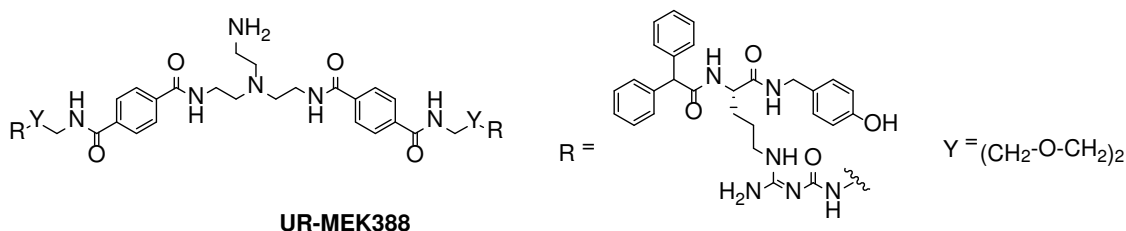
This chapter is dealing with the exploration of two label-free assays (ECIS and DMR) with respect to the functional characterization of the NPY Y₂ and Y₄ receptor, respectively. For this purpose, selected receptor ligands were analysed and the data were compared with those from conventional calcium assays. Furthermore, the influence of the G α_i inhibitor pertussis toxin and the G α_q inhibitor FR900359 (UBI-QIC) on the response in the label-free and the calcium assay was investigated.

5.2 Materials and Methods

All chemicals were from commercial suppliers, unless otherwise indicated, as specified in chapters 3 and 4.

5.2.1 Human neuropeptide Y₂ and Y₄ receptor ligands

The porcine NPY and [⁴K]hPP was kindly provided by Prof. Dr. Chiara Cabrele (University of Salzburg). Stock solutions (1 mM) were prepared in 10 mM HCl and stored at -20 °C. Compounds **1-4** [21] and (UR-MEK388 [22] (5 mM stock solution in 100 % DMSO) as well as BIIE 0246 (10 mM stock solution in 10 % DMSO) [23] were synthesized in our lab [23]. For label-free measurements, stock solutions were thawed and diluted with Leibovitz' L-15 medium supplemented with 1 % bovine serum albumin (BSA, Serva Electrophoresis, Heidelberg, Germany) and 0.1 mg/mL Bacitracin (Sigma-Aldrich, Taufkirchen, Germany). Y₄ receptor ligands were diluted in "siliconized" Eppendorf reaction vessels to prevent adsorption. For fura-2 and aequorin calcium assay, stock solutions aliquots were diluted in loading buffer (pH 7.4; 25 mM HEPES, 120 mM NaCl, 1.5 mM CaCl₂, MgCl₂, 5 mM KCl, 10 mM D-glucose) supplemented with 1 % BSA and 0.1 mg/mL bacitracin as previously described [20].

hY₂R agonistYPSKPDNPGEDAPAEDLARYYSALRHYINLITRQRY-NH₂ **pNPY****hY₂R antagonist****hY₄R agonists**APLKPVYPGDNATPEQMAQYAADLRRYINMLTRPRY-NH₂ [**K⁴**]hPP**hY₄R antagonist****Fig. 5.1:** Chemical structures of selected hY₂ and hY₄ receptor agonists and antagonists.**5.2.2 Cell culture**

CHO-K1 [19], CHO-hY₂-mtAEQ [19], CHO-hY₂-G_{qi5}-mtAEQ [19] and CHO-hY₄-G_{qi5}-mtAEQ [20] cells were cultured as described elsewhere.

5.2.3 Aequorin calcium assay

The assay was performed as described previously [19,20].

5.2.4 Fura-2 calcium assay

The fura-2 calcium assay was performed as described in chapter 4.

5.2.5 Impedimetric assay

For the investigation of hY₂R agonists, PTX and FR900359 (UBO-QIC) on CHO cells, the assay was performed as described in chapters 3 and 4. The frequency scans were performed with an ECIS-Z θ device for 8-well electrode arrays (type 8W10E+) from Applied BioPhysics (Troy, NY, USA). A volume of 400 μ L of cell suspension, prepared in HAM's F12 nutrient mixture (Sigma Aldrich) containing 10% FCS from an almost confluent cell layer trypsinized from a cell culture flask, was dispensed at a density of $1.2 \cdot 10^5$ cells per well. Approximately 60 min before the assay the culture medium was replaced by 200 μ L of serum-free L-15 medium supplemented with 1% BSA and 0.1 mg/mL bacitracin. The impedance-based experiments were performed with an ECIS-Z device for 96-well electrode arrays (type 96W1E+) from Applied BioPhysics. A volume of 300 μ L of cell suspension, prepared in HAM's F12 nutrient mixture containing 10% FCS was dispensed at a density of $4.5 \cdot 10^4$ cells per well. About 60 min before the assay the culture medium was replaced by 150 μ L of serum-free L-15 medium supplemented with 1% BSA and 0.1 mg/mL bacitracin. Data were recorded with the ECIS device placed in an incubator (Galaxy 48S, New Brunswick, USA), containing a humidified atmosphere at 37 °C at an AC frequency of 10 kHz. For data processing cf. [24]. Antagonists and the agonist were applied simultaneously.

5.2.6 Dynamic mass redistribution assay

The assay was performed as described in chapters 3 and 4, using CHO cells expressing the receptor of interest. A volume of 40 μ L of cell suspension, prepared by trypsinization from 80 % confluent cell layers, in HAM's F12 nutrient mixture supplemented with 10% FCS was dispensed at a density of $2 \cdot 10^4$ cells per well into uncoated 384-well EnSpire microplates. The cells were washed four times with serum-free L-15 medium supplemented with 1% BSA and 0.1 mg/mL bacitracin and allowed to equilibrate in a volume of 30 μ L of the same medium per well in the multimode reader at 37 °C for about 60 min. For data processing cf. [24]. Antagonists and the agonist were applied simultaneously.

5.3 Results and discussion

5.3.1 Determination of the optimal cell density for CHO-hY₂-G_{qi5}-mtAEQ cells in label-free assays

To characterize the DMR and impedance response of the hY₂ receptor, the cell density was optimized for both assays (Fig. 5.2). The addition of 300 nM (DMR) or 10 nM (ECIS) pNPY caused a positive mass redistribution and an increase of the recorded impedance. pNPY was chosen instead of human NPY, because hNPY contains a methionine residue in position 17 that is susceptible to oxidation. The maximal cellular response was observed at a density of $2.0 \cdot 10^4$ cells/well for DMR and $4.5 \cdot 10^4$ cells/well for impedance experiments.

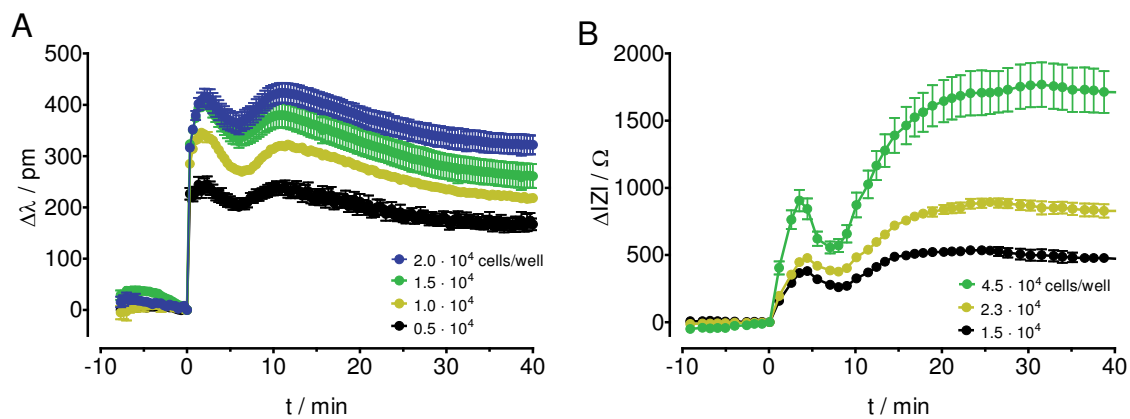


Fig. 5.2: Dependence of the pNPY induced response on the density of CHO-hY₂ cells, recorded by DMR (A) and ECIS (B). (A) DMR response caused by 300 nM pNPY at various CHO-Y₂ cell densities in 384-well plates. (B) Cell density dependent signal intensity in the ECIS assay after addition of 10 nM pNPY. Cells were plated in a range from $1.5 \cdot 10^4$ to $4.5 \cdot 10^4$ cells per well.

5.3.2 Effective range of measurement depending on the frequency of the alternating current (AC)

Frequency scans were performed to compare the impedance measured with cell-free electrodes and electrodes covered with monolayers of CHO-hY2-G_{q15}-mtAEQ cells. The impedance as a function of frequency for an electrode with an area of 0.49 cm² (8W10E: 8 wells à 10 electrodes) is shown in Fig. 5.3A. The effective range of measurement was recorded between 10³ and 10⁵ Hz. The maximum of the normalized impedance as a function of frequency becomes obvious from Fig. 5.3B. As the maximum of this curve is supposed to reflect highest sensitivity [25] for this type of cells, ECIS experiments were performed at a frequency of 10 kHz.

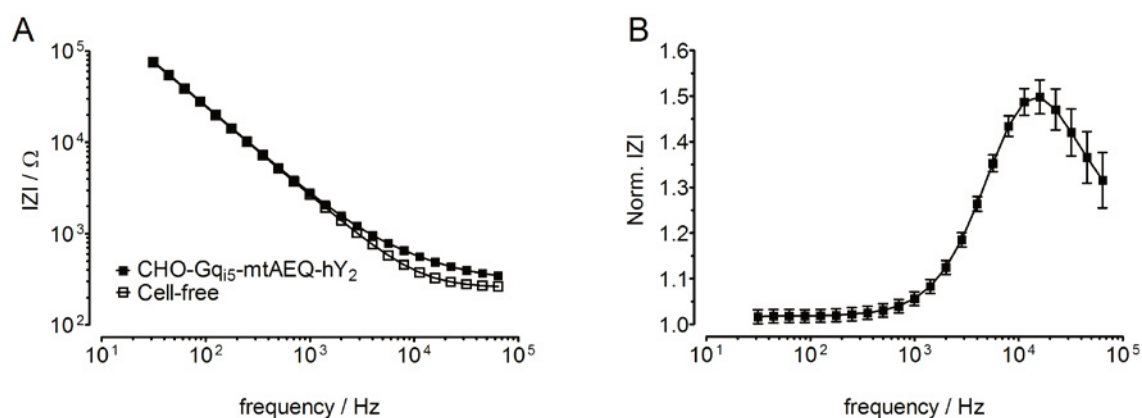


Fig. 5.3: (A) Frequency-dependent impedance traces of electrodes covered with a confluent monolayer of CHO-hY₂ cells in L15 + 1 % BSA + 0.1 mg/mL bacitracin and cell-free electrodes in the same culture medium. (B) Normalized impedance corresponding to the ratio of impedance of the cell-covered electrode and the impedance of the cell-free electrode measured at the same frequency.

5.3.3 Functional characterization of hY₂ receptor ligands

Porcine neuropeptide Y and the selective hY₂ receptor antagonist BIIE 0246 were studied in with ECIS and DMR using CHO-hY₂ cells. The results were compared with those obtained from conventional functional assays, namely mobilization of intracellular calcium in the fura-2 and in an aequorin-based assay. Activation of the G $\alpha_{i/o}$ coupled hY₂ receptor induced an increase in cellular impedance in ECIS (Fig. 5.4A) and a shift towards longer wavelengths in DMR (Fig. 5.4C). Control experiments performed with CHO cells devoid of hY₂ receptors did not respond to agonist addition. The shape of the curves (Fig. 5.4) was similar in both label-free assays. pNPY induced an immediate sharp rise after compound addition. The signal peaked in a first maximum at approximately 5 min. The transient minimum was reached in both assays within minute 5 to 10. Subsequently, an increase was observed within 10 to 20 minutes, before the signal decayed slowly. The signalling fingerprints of the major G α protein classes were reported for both label-free techniques [26-28] (cf. Figure 1.3, chapter 1). According to these studies, the overall response can be assigned to the G α_i protein, regardless of minor differences, which may arise from the chimeric G-protein G $_{q15}$. The G α_i

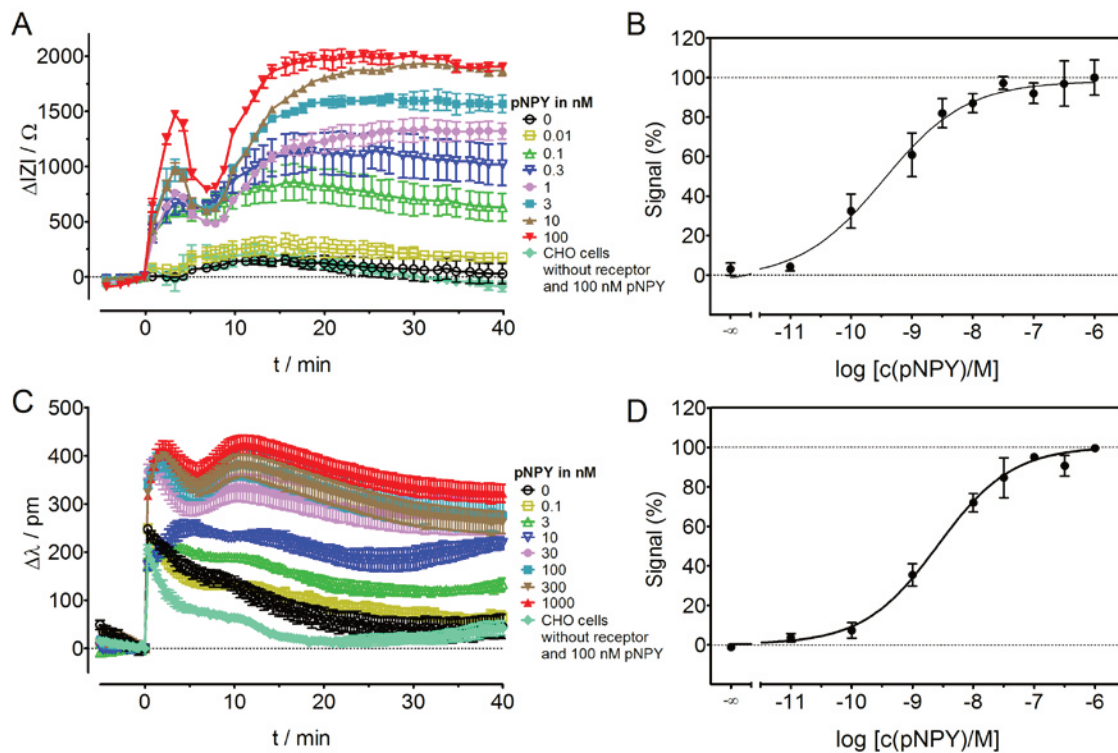


Fig. 5.4: pNPY-induced response of CHO-hY₂-G_{q15}-mtAEQ cells recorded by ECIS (A, B) and DMR (C, D). (A) Representative time courses (performed in triplicate) of the concentration-dependent change of impedance (recorded at 10 kHz) or resonance wavelength (C). (B,D) Concentration-response curves derived from areas-under-the-curve (AUC) of baseline-corrected data integrated from 0 – 40 min for at least four independent experiments, each performed in triplicate.

protein mainly contributes to the impedimetric readout, because the characteristic $G\alpha_q$ protein associated dip immediately after agonist addition [29] (cf. Fig. 1.3, chapter 1) is missing. Moreover, a second maximum, typical for a $G\alpha_i$ mediated signal, was recorded. The pEC_{50} values determined for pNPY depended on the type of label-free and calcium assay (Table 5.1). ECIS revealed the highest potency of pNPY with an pEC_{50} of 9.37, whereas the DMR and the fura-2 assay gave comparable results (pEC_{50} values: 8.58 and 8.47), and the aequorin calcium assay gave the lowest pEC_{50} value. Interestingly, the differences between

Tab. 5.1: Potencies ($pEC_{50} \pm SEM$) of pNPY determined in the optical and impedimetric label-free assay compared to calcium assays

Cells	DMR ^a	ECIS ^a	fura-2 ^a	Aequorin ^a
CHO-hY ₂ -G _{qi5} -mtAEQ	8.58 ± 0.08	9.37 ± 0.12	8.47 ± 0.09	7.84 ± 0.19
CHO-hY ₂ -mtAEQ	8.29 ± 0.13	n.d.	n.d.	n.d.

^aAssays on CHO-hY₂-G_{qi5}-mtAEQ cells. Data were analyzed by nonlinear regression and were best fitted to four-parameter sigmoidal concentration-response curves. Data shown are the means ± SEM of at least two independent experiments. Investigations in label-free and aequorin assay were performed in triplicate. Fura-2 calcium assay: one experiment performed in triplicate.

binding ($K_d = 0.7 \pm 0.2$ nM [19]) and functional data was less pronounced in the impedimetric. It may be speculated that cellular signalling mechanisms other than the calcium response contribute to the holistic readout. Moreover, the pNPY potency obtained in the fura-2 calcium assay was higher than the value, generated in the aequorin assay. A similar result was already reported before [19], although the discrepancy between the assays was much higher in the recent experiments. Apparent discrepancies between the data from the calcium assays could result from the different assay procedures. Especially, the shear stress caused by the injection of the cell into the pNPY-containing wells in the aequorin assay could be a critical issue.

To investigate the effect of the chimeric G-protein G_{qi5}, the CHO-hY₂-G_{qi5}-mtAEQ cells were compared with the CHO-hY₂-mtAEQ cells in the optical label-free assay (Fig. 5.5). Surprisingly, concentration-dependent signals of similar curve shapes were recorded with both cell types. The determined potency of pNPY was slightly lower in the cells without chimeric G-protein (pEC_{50} : 8.29) compared with the cells expressing the G_{qi5} construct (pEC_{50} : 8.58). The efficacy of pNPY in the cells without G_{qi5} was about 80 % of the maximal agonist signal measured with the cells expressing the chimeric G-protein. In contrast to the fact that mobilisation of

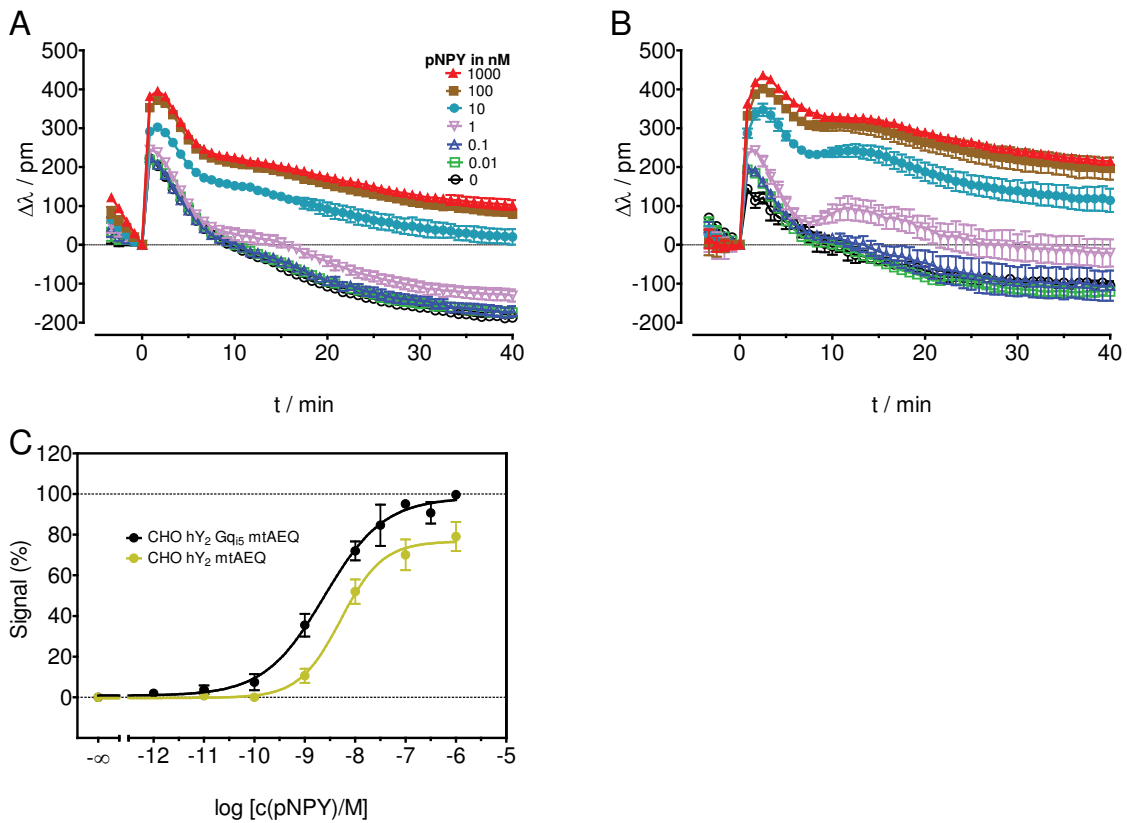


Fig. 5.5: (A, B) pNPY-induced DMR response of CHO-hY₂ cells devoid of (A, CHO-hY₂-mtAEQ cells) or expressing the G α_{qi5} protein (B, CHO-hY₂-G α_{qi5} -mtAEQ cells). Peptide solutions contained 1% BSA to reduce adsorption to the surface of plate and 0.1 mg/mL bacitracin in order to prevent protease-mediated degradation of pNPY. (C) Comparison of the concentration-response curves of pNPY. The response was normalized to a solvent control and referred to the maximal effect of pNPY in the CHO-hY₂-G α_{qi5} -mtAEQ cells, expressing the chimeric G-protein. Data are means \pm SEM of at least 3 independent experiments, each performed in triplicate.

intracellular calcium by pNPY in the fura-2 assay was weak in CHO-Y₂ cell devoid of the chimeric G-protein [19], the DMR assay revealed nearly full intrinsic activity on cells without G α_{qi5} . Obviously, the G-proteins endogenously expressed in CHO cells suffice to give apply DMR as a functional readout, making genetic engineering with regard to re-direction of the cellular signal unnecessary. To explore whether the measured DMR signal is Y₂ receptor-mediated, the selective high affinity NPY Y₂ receptor antagonist BIIE 0246 was investigated in the optical label-free assays (Fig. 5.6). It was reported in previous studies that BIIE 0246 behaves as an insurmountable antagonist after pre-incubation [19,30]. Therefore, BIIE 0246 at different concentrations was co-administered with a constant submaximal agonist ($c(\text{pNPY}) = 30 \text{ nM}$) concentration. The

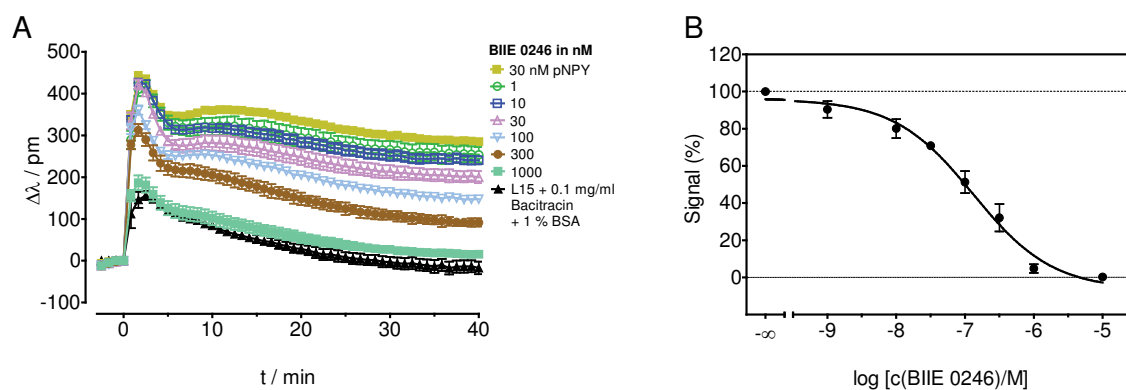


Fig. 5.6: Inhibition of the NPY induced signal by BIIE 0246 on CHO cells stably co-expressing the hY_2 receptor, G_{q15} and mtAEQ in the DMR assay. (A) Inhibition of the pNPY (30 nM) induced response by co-applied BIIE 0246. (B) Concentration-response curve of BIIE 0246 (pK_B : 7.98 ± 0.13). Data are means \pm SEM of 2 independent experiments, each performed in triplicate.

determined K_B value of BIIE 0246 ($K_B = 10.47$ nM) was in good agreement with previously reported data for the fura-2 assay ($K_B = 28.9$ nM) [19]. The antagonist could suppress the pNPY induced signal in the impedimetric assay as well (data not shown). Because of technical problems with the ECIS apparatus, the experiment could not be repeated.

5.3.4 Investigation of G-protein coupling of the human NPY Y_2 receptor

To analyse the contribution of $G_{ai/o}$ and $G_{aq/11}$ proteins, concentration-response curves of pNPY were constructed in the presence of pertussis toxin or the $G_{aq/11}$ inhibitor FR900359 (UBO-QIC) [31,32], respectively. Pertussis toxin catalyzes the ADP-ribosylation of the α_i subunit of the heterotrimeric G protein, preventing the interaction with GPCRs, due to the G_i subunits remaining locked in the GDP-bound state [33-35]. Pertussis toxin influences cellular response by different mechanisms. The inhibition is resulting in an uncoupling of the $G_{ai/o}$ protein from the receptor and the final suppression of the intracellular signal transduction. The depsipeptide FR900359 is structurally very similar to YM-254890 and shows similar pharmacological activity [36]. The reason for the YM-254890 mediated inhibition of the $G_{aq/11}$ signal transduction is the prevention of the GDP-GTP exchange in $G_{aq/11}$ [37].

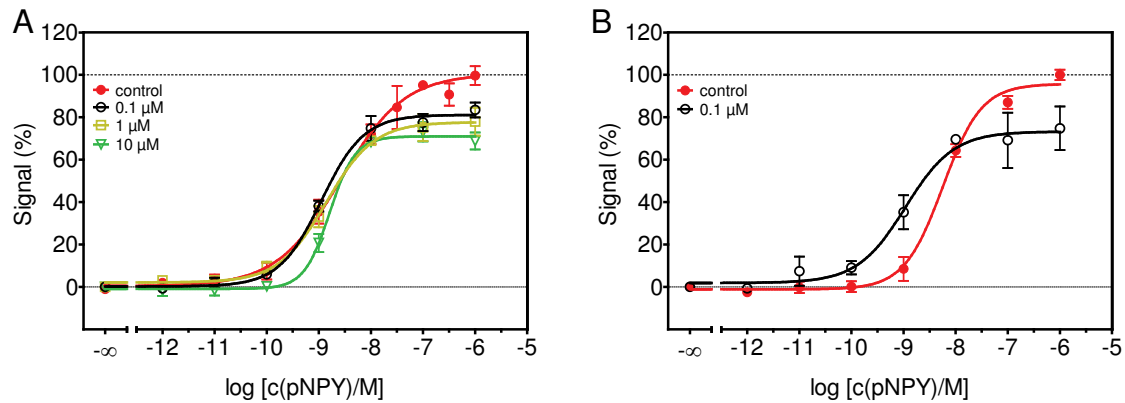


Fig. 5.7: Effect of the $G\alpha_q$ -inhibitor FR900359 on the pNPY-induced response in the DMR assay. Experiments were performed using (A) CHO-hY₂-G_{qi5}-mtAEQ and (B) CHO-hY₂-mtAEQ cells. Data were normalized to a solvent control and the maximal activation by the agonist pNPY on the cells of interest. Data represent means \pm SEM of at least 2 independent experiments performed in triplicate.

As becomes obvious from Fig. 5.7, the pNPY response was reduced by the $G\alpha_{q/11}$ inhibitor FR900359 in both, CHO-hY₂-G_{qi5}-mtAEQ and CHO-hY₂-mtAEQ cells. In case of the cells expressing the chimeric G-protein the concentration-response curve of pNPY was not shifted but depressed by approximately 20% to 30% in the presence of FR900259 at increasing concentrations. The depression of the pNPY signal in the presence of 10 μ M FR900259 was almost on the same level as the signal suppression caused by 1 μ M $G\alpha_{q/11}$ inhibitor. Interestingly, 0.1 μ M of FR900259 reduced the pNPY signal in cells without chimeric G-protein by roughly 20% as well, and the concentration-response curve was leftward shifted. It seems that in DMR the chimeric G-protein is less involved in the neuropeptide Y₂ receptor signalling than expected. This is in contrast to the fura-2 (data not shown) and aequorin calcium (Fig. 5.8) assays. Both, the aequorin and the fura-2 assay, revealed a complete lack of response to pNPY in the presence of FR900359 at concentrations ≥ 0.1 μ M. By contrast, in the presence of 5 and 50 ng/mL pertussis toxin, only a depression and a slight rightward shift became obvious. These results suggest that the pNPY induced DMR signal is in part and the calcium signal is completely mediated by endogenously expressed $G\alpha_{q/11}$ and/or the chimeric G-protein, respectively. The capability of the Y₂ receptor to couple to the $G\alpha_{q/11}$ protein was described for rabbit smooth muscle cells [38].

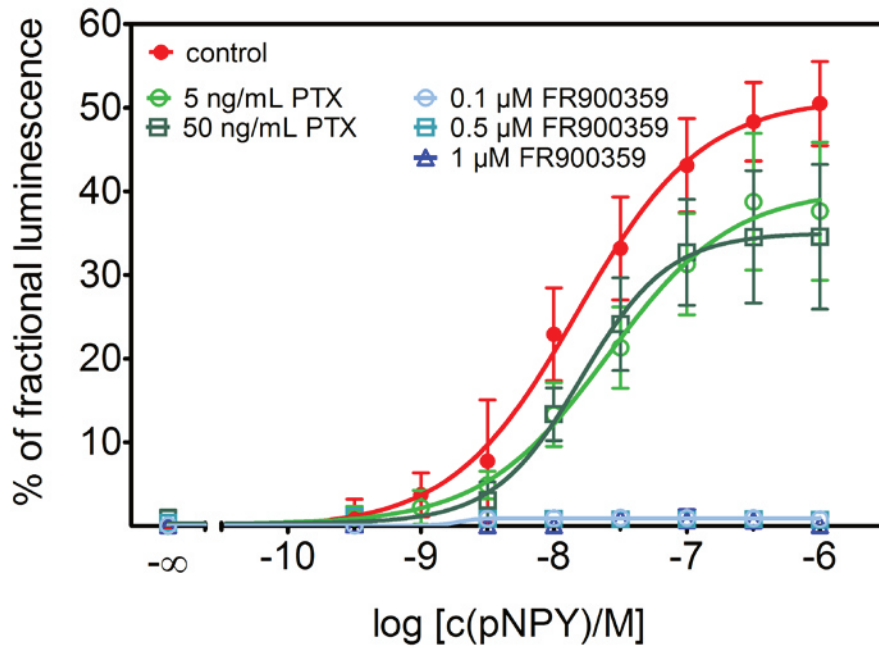


Fig. 5.8: Aequorin assay with CHO-hY₂-G_{q15}-mtAEQ cells. Concentration-response curves of pNPY in the presence of FR900359, PTX or without inhibitor. (Mean values \pm SEM, n=3)

As the inhibition of the hY₂ receptor mediated DMR signal by the FR900359 was incomplete and the hY₂ receptor is known to preferentially couple to the G $\alpha_{i/o}$ protein [3], the effect of pertussis toxin (PTX) was investigated. In the presence of pertussis toxin at concentrations from 1 to 100 ng/mL, the DMR signal of the pNPY-stimulated cells was reduced in a concentration-dependent manner resulting in an almost completely blocked response (Fig. 5.9).

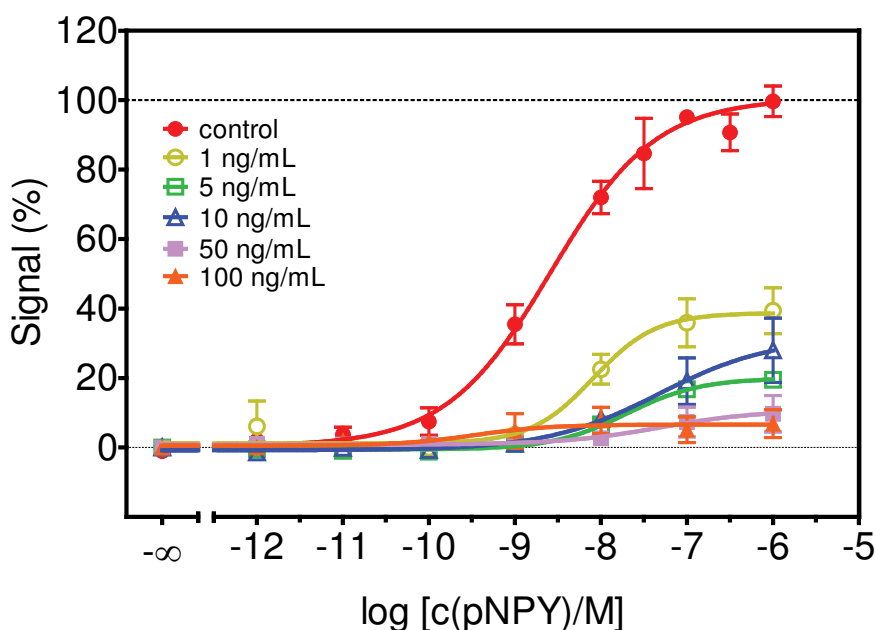


Fig. 5.9: DMR response in CHO-hY₂-G_{q15}-mtAEQ cells in the absence and presence of the G $\alpha_{i/o}$ inhibitor PTX. Data were normalized to a solvent control and the maximal activation by the agonist pNPY. Data represent means \pm SEM of at least 2 independent experiments performed in triplicate.

Compared to the DMR method the pNPY induced effect was just partly inhibited in the fura-2 (data not shown) and aequorin calcium assay (Fig. 5.8). Due to the expression of the chimeric G-protein in CHO-hY₂-G_{q15}-mtAEQ cells an almost complete reduction of the pNPY signal by PTX was not expected. These findings suggest not only a specific G_{i/o} inhibition but also a partly blockade of the chimeric G-protein in the presence of PTX. It could be possible that the PTX mechanism of action is responsible for these findings. Pertussis toxin ADP-ribosylates the amino acid cysteine in the carboxyl terminus of the α subunit of the G $\alpha_{i/o}$ protein and inhibits the signal transduction [39]. This cysteine residue belongs to those five C-terminal amino acids of the G $\alpha_{i/o}$ protein, which were used to engineer the chimeric G protein G α_{q15} by replacing the C-terminus in G $\alpha_{q/11}$ to improve the coupling efficiency to the hY₂ receptor [40]. Whereas the DMR response was strongly pertussis toxin sensitive, the results from the calcium assays suggested a predominantly G $\alpha_{q/11}$ mediated response.

5.3.5 Functional characterization of hY₄ receptor ligands in the DMR and aequorin calcium assay

A selection of structurally different agonists and antagonists (cf. section 5.2.1) were studied in the DMR and aequorin calcium assay, respectively. Cells expressing the hY₄ receptor were seeded to perform the DMR assay by analogy with the experiments described for CHO cells expressing the hY₂ receptor. The results for hY₄ receptor agonists in the DMR assay and the aequorin calcium assay are summarized in Table 5.2 and Fig. 5.10.

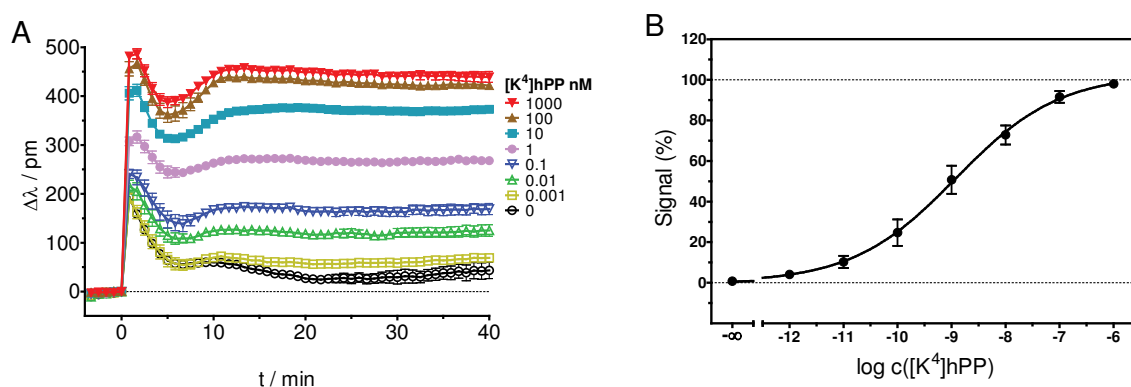


Fig. 5.10: [K⁴]hPP induced DMR signal on CHO cells expressing the hY₄ receptor. (A) Representative agonist induced traces. (B) Concentration response curve from the area under the curve (0 – 40 min). Data represent means \pm SEM of at least 2 independent experiments performed in triplicate.

[K⁴]hPP induced an immediate sharp increase after addition. The signal peaked in a first maximum at approximately two minutes. A transient relative minimum was reached after approximately five minutes. Subsequently, a second positive wavelength shift was recorded. The DMR signal resulted in a constant level from minute 15 on. The shape of the curves suggest a G α_i protein mediated response [26,27]. The pEC₅₀ values of the analysed agonists were comparable to data from other assays [21]. As reported, the configuration of the stereo centers in the 2,7-diaminosuberic acid linker of Y₄R agonists derived from the C-terminal pentapeptide of hPP has an impact on Y₄R potency [21]. In the label-free assay (2*R*,7*R*)-**3** was 3.5 times more potent than (2*S*,7*S*)-**3** (stereochemical discriminators refer to the chiral centers in the linker). A similar difference was determined in the calcium assay (pEC₅₀ values: 8.17 (2*R*,7*R*)-**3** vs. 7.76 (2*S*,7*S*)-**3**). Similarly, a stereochemical discrimination was determined for the propionylated analogues (2*R*,7*R*)-**4** and (2*S*,7*S*)-**4**. As demonstrated recently [21], the replacement of one of the ‘inner arginines’ in **1** by the N^G-carbamoylated arginine results in an increased Y₄R agonist potency. In the DMR assay, **2** was about 25 times more potent than **1**. Both compounds showed the same or slightly lower efficacy than [K⁴]hPP. Most agonists showed a higher potency in the label-free assay compared to the aequorin calcium assay.

Tab. 5.2: NPY Y₄R agonist potencies (pEC₅₀) of ‘dimeric’ pentapeptides and reference compound [K⁴]hPP.

Compound	DMR ^a		Aequorin assay ^{a,b}	
	pEC ₅₀ ± SEM	E _{max}	pEC ₅₀ ± SEM	E _{max}
[K ⁴]hPP	8.97 ± 0.17	1.00	8.07 ± 0.03 ^[20]	1.00
1	8.04 ± 0.15	0.99	7.35 ± 0.10 ^[21]	0.75
2	9.44 ± 0.23	0.85	8.25 ± 0.12 ^[21]	0.80
(2 <i>R</i> ,7 <i>R</i>)- 3	8.29 ± 0.13	n.d.	8.17 ± 0.03 ^[21]	0.80
(2 <i>S</i> ,7 <i>S</i>)- 3	7.75 ± 0.18	n.d.	7.76 ± 0.04 ^[21]	n.d.
(2 <i>R</i> ,7 <i>R</i>)- 4	8.12 ± 0.08	n.d.	7.87 ± 0.06 ^[21]	n.d.
(2 <i>S</i> ,7 <i>S</i>)- 4	7.67 ± 0.17	n.d.	7.24 ± 0.04 ^[21]	n.d.

^aAssays on CHO-hY₄-G_{q15}-mtAEQ cells. Data were analyzed by nonlinear regression and were best fitted to four-parameter sigmoidal concentration-response curves. E_{max}: maximal response relative to [K⁴]hPP (E_{max} = 1.00). pEC₅₀: -logEC₅₀. Data shown are the means ± SEM of at least two independent experiments. ^bData were taken from Kuhn et al. (2016), ref. [21]

The $[K^4]hPP$ induced signal was suppressed by the hY_4R antagonist UR-MEK388 in the DMR ($pK_B : 6.67 \pm 0.12$) and in aequorin calcium assay

5.4 Conclusion

The applicability of label-free techniques (DMR and ECIS) was explored in comparison to two calcium assays (fura-2 and aequorin) for the characterization of hY_2 and hY_4 receptor ligands on cells expressing the receptor of interest, the chimeric G-protein G_{qi5} and mitochondrially targeted aequorin. Moreover, the effect of the $G\alpha_{q/11}$ and $G\alpha_{i/o}$ proteins inhibitors FR900359 (UBO-QIC) and pertussis toxin (PTX) was investigated.

hY_2 receptor. The stimulation of the hY_2 receptor by pNPY resulted in concentration-dependent signals in ECIS and DMR. The inhibition of the $G\alpha_{q/11}$ protein with FR900359 caused a partial reduction of the DMR signal, whereas in the presence of the $G\alpha_{i/o}$ inhibitor PTX, the DMR signal was almost completely inhibited. Similar findings were recorded in cells which do not express a chimeric G-protein. Obviously, the endogenously expressed G-proteins are sufficient to give a cellular response. In the presence of FR900359, the calcium signal was completely suppressed, whereas PTX only slightly reduced the signal. Depending on the assay, stimulation of the hY_2 receptor preferentially activates different signalling patterns characteristic of either the $G\alpha_{q/11}$ or the $G\alpha_{i/o}$ pathway.

hY_4 receptor. The stimulation of the hY_4 receptor by $[K^4]hPP$ and other agonists caused a concentration-dependent effect in the DMR assay. Most of the investigated agonists were more potent in the optical label-free assay than in the aequorin calcium assay.

It may be speculated that, in addition to Ca^{2+} mobilization, other cellular signalling mechanisms contribute to the holistic readout. The contribution of either the $G\alpha_{q/11}$ or the $G\alpha_{i/o}$ pathway could not be unambiguously elucidated. The discrepancies between the effects of the applied G-protein inhibitors on the different cells in the conventional and label-free assays may be attributed to the chimeric G-protein.

5.5 References

- 1 Balasubramaniam A. Neuropeptide Y family of hormones: receptor subtypes and antagonists. *Peptides* 1997;18
- 2 Reichmann F, Holzer P. Neuropeptide Y: A stressful review. *Neuropeptides* 2016;55:99-109.
- 3 Michel MC, Beck-Sickinger A, Cox H, Doods HN, Herzog H, Larhammar D, Quirion R, Schwartz T, Westfall T. XVI. International union of pharmacology recommendations for the nomenclature of neuropeptide Y, peptide YY, and pancreatic polypeptide receptors. *Pharmacol Rev* 1998;50:143-150.
- 4 Cabrele C, Beck-Sickinger AG. Molecular characterization of the ligand–receptor interaction of the neuropeptide Y family. *J Pept Sci* 2000;6:97-122.
- 5 Cerda-Reverter JM, Larhammar D. Neuropeptide Y family of peptides: structure, anatomical expression, function, and molecular evolution. *Biochem Cell Biol* 2000;78
- 6 Kormos V, Gaszner B. Role of neuropeptides in anxiety, stress, and depression: From animals to humans. *Neuropeptides*;47:401-419.
- 7 Parker SL, Balasubramaniam A. Neuropeptide Y Y2 receptor in health and disease. *Br J Pharmacol* 2008;153:420-431.
- 8 Zhang L, Bijker MS, Herzog H. The neuropeptide Y system: Pathophysiological and therapeutic implications in obesity and cancer. *Pharmacol Ther* 2011;131:91-113.
- 9 Weinberg DH, Sirinathsinghji DJS, Tan CP, Shiao L-L, Morin N, Rigby MR, Heavens RH, Rapoport DR, Bayne ML, Cascieri MA, Strader CD, Linemeyer DL, MacNeil DJ. Cloning and expression of a novel neuropeptide Y receptor. *J Biol Chem* 1996;271:16435-16438.
- 10 Starbäck P, Wraith A, Eriksson H, Larhammar D. Neuropeptide Y receptor gene $\gamma 6$: Multiple deaths or resurrections? *Biochem Biophys Res Commun* 2000;277:264-269.
- 11 Silva AP, Cavadas C, Grouzmann E. Neuropeptide Y and its receptors as potential therapeutic drug targets. *Clin Chim Acta* 2002;326:3-25.
- 12 Herzog H, Hort YJ, Ball HJ, Hayes G, Shine J, Selbie LA. Cloned human neuropeptide Y receptor couples to two different second messenger systems. *Proc Natl Acad Sci U S A* 1992;89:5794-5798.
- 13 Merten N, Beck-Sickinger AG. Molecular ligand-receptor interaction of the NPY/PP peptide family. In: Zukowska Z, Feuerstein GZ, eds. *NPY family of peptides in neurobiology, cardiovascular and metabolic disorders: From genes to therapeutics*. Basel: Birkhäuser Basel, 2006: pp 35-62.
- 14 Bischoff A, Püttmann K, Kötting A, Moser C, Buschauer A, Michel MC. Limited signal transduction repertoire of human Y5 neuropeptide Y receptors expressed in HEC-1B cells. *Peptides* 2001;22:387-394.
- 15 Dautzenberg FM, Higelin J, Pflieger P, Neidhart W, Guba W. Establishment of robust functional assays for the characterization of neuropeptide Y (NPY) receptors: identification of 3-(5-benzoyl-thiazol-2-ylamino)-benzonitrile as selective NPY type 5 receptor antagonist. *Neuropharmacology* 2005;48:1043-1055.
- 16 Gerald C, Walker MW, Vaysse PJ-J, He C, Branchek TA, Weinshank RL. Expression cloning and pharmacological characterization of a human hippocampal neuropeptide Y/ peptide YY Y2 receptor subtype. *J Biol Chem* 1995;270:26758-26761.
- 17 Lundell I, Blomqvist AG, Berglund MM, Schober DA, Johnson D, Statnick MA, Ganski RA, Gehlert DR, Larhammar D. Cloning of a human receptor of the NPY receptor family with high affinity for pancreatic polypeptide and peptide YY. *J Biol Chem* 1995;270:29123-29128.

- 18 Parker EM, Babij CK, Balasubramaniam A, Burrier RE, Guzzi M, Hamud F, Gitali M, Rudinski MS, Tao Z, Tice M, Xia L, Mullins DE, Salisbury BG. GR231118 (1229U91) and other analogues of the C-terminus of neuropeptide Y are potent neuropeptide Y Y1 receptor antagonists and neuropeptide Y Y4 receptor agonists. *Eur J Pharmacol* 1998;349:97-105.
- 19 Ziemek R, Brennauer A, Schneider E, Cabrele C, Beck-Sickinger AG, Bernhardt G, Buschauer A. Fluorescence- and luminescence-based methods for the determination of affinity and activity of neuropeptide Y2 receptor ligands. *Eur J Pharmacol* 2006;551:10-18.
- 20 Ziemek R, Schneider E, Kraus A, Cabrele C, Beck-Sickinger AG, Bernhardt G, Buschauer A. Determination of affinity and activity of ligands at the human neuropeptide Y Y4 receptor by flow cytometry and aequorin luminescence. *J Recept Signal Transduct Res* 2007;27:217-233.
- 21 Kuhn KK, Ertl T, Dukorn S, Keller M, Bernhardt G, Reiser O, Buschauer A. High affinity agonists of the neuropeptide Y (NPY) Y4 receptor derived from the C-terminal pentapeptide of human pancreatic polypeptide (hPP): Synthesis, stereochemical discrimination and radiolabeling. *J Med Chem* 2016
- 22 Keller M, Kaske M, Holzammer T, Bernhardt G, Buschauer A. Dimeric argininamide-type neuropeptide Y receptor antagonists: Chiral discrimination between Y1 and Y4 receptors. *Bioorg Med Chem* 2013;21:6303-6322.
- 23 Doods H, Gaida W, Wieland HA, Dollinger H, Schnorrenberg G, Esser F, Engel W, Eberlein W, Rudolf K. BIIE0246: A selective and high affinity neuropeptide Y Y2 receptor antagonist. *Eur J Pharmacol* 1999;384:R3-R5.
- 24 Lieb S, Michaelis S, Plank N, Bernhardt G, Buschauer A, Wegener J. Label-free analysis of GPCR-stimulation: The critical impact of cell adhesion. *Pharmacol Res*
- 25 Stolwijk J, Michaelis S, Wegener J. Cell growth and cell death studied by electric cell-substrate impedance sensing. *Electric Cell-Substrate Impedance Sensing and Cancer Metastasis* 2012
- 26 Fang Y. Non-invasive optical biosensor for probing cell signaling. *Sensors* 2007;7:2316-2329.
- 27 Schröder R, Janssen N, Schmidt J, Kebig A, Merten N, Hennen S, Müller A, Blattermann S, Mohr-Andra M, Zahn S, Wenzel J, Smith NJ, Gomeza J, Drewke C, Milligan G, Mohr K, Kostenis E. Deconvolution of complex G protein-coupled receptor signaling in live cells using dynamic mass redistribution measurements. *Nat Biotechnol* 2010;28:943-949.
- 28 Verdonk E, Johnson K, McGuinness R, Leung G, Chen Y-W, Tang HR, Michelotti JM, Liu VF. Cellular dielectric spectroscopy: A label-free comprehensive platform for functional evaluation of endogenous receptors. *Assay Drug Dev Technol* 2006;4:609-619.
- 29 Fang Y, Frutos AG, Verklereen R. Label-free cell-based assays for GPCR screening. *Comb Chem High Throughput Screen* 2008;11:357-369.
- 30 Dautzenberg FM, Neysari S. Irreversible binding kinetics of neuropeptide Y ligands to Y2 but not to Y1 and Y5 receptors. *Pharmacology* 2005;75:21-29.
- 31 Fujioka M, Koda S, Morimoto Y, Biemann K. Structure of FR900359, a cyclic depsipeptide from *Ardisia crenata* Sims. *J Org Chem* 1988;53:2820-2825.
- 32 Schrage R, Schmitz A-L, Gaffal E, Annala S, Kehraus S, Wenzel D, Büllsbach KM, Bald T, Inoue A, Shinjo Y, Galandrin S, Shridhar N, Hesse M, Grundmann M, Merten N, Charpentier TH, Martz M, Butcher AJ, Slodczyk T, Armando S, Efferm M, Namkung Y, Jenkins L, Horn V, Stößel A, Dargatz H, Tietze D, Imhof D, Galés C, Drewke C, Müller CE, Hölzel M, Milligan G, Tobin AB, Gomeza J, Dohlman HG, Sondek J, Harden TK, Bouvier M, Laporte SA, Aoki J, Fleischmann BK, Mohr K, König GM, Tüting T, Kostenis E. The

- experimental power of FR900359 to study Gq-regulated biological processes. *Nat Commun* 2015;6:10156.
- 33 Mangmool S, Kurose H. G(i/o) protein-dependent and -independent actions of pertussis toxin (PTX). *Toxins* 2011;3:884-899.
 - 34 Passador L, Iglewski W. ADP-ribosylating toxins. *Methods Enzymol: Academic Press*, 1994: pp 617-631.
 - 35 Katada T. The inhibitory G-Protein Gi identified as pertussis toxin-catalyzed ADP-ribosylation. *Biol Pharm Bull* 2012;35:2103-2111.
 - 36 Kamato D, Thach L, Bernard R, Chan V, Zheng W, Kaur H, Brimble M, Osman N, Little PJ. Structure, function, pharmacology, and therapeutic potential of the G-Protein, G α (q/11). *Front Cardiovasc Med* 2015;2:14.
 - 37 Takasaki J, Saito T, Taniguchi M, Kawasaki T, Moritani Y, Hayashi K, Kobori M. A novel G α q/11-selective inhibitor. *J Biol Chem* 2004;279:47438-47445.
 - 38 Misra S, Murthy KS, Zhou H, Grider JR. Coexpression of Y1, Y2, and Y4 receptors in smooth muscle coupled to distinct signaling pathways. *J Pharmacol Exp Ther* 2004;311:1154-1162.
 - 39 West RE, Moss J, Vaughan M, Liu T, Liu TY. Pertussis toxin-catalyzed ADP-ribosylation of transducin. Cysteine 347 is the ADP-ribose acceptor site. *J Biol Chem* 1985;260:14428-14430.
 - 40 Ziemek R. Development of binding and functional assays for the neuropeptide Y Y2 and Y4 receptors. *Faculty of Chemistry and Pharmacy: Regensburg*, 2006.

6 Summary

Label-free cell-based assays have been attracting growing attention in drug research. In this context, optical approaches based on evanescent electric fields (e.g. resonant waveguide grating, RWG; dynamic mass redistribution, DMR) and electrochemical impedance analysis (e.g. electric cell-substrate impedance sensing, ECIS) are the most widespread techniques. The aim of this doctoral thesis was to optimize and to explore the potential of two label-free methods, DMR and ECIS, to functionally characterize ligands of prototypical aminergic and peptidergic G-protein coupled receptors (GPCRs). For this purpose, histamine H_1 and neuropeptide Y (NPY) Y_2 and Y_4 receptors were selected as examples.

With respect to the optimization of the conditions for the investigation of the human histamine H_1 receptor (H_{1R}), native U-373 MG glioblastoma and genetically engineered HEK 293T cells, either expressing the H_{1R} alone or in combination with the adhesion protein hMSR1 were used. Reduced cell adhesion to the surface of the sensing devices affected both, the optical and the impedance-based readout, but became much more obvious in case of the DMR-assay. The co-expression of hH_{1R} and hMSR1 in HEK 293T cells strongly enhanced the signal compared to hH_{1R} expression alone. As the sensitivity of the optical readout is confined to a distance of 100-200 nm from the surface, depending on the wavelength of the incident light, this observation is in accordance with tighter adhesion of the co-transfectants, inducing a shorter distance between the cell membrane and the substrate. Cell adhesion was found to have a critical impact on the results of label-free cell monitoring, in particular when techniques based on evanescent electric fields are applied.

To explore the applicability and the potential of label-free assays, a set of H_{1R} agonists and antagonists was characterized by DMR, ECIS and the data were compared with those from various signaling pathway specific readouts (Fura-2 and aequorin calcium assays, arrestin recruitment (luciferase fragment complementation) assay, luciferase gene reporter assay), gained from genetically engineered HEK293T cells. Additionally, reference data from GTPase assays and radioligand binding were considered. Histamine and other H_{1R} agonists (betahistine, UR-KUM530) gave different assay-related pEC_{50} values, however, the order of potency was retained. In the luciferase fragment complementation assay, the H_{1R} preferred β -arrestin2 over β -arrestin1. The calcium and the impedimetric assay depended on $G\alpha_q$ coupling of the H_{1R} , as demonstrated by complete inhibition of the histamine-induced signals

in the presence of the $G\alpha_q$ inhibitor FR900359 (UBO-QIC). Whereas partial inhibition by FR900359 was observed in DMR and the gene reporter assay, pertussis toxin (PTX) substantially decreased the response in DMR, but increased the luciferase signal, reflecting the contribution of both, $G\alpha_q$ and G_i , to signalling in these assays. For antagonists, the results from DMR were essentially compatible with those from conventional readouts, whereas the impedance-based data revealed a trend towards higher pK_b values. ECIS and calcium assays apparently only reflect $G\alpha_q$ signaling, whereas DMR and gene reporter assays appear to integrate both, $G\alpha_q$ and $G\alpha_i$ mediated signaling. Regardless of that, the results confirm the value of the label-free methods, DMR and ECIS, for the characterization of H_1R ligands.

As a model for peptidergic GPCRs, CHO- G_{q15} -mtAEQ cells co-expressing the human NPY Y_2 (Y_2R) or Y_4 receptor (Y_4R), the chimeric $G\alpha$ protein G_{q15} and mitochondrially tagged aequorin were selected. The applicability of DMR and ECIS was explored in comparison to two calcium assays (Fura-2 and aequorin). The stimulation of the Y_2R by pNPY resulted in concentration-dependent signals in ECIS and DMR. The inhibition of $G\alpha_{q/11}$ by FR900359 caused a partial reduction of the DMR signal, whereas in the presence of the $G\alpha_{i/o}$ inhibitor PTX, the DMR signal was almost completely inhibited. In CHO cells which do not express a chimeric G-protein, pNPY gave a strong DMR signal, suggesting that endogenously expressed G-proteins are sufficient to give a cellular response. This effect was only slightly reduced by FR900359. In both calcium assays with CHO-h Y_2 - G_{q15} -mtAEQ cells, PTX only slightly reduced the signal, whereas FR900359 completely suppressed the response. Depending on the assay, stimulation of the Y_2R preferentially resulted in different signalling patterns characteristic of either the $G\alpha_{q/11}$ or the $G\alpha_{i/o}$ pathway.

The stimulation of the h Y_4 receptor by [K^4]hPP and other agonists caused a concentration-dependent effect in the DMR assay. Most of the investigated agonists were more potent in the optical label-free assay than in the aequorin calcium assay. It may be speculated that, in addition to Ca^{2+} mobilization, other cellular signalling mechanisms contribute to the holistic readout. The contribution of either the $G\alpha_{q/11}$ or the $G\alpha_{i/o}$ pathway could not be unambiguously demonstrated. The discrepancies between the effects of the applied G-protein inhibitors on the different cells in the conventional and label-free assays may be attributed to the chimeric G-protein.

In summary, both noninvasive techniques are complementary to each other, but cannot fully replace reductionist signaling pathway focused assays.

Eidesstattliche Erklärung

Ich erkläre hiermit an Eides statt, dass ich die vorliegende Arbeit ohne unzulässige Hilfe Dritter und ohne Benutzung anderer als der angegebenen Hilfsmittel angefertigt habe; die aus anderen Quellen direkt übernommenen Daten und Konzepte sind unter Angabe des Literaturzitats gekennzeichnet.

Einige der experimentellen Arbeiten wurden in Zusammenarbeit mit anderen Personen durchgeführt. Entsprechende Vermerke finden sich in den betreffenden Kapiteln. Eine detaillierte Auflistung aller Kooperationen enthält zudem der Abschnitt „Acknowledgements and declaration of collaborations“.

Weitere Personen waren an der inhaltlich-materiellen Herstellung der vorliegenden Arbeit nicht beteiligt. Insbesondere habe ich hierfür nicht die entgeltliche Hilfe eines Promotionsberaters oder anderer Personen in Anspruch genommen. Niemand hat von mir, weder unmittelbar noch mittelbar, geldwerte Leistungen für Arbeiten erhalten, die im Zusammenhang mit dem Inhalt der vorgelegten Dissertation stehen.

Die Arbeit wurde bisher weder im In- noch im Ausland in gleicher oder ähnlicher Form einer anderen Prüfungsbehörde vorgelegt.

Regensburg, _____

Sebastian Lieb

